ABSTRACT

DEGRADATION OF POLYLACTIC ACID IN THE PRESENCE OF MICROSIZE AND NANOSIZE FILLERS

by
Quyuan Zhou

Polylactide (PLA)-cationic (montmorillonite, MMT) and anionic (hydrotalcite, HT) clay micro- or nanocomposites based on semicrystalline and amorphous polymers and unmodified and organomodified as well as calcined or non-calcined clays at 5wt% concentration are produced by melt mixing. Depending on the clay type, presence of organomodifiers and calcination, micro- or nanocomposites are produced, as confirmed by XRD and SEM analysis.

Unfilled polymers and their composites are subjected to isothermal degradation in air at 180°C and 200°C. Degradation rate constants are calculated from novel equations incorporating *IV*. Results show that the thermal degradation rate constants of the amorphous PLA and its composites are lower than those of the semicrystalline PLA and its composites due to the higher initial MW of the amorphous PLA based on *IV* (Intrinsic Viscosity) measurements. Due to better filler dispersion in the polymer matrix the thermal degradation rates of the nanocomposites are significantly lower than those of the unfilled polymers under air. The thermal degradation rate constants of calcined clay composites are higher than those of the non-calcined clay composites due to the porous structure of the calcined clays. As per dynamic TGA data and thermal kinetics analysis organomodified nanofillers have a complex effect on the polymer thermal stability, whereas all unmodified fillers reduce polymer thermal stability. The thermal stability of calcined clay composites is higher than that of their non-calcined clay counterparts. It is

shown that the effect of the unmodified cationic fillers on the polymer thermal stability depends on the heating rate by contrast to the heating rate independent effect of the unmodified anionic clays. In general, mathematical modeling based on random thermal scission equations was satisfactory for fitting the TGA experimental data.

Unfilled polymers and their composites subjected to accelerated hydrolytic degradation over a temperature range of 50°C-70°C show significant morphological differences after four weeks. Degradation rate constants were higher for the amorphous PLA and its composites than for semicrystalline PLA and its composites as a result of increased permeation through the amorphous domains. Since the effective pH of the cationic nanofillers and their hydrophilicity change through treatment with organomodifiers, the degradation rate constants of the nanocomposites are significantly higher than those of the unfilled polymers; by contrast, those of cationic microcomposites and anionic nanocomposites are lower or slightly lower than those of the unfilled polymers, possibly due to the reduction of the carboxylic group catalytic effect through neutralization with the hydrophilic alkaline filler. As a result of the stronger neutralizing ability of the anionic vs. the cationic clays, the hydrolytic degradation rates of the anionic clay composites were lower than those of the cationic clay composites and the unfilled polymers. In the case of semicrystalline PLA, calcined HT and MMT clays can reduce hydrolytic degradation rates through their stronger neutralization ability. Although the degradation rate constants increased with increasing temperature, based on the calculated activation energies the degradation kinetics did not differ significantly above and below the assumed T_g of 58°C~60°C. From SEM examination of the degraded samples it appears that bulk hydrolytic degradation starts at the polymer/filler interface

DEGRADATION OF POLYLACTIC ACID IN THE PRESENCE OF MICROSIZE AND NANOSIZE FILLERS

by
Quyuan Zhou

A Dissertation
Submitted to the Faculty of
New Jersey Institute of Technology
in Partial Fulfillment of the Requirements for the Degree of
Doctor of Philosophy in Chemical Engineering

Otto H.. York Department of Chemical, Biological and Pharmaceutical Engineering

August 2008

APPROVAL PAGE

DEGRADATION OF POLYLACTIC ACID IN THE PRESENCE OF MICROSIZE AND NANOSIZE FILLERS

Quyuan Zhou

Dr. Marino Xanthos, Dissertation Advisor — Date
Professor, Otto H. York Department of Chemical, Biological and Pharmaceutical Engineering, NJIT

Dr. George Collins, Committee Member — Date
Research Professor of Biomedical Engineering, NJIT

Dr. Michael Jaffe, Committee Member — Date
Research Professor of Biomedical Engineering, NJIT

Dr. Boris Khusid, Committee Member — Date
Professor, Otto H. York Department of Chemical, Biological and Pharmaceutical Engineering, NJIT

Dr. Laurent Simon, Committee Member — Date
Associate Professor, Otto H. York Department of Chemical, Biological and Pharmaceutical Engineering, NJIT

Dr. Xianqin Wang, Committee Member — Date
Assistant Professor, Professor, Otto H.. York Department of Chemical, Biological and Pharmaceutical Engineering, NJIT

BIOGRAPHICAL SKETCH

Author: Quyuan Zhou

Degree: Doctor of Philosophy

Date: August 2008

Undergraduate and Graduate Education:

- Doctor of Philosophy in Chemical Engineering,
  New Jersey Institute of Technology, Newark, NJ, 2008

- Master of Science in Chemical Engineering,
  Manhattan College, Riverdale, New York, 2003

- Bachelor of Science in Chemical Engineering,
  Zhejiang University, Hangzhou, P. R. China, 1987

Major: Chemical Engineering

Publications and Presentations

Q. Zhou and M. Xanthos
"Nanoclay and Crystallinity Effects on the Hydrolytic Degradation of Polylactides,"*Polym. Degrad. Stab.*, DOI 10.1016/jpolymdegradstab.2008.05.014

Q. Zhou and M. Xanthos
"Hydrolytic Degradation of Polylactic Acid Micro- and Nanocomposites", *Proc.66th Annual Technical Conference Society of Plastics Engineers*, *SPE,* 54, 576-580 (2008).

M. Xanthos and Q. Zhou
"Thermal And Hydrolytic Degradation of Polylactic Acid Nanocomposites",*Proc. Polymer Processing Society PPS-24 Annual Meeting,* Paper S17-237, June 15-19, 2008, Salerno, Italy.

Dedicated to my parents, my husband Wei Wang and my lovely daughters Mengqi Wang and Mengfan Wang

谨以此文献给我的亲人们

ACKNOWLEDGMENT

As I look back on the four and half years that it took me to complete this work, I would like to make special mention of the people listed below:

First, I would like to express my deepest appreciation to my Ph.D. advisor, Prof. Marino Xanthos for his constructive guidance, encouragement and suggestions throughout the course of this research. I especially acknowledge him for his devotion in uncovering my abilities. He gave me the opportunity to learn and strengthen my background in polymer chemistry. Particularly, I would like to thank him for the many hours spent in improving my English and I'll always remember those pleasant discussions on the research that we shared.

Special thanks are given to Dr. George Collins, Dr. Michael Jaffe and Dr. Laurent Simon for providing me insightful comments on polymer crystallization and model fitting. Also, special thanks are given to Dr. Boris Khusid and Dr. Xianqin Wang for actively participating in my committee.

I would like to thank the staff of the Medical Device Concept Laboratory (MDCL) and Polymer Processing Institute (PPI), Newark, NJ for providing a friendly and productive environment. Their invaluable assistance is greatly appreciated.

In addition, I would like to thank Dr. Victor Tan for his guidance and help with the characterization experiments and Mr. Dale Conti as well as Mr. Michael Zawisa for their timely support and assistance with experimental equipment in the PPI Laboratory. I also would like to thank Dr. Jing Wu and Mr. Yogesh Gandhi for providing the PLLA polymer and experimental apparatus and chemicals, respectively.

I am grateful to all of my colleagues and friends, Dr. Fei He, Dr. Byeong J Jeong, Mr. Kuan-Yin Lin, Mr. Shuli Teng, Dr. Chen Wan, Dr. Peng Wang, Dr. Seung Uk Yoo and Dr. Linjie, Zhu for their unconditional help and suggestions.

It would be inexcusable not to mention my mentor, Dr. Helen C. Hollein, for her confidence in me. It would have been difficult for me to begin my Ph. D studies without her great help. Also, my appreciation is given to Dr. Wei Kuo Lee for his enthusiastic encouragement during those difficult days.

I take this opportunity to sincerely thank my parents for their love and unceasing support since the day I was born. Their advice, inspiration and encouragement help me to stay focused and go in the right direction.

It is hard to express my appreciation in words to my husband for his endless love and support. His dedication to our marriage and children is unequaled. He has often been a light at the end of very dark tunnel for me. Without his help I could not have done it.

And finally, I would like to let my daughters know that this was for them. I want you both to live your life like every day is your last. And remember, "*Climb every mountain, cross every stream, follow every rainbow, till you find your dream.*"

TABLE OF CONTENTS

TABLE OF CONTENTS
(Continued)

TABLE OF CONTENTS
(Continued)

Chapter **Page**

LIST OF TABLES

LIST OF TABLES
(Continued)

Table **Page**

LIST OF FIGURES

LIST OF FIGURES
(Continued)

LIST OF FIGURES
(Continued)

Figure **Page**

LIST OF FIGURES
(Continued)

Figure **Page**

LIST OF FIGURES
(Continued)

Figure **Page**

k	Rate constant based on α in equation 5.8
k'	Rate constant based on [a] in equation 5.5
k_1	General hydrolytic degradation rate constant
k_2	Autocatalyzed hydrolytic degradation rate constant
k_2^*	Autocatalyzed hydrolytic degradation rate constant based on *IV*
k_3	Non-autocatalyzed hydrolytic degradation rate constant
k_{iv}	Isothermal degradation rate constant based on *IV*
k_{iv1}	Isothermal degradation rate constant based on *IV* at 180°C
k_{iv2}	Isothermal degradation rate constant based on *IV* at 200°C
k_n	Rate constant based on the number average molecular weight
k_v	Isothermal degradation rate constant based on M_v
M_{v0}	Viscosity molecular weight before degradation
$\overline{M_v}$	Viscosity average molecular weight
$\overline{M_n}$	Number average molecular weight
$\overline{M_{n0}}$	Initial number average molecular weight
$\overline{M_{nt}}$	Number average molecular weight at time t
$\overline{M_w}$	Weight average molecular weight

n	Reaction order
R	Ideal gas constant
r^2	Linear correlation coefficient
$\overline{r^2}$	Average linear correlation coefficient
s	Shape index of the differential thermal analysis curve for nonisothermal dynamic degradation.
T	Absolute temperature
T_c	Crystallization temperature
T_{cc}	Cold crystallization temperature
T_g	Glass transition temperature
T_p	Peak temperature determined at the DTG maximum peak
T_m	Melting temperature
T_m'	Temperature at maximum rate of weight loss
T_{10}	Temperature at weight loss of 10%
T_{50}	Temperature at weight loss of 50%
t	Time
W	Apparent weight fraction remaining
W_w	Sample wet weight
W_d	Sample dry weight

w	Molecular weight of the repeat unit
X	Number-average degree of polymerization
X_t	Number-average degree of polymerization at time t
X_0	Number-average degree of polymerization before degradation
α	Degree of conversion
$[\eta]$	Intrinsic viscosity
η_r	Relative viscosity
η_{sp}	Specific viscosity
θ	Diffraction angle
θ'	Difference between T and T_m'
v	Mark-Houwink parameter
φ	Heating rate

LIST OF ACRONYMS

ASTM	American Society for Testing of Materials
BPs	Biodegradable polymers
DSC	Differential Scanning Calorimetry
DTGA	Derivative differential thermogravimetric analysis
EDX	Energy Dispersive X-ray Analysis
HT	Hydrotalcite
HT(C)	Calcined Hydrotalcite
ISO	International Standards Organization
LDH	Layered double hydroxides
MCL	Medium-chain-length
MFI	Melt flow index
MMT	Montmorillonite
MMT-Na^+(C)	Calcined MMT-Na^+
OMLS	Organically modified layered silicate
PBS	Poly(butylene succinate)
PCL	Pol(ε-caprolactone)
PDLLA	Poly(DL-lactide)
PHAs	Polyhydroxyalkanoates
PLA	Polylactic Acid or Polylactide
PLAB	A polymer blend produced by melt mixing PLLA (A) and PDLLA (B)

PLGA	Poly(lactide-co-glycolide)
PLLA	Poly(L-lactide)
PLS	Polymer layered silicate
ROP	Ring opening polymerization
SCL	Short-chain length
SEM	Scanning Electron Microscopy
TGA	Thermogravimetric analysis
XRD	Wide-angle X-ray diffraction
15A	Cloisite® 15A
30B	Cloisite® 30B

CHAPTER 1

INTRODUCTION

Biodegradable polymers (BPs) or biopolymers have been highlighted as ''green polymers''. They have received much attention in major applications, such as tissue engineering, drug delivery and packaging based on one of the main characteristics of biodegradable polymers, i.e., their hydrolytic/enzymatic degradation. Since the mechanical properties of most biodegradable polymers are comparable to those of conventional thermoplastics, they can be reasonably substituted for certain commodity polymers in high volume applications. As a result, BPs must possess adequate thermal stability to minimize thermal degradation and maintain their molecular weight and properties during melt processing. Among the methods to control thermal and hydrolytic degradation of BPs is to prepare micro- or nanocomposites by adding different size fillers which, in addition, may enhance mechanical and other physical properties. Therefore, the objective of this study is to report on the degradation (including hydrolytic and thermal) of biodegradable polylactic acid polymers in the presence of micro- and nano- sized fillers. This chapter serves as an introduction to biodegradable polymers, micro- and nano- sized fillers as well as biopolymer composites.

1.1 Biodegradable Polymers

Biodegradable polymers began to spark interest during the oil crisis in the 1970's. As oil prices increased, efforts to develop biodegradable materials intensified. The 1980's brought items such as biodegradable films, sheets, and foamed materials.

The American Society for Testing of Materials (ASTM) and the International Standards Organization (ISO) define degradable polymers as those which undergo a significant change in chemical structure under specific environmental conditions. These changes result in a loss of physical and mechanical properties, as measured by standard methods. Biodegradable polymers undergo degradation from the action of naturally occurring microorganisms such as bacteria, fungi, and algae. Polymers may also be designated as photodegradable, oxidatively degradable, hydrolytically degradable, or compostable (Kolybaba et al., 2003).

BPs are becoming increasingly more popular. This is due in part to the fact that they may be produced from renewable resources and, thus, may be much more economical than conventional polymers. BPs disposed in bioactive environments degrade by the enzymatic action of microorganisms such as bacteria, fungi, and algae. Their polymer chains are also broken down by nonenzymatic processes such as chemical hydrolysis. BPs are often derived from plant processing of atmospheric CO_2. Biodegradation converts them to CO_2, CH_4, water, biomass, humic matter, and other natural substances. BPs are, thus, naturally recycled by biological processes (Figure. 1.1) (Gross et al., 2002).

Biodegradable polymers can be either natural or synthetic polymers. The natural polymers fall into four main groups:

- Proteins and polyamides. Examples include: Collagen, Fibrinogen and fibrin, Gelatin, Casein.
- Polysaccharides. Examples include: Cellulose, Starch and amylase, Chitin and chitosan, Dextran.
- Polynucleotides, e.g. DNA and RNA,

- Others, such as Lignin, Shellac, Natural Rubber

Synthetic polymers may include aliphatic polyesters, polyamides, polyanhydrides, polyethers, polyalkylene esters, polyvinyl alcohol, and polyvinyl esters.

Compared to natural polymers, synthetic polymers are preferable since they have tailorable properties and may be produced from reliable sources of new materials.

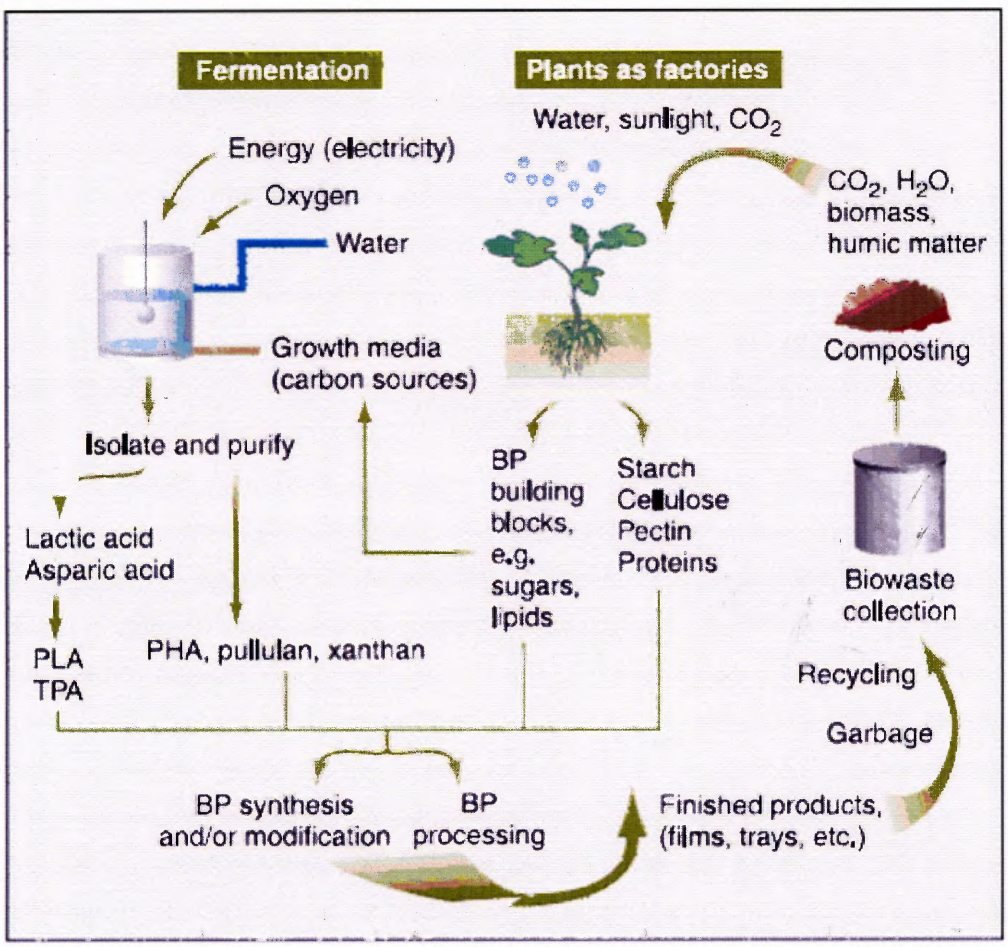

Figure 1.1 Biodegradable polymers naturally recycled by biological processes. (Gross et al., 2002)

1.1.1 Synthesis and Properties

Two general routes are used to develop synthetic biodegradable polymers. They are step (condensation) polymerization and addition (chain) polymerization including ring opening polymerization. The step process is used to prepare a variety of hydrolytically sensitive polymer classes. Ring opening polymerization (ROP) is an extensively investigated polymerization route to develop hydrolytically sensitive polymers, including poly (α-esters) and polyphosphazenes. Radical polymerization mostly results in the formation of non-degradable polymers; however, recent studies have demonstrated the feasibility of developing synthetic degradable polymers or cross-linked gels by radical polymerization processes (Nair et al., 2007). Synthetic biodegradable polymers may be made from biosources like corn, wood cellulose, etc. or can also be synthesized by bacteria. Other biodegradable polymers can be derived from petroleum sources or may be obtained from mixed sources of biomass and petroleum.

1.1.1.1 Biodegradable Synthetic Polymers from Renewable Resources. Renewable sources of polymeric materials offer an alternative to maintaining sustainable development of economically and ecologically attractive technologies. Innovations in the development of materials from biodegradable polymers, preservation of fossil-based raw materials, complete biological degradability, reduction in the volume of industrial and municipal waste and compostability in the natural cycle, protection of the climate through the reduction of carbon dioxide released, as well as the possibilities of agricultural resources to produce green materials are some of the reasons why such materials have attracted academic and industrial interest (Mohanty et al., 2003). Examples of aliphatic polyesters, the most important class of such materials are given below:

Polylactic Acid or Polylactide (PLA)

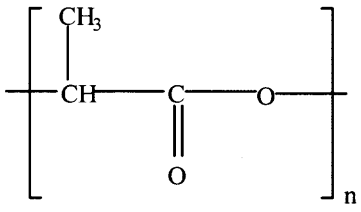

PLA is not new to the world of polymers. Carothers et al. (1932) investigated the production of PLA from the cyclic dimer (lactide) of lactic acid as early as 1932. Even before that, low molecular weight dimers and oligomers were detected when water was removed from an aqueous solution of lactic acid. Cargill Dow LLC, in 1997 started to focus on the production and marketing of PLA with the intention of significantly reducing its production cost and making it a large-volume plastic (Mohanty et al., 2005).

The conversion of lactic acid into high-molecular-weight PLA can follow two different routes of polymerization, as depicted in Figure 1.2. Lactic acid is condensation polymerized to yield a low-molecular-weight polymer which is unusable unless external coupling agents are employed to increase its molecular weight. Low molecular weight is the result in a high viscosity polymer melt, the formation of water, the presence of impurities, the statistical absence (low concentration) of reactive end-groups, and the "back-biting" equilibrium reaction that forms the six-member lactide ring. The second route of producing PLA is to convert the prepolymer to lactide followed by purification and ring-open polymerization to yield high-weight average molecular weight ($\overline{M_w}$ 100,000) PLA. The lactide method was the only method of producing pure, high-molecular-weight PLA until Mitsui Toatsu Chemicals recently commercialized a process wherein lactic acid and catalyst are azeotropically dehydrated in a refluxing, high-boiling,

aprotic solvent under reduced pressure to obtain PLA with $\overline{M_w}$ greater than 300,000 (Garlotta et al. 2001).

Cargill Dow LLC has developed a patented, low-cost continuous process for the production of lactic acid-based polymers. The process combines the substantial environmental and economic benefits of synthesizing both lactide and PLA in the melt rather than in solution and, for the first time, provides a commercially viable biodegradable commodity polymer made from renewable resources. Unlike conventional lactic acid, the lactic acid used in this process is produced by fermentation of dextrose (Figure 1.3) (Mohanty et al., 2005).

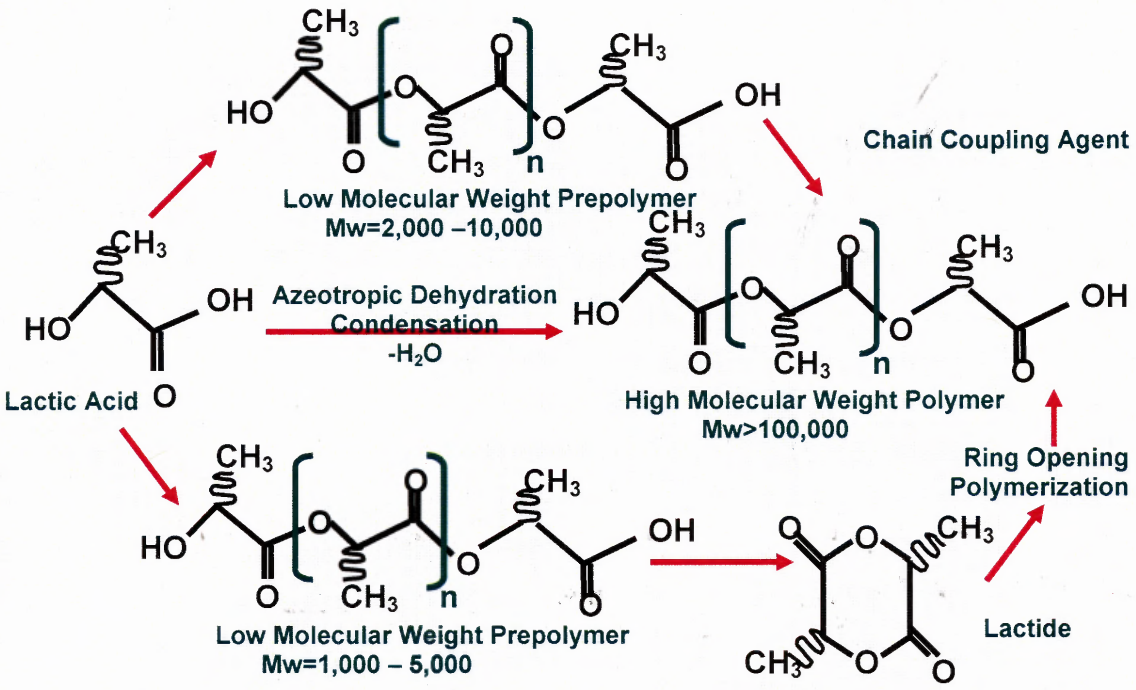

Figure 1.2 Synthesis of lactic acid into high-molecular-weight PLA. (Garlotta et al. 2001).

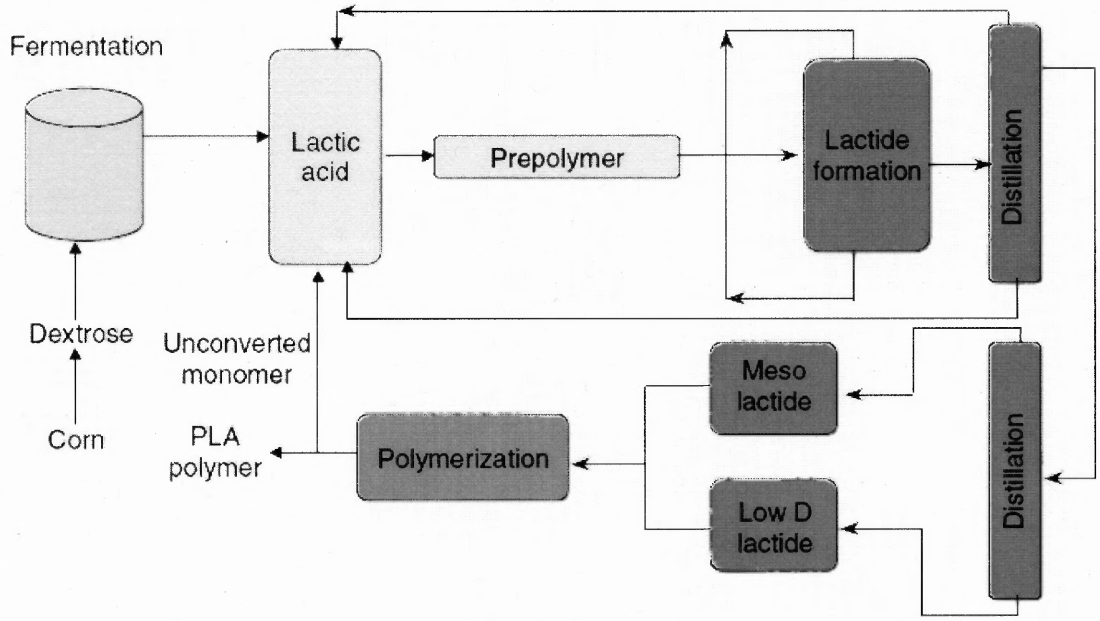

Figure 1.3 Cargill's nonsolvent process to prepare polylactic acid.
(Mohanty et al., 2005)

Poly (lactic acid) is present in three isomeric forms D (-), L (+) and racemic (D, L) and the polymers are usually abbreviated to indicate their chirality. Lactide is obtained by the depolymerization of high molecular-weight PLA under reduced pressure to give a mixture of L-lactide, D-lactide, or meso-lactide (Figure 1.4). Since lactic acid is enantiomeric, its polymers involve poly(L-lactide) PLLA, poly(D-lactide) (PDLA), poly(DL-lactide) (PDLLA), poly(meso-lactide), and their copolymers having different enantiomeric structure and/or optical activity of the monomeric units. While both PDLLA and poly (meso-lactide) are amorphous, the enantiomeric PLLA and PDLA are crystalline, showing a melting temperature (T_m) around 180°C. PLLA is the product resulting from polymerization of lactid acid in the L form. PDLA is the product resulting from polymerization of lactide acid in the D form (Urayama et al., 2003). Usually, PLLA has D-lactic acid content less than 6% (Feijoo et al., 2005).

Polylactic acid can be processed like most thermoplastics into fibers (for example using conventional melt spinning processes) and films. Its mechanical properties are comparable to those of thermoplastic polymers (Royte, 2006). The melting temperature of PLLA can be increased by 40-50 °C and its heat deflection temperature can be increased from approximately 60° C to up to 190 °C by physically blending the polymer with PDLA. PDLA and PLLA form a highly regular stereocomplex with increased crystallinity. The melting temperature is maximized when a 50:50 blend of PLLA and PDLA is used, but even at lower concentrations of 3-10% of PDLA, there is still a substantial improvement.

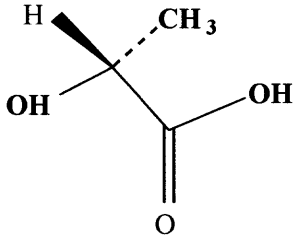

D(-) Lactic Acid

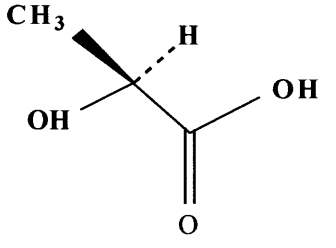

L (+) Lactic Acid

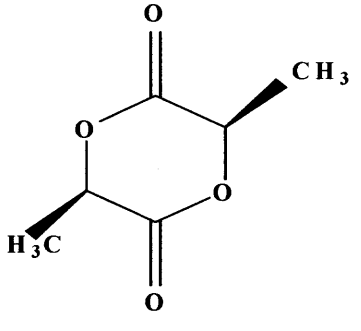

D-Lactide

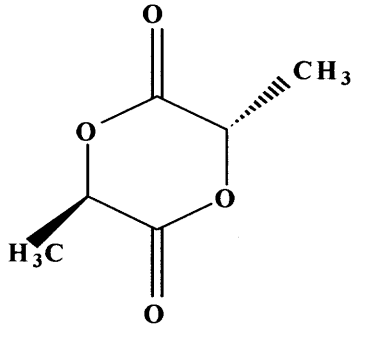

Meso-Lactide

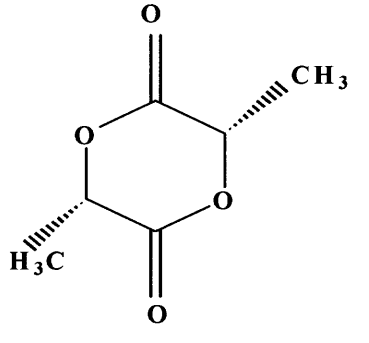

L-Lactide

Figure 1.4 Lactic acid and lactide structures.
(Garlotta et al. 2001)

Polyhydroxyalkanoates (PHAs)

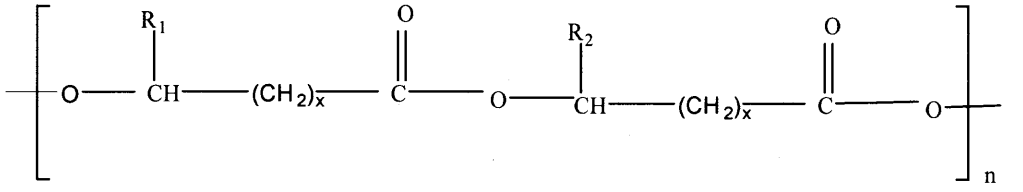

General Structure of Polyhydroxyalkanoates, R_1/R_2=alkyl group C1-C13, X=1-4, n=100-30,000

Polyhydroxyalkanoates (PHAs) are a family of linear polyesters that may divide into two groups based on the number of constituent carbon atoms in their monomer units – short-chain-length (SCL) PHAs and medium-chain-length (MCL) PHAs. The former consists of monomers with 3–5 carbon atoms and the latter contains monomers with 6–14 carbon atoms (Anderson et al., 1990).

PHAs can be synthesized by a wide variety of bacteria through the fermentation of sugars, lipids, alkanes, alkenes and alkanoic acids. Depending on the particular carbon source, different metabolism pathways can produce different hydroxy alkanale monomer. Details may be found in refs (Philip et al., 2007) (Fukui et al., 1997 and 1998) (Tsuge et al., 2000) (Huijberts et al., 1992).

PHASCL's are stiff and brittle with a high degree of crystallinity whereas PHAMCL's are flexible, have low crystallinity, tensile strength and melting point (Philip et al., 2007). The most common PHA biopolymer is PHB (polyhydroxybutyrate). PHB is often compared to polypropylene (PP) with regard to its physical properties because they have similar melting points, degree of crystallinity, and glass transition temperatures (Hakkarainen et al., 2002). Although PHB has many interesting properties, its inherent brittleness and low strength restrict its wider range of applications (Xing et al., 1998).

However, the introduction of different HA monomers such as 3-hydroxyvalerate (3HV) or 3-hydroxyhexanoate (3HHx) into the chain greatly improves the properties of PHB.

1.1.1.2 Biodegradable Synthetic Polymers from Petroleum Sources. Synthetic biodegradable polyesters are generally made by polycondensation methods with raw materials obtained from petrochemical feed stocks. Unlike other petrochemical-based resins that take centuries to degrade after disposal, these synthetic polyesters break down rapidly into carbon dioxide, water, and humus when they are exposed to the combined attack of water and microorganisms. Several examples are given below:

Poly (lactide-co-glycolide) (PLGA)

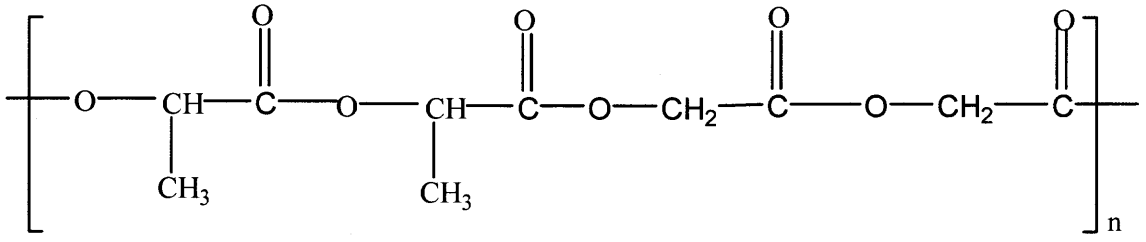

PLGA copolymers are prepared by ring opening polymerization of lactide (LA) and glycolide (GA) in the presence of stannous octoate as catalyst (Usuki et al., 1993) as shown in Figure 1.5.

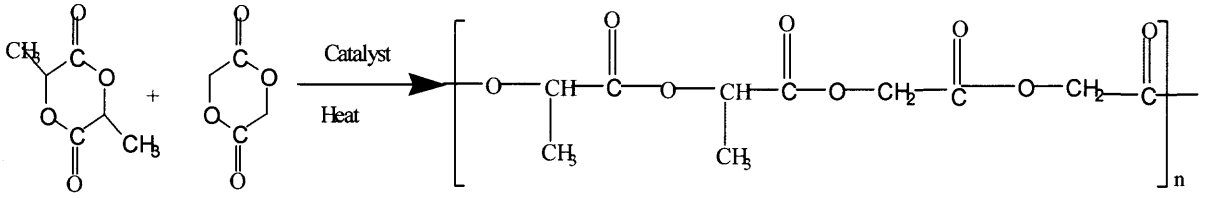

Figure 1.5 Synthesis of PLGA from lactic acid and glycolide.
(Porjazoska et al., 2002)

In general, glycolic acid-rich PLGA copolymers (up to 70%) are amorphous in nature and degrade quite rapidly. As the molecular weight of the polymer decreases,

hydrolytic degradation becomes faster because of the higher content of carboxylic groups at the end of the polymer chain which accelerates the acid-catalyzed degradation. The PLGA matrix undergoes random chain scission while preserving the original shape and mass until significant degradation (~ 90%) has occurred.

Poly(ε-caprolactone) (PCL)

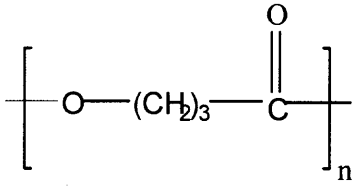

Poly(ε-caprolactone) is prepared by the ring-opening polymerization of the cyclic monomer ε-caprolactone. Catalysts such as stannous octoate are used and low molecular weights alcohols can be used as initiators which can also control the molecular weight of the polymer (Veld et al., 1997) (Storey et al., 1998) (Figure 1.6)

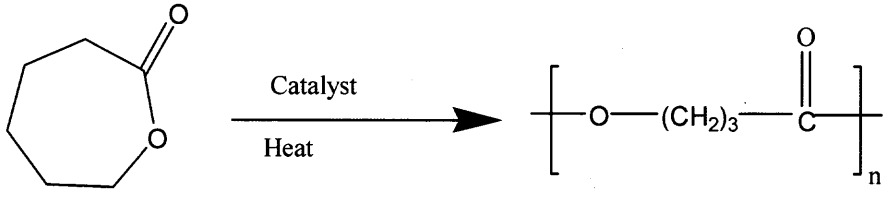

ε-caprolactone Poly (ε-caprolactone)

Figure 1.6 Synthesis of ε-caprolactone into Poly (ε-caprolactone).
(Veld et al., 1997)

Poly (ε-caprolactone) (PCL) is a biodegradable, semicrystalline polymer having a low melting temperature (~60°C). Due to its crystallinity and hydrophobicity, degradation of PCL is very slow, rendering it suitable for long-term drug delivery over a period of more than one year (Youan et al., 1999) (Sinha et al., 2004). It has the ability to form compatible blends with other polymers, which provides opportunities to manipulate the

drug release rate from microparticles (Sinha et al., 2004). The PCL-based devices maintain their shape and weight during the initial phase of biodegradation, where the molecular weight decreases by up to 5000 through bulk hydrolysis of the ester bonds. The second phase of PCL degradation is characterized by the onset of weight loss because the continuous chain cleavage produces a fragment small enough to diffuse out of the polymer matrix. On the other hand, the hydrolysis rate is known to decrease at the second phase, due to the increased crystallinity.

Poly (butylene succinate) (PBS)

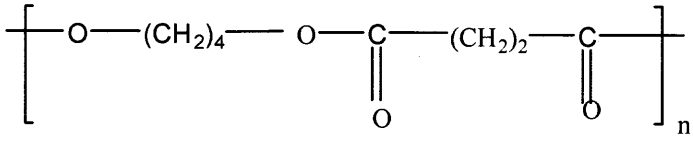

One of the most promising polymers in the family of synthetic biodegradable polyesters is PBS under the trade name of "BIONOLLE". It is chemically synthesized by the polycondensation of 1, 4-butanediol with succinic acid. (Bhari et al., 1998) (Doi et al., 1996). High molecular weight PBS is generally prepared by a coupling reaction of relatively low molecular weight PBS in the presence of hexamethylene diisocyanate (OCN-C_6H_{12}-NCO) as a chain extender (Yasuda et al., 1995). For obtaining high molecular weight polyesters by polycondensation, two methodologies have been adopted; i.e., one is the use of transition metal alkoxides having transesterification ability, and the other is the above chain extension reaction (Sirahama et al., 2001).

PBS has excellent processability, so it can be processed in the field of textiles into melt blown, multifilament, monofilament, flat, and split yarns and also in the field of plastics into injection molded products, thus being a promising polymer for various

potential applications (Fujimaki et al., 1998) (Mani et al., 2001). Main chain regularity is an important parameter for the polymer's ability to crystallize.

Polyanhydrides

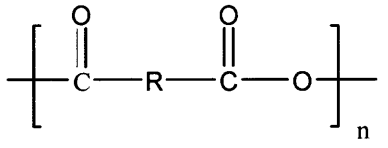

Polyanhydrides are synthesized via melt condensation of diacids/diacid esters, ROP of anhydrides, interfacial condensation, dehydrochlorination of diacids and diacid chlorides or by the reaction of diacyl chlorides with coupling agents such as phosgene or diphosgene. A variety of catalyst systems for polymerization have been identified, which enabled the synthesis of high molecular weight polyanhydrides. Both homo- and co-polyanhydrides having different properties have been developed by the melt condensation method (Nair et al., 2007). These classes are characterized by differences in crystallinity, melting point, solubility and ease of degradability (Vogel and Mallapragada, 2005).

Polyanhydrides are surface eroding polymers which do not allow water to penetrate into the material, eroding layer by layer. The hydrophobic backbone with hydrolytically labile anhydride linkages allows hydrolytic degradation to be controlled by manipulating the polymer composition (Nair et al., 2007).

Polyvinyl Alcohol (PVA)

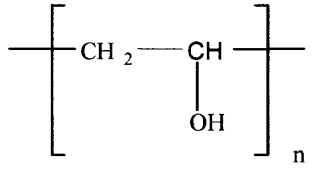

The primary raw material used in the manufacture of polyvinyl alcohol is vinyl acetate monomer. PVA is manufactured by the polymerization of vinyl acetate followed by

partial hydrolysis. The process of hydrolysis is based on the partial replacement of ester group in vinyl acetate with the hydroxyl group, and is completed in the presence of aqueous sodium hydroxide, following the gradual addition of the aqueous saponification agent. Polyvinyl alcohol is precipitated, washed and dried. The degree of hydrolysis is determined by the time point at which the saponification reaction is stopped. (Saxena, 2004)

PVA has a melting point of 230°C and 180–190°C for the fully hydrolysed and partially hydrolysed grades. It decomposes rapidly above 200°C as it can undergo pyrolysis at high temperatures. PVA is an atactic material but exhibits crystallinity as the hydroxyl groups are small enough to fit into the lattice without disrupting it.

1.1.2 Applications

Biopolymers that may be employed in packaging continue to receive more attention than those designated for any other application. For example, biodegradable plastic films may be employed as garbage bags, disposable cutlery and plates, food packaging, and shipping materials (Guan and Hanna, 2002). Biopolymer applications in the field of medicine are as involved as artificial organs (Mukhopadhyay, 2002). One example is artificial bone material which adheres and integrates onto bone in the human body. Another application for biopolymers is in the controlled release delivery of medications (Sakiyama and Hubbell, 2001). The bioactive material releases medication at a rate determined by its enzymatic degradation. PLA materials have been developed for medical devices such as resorbable screws, sutures, and pins. These materials reduce the risk of tissue reactions to the devices, shorten recovery times, and decrease the number of

doctor visits needed by patients. The automotive sector is responding to societal and governmental demands for environmental responsibility (Lammers and Kromer, 2002). Biobased cars are lighter, making them a more economical choice for consumers, as fuel costs are reduced. Natural fibers are substituted for glass fibers as reinforcement materials in plastic parts of automobiles and commercial vehicles. An additional advantage of using biodegradable polymer materials is that waste products may be composted. Natural fibers (from flax or hemp) are usually applied in formed interior parts. The components do not need load bearing capacities, but dimensional stability is important. There are a number of novel applications for biopolymers, which do not fit into any of the previous categories. One such example is the use of biopolymer systems to modify food textures. For example, biopolymer starch (gelatin-based) fat replacements possess fat-like characteristics of smooth, short plastic textures that remain highly viscous after melting. Research continues to focus on biopolymers that can be manipulated into food products at high pressure. The eventual goal is improved physical characteristics such as foaming, gelling, and water- or fat-binding abilities. Biopolymer materials are currently incorporated into adhesives, paints, engine lubricants, and construction materials (Ledward, 1998).

Biodegradable golf tees and fishing hooks have also been invented. The attraction of biopolymers in all of these areas is their derivation from renewable sources that slow the depletion of the global fossil fuel resources (Kolybaba et al., 2003).

1.2 Clay Reinforcements

The term "clay" firstly formalized in 1546 by Agricol, refers to a naturally occurring material composed primarily of fine-grained minerals, which is generally plastic at appropriate water contents and will harden when dried or fired. (Guggenheim and Martin, 1995).

Historically the term "clay" has referred to the small inorganic particles in diameter<2 μm of a soil fraction without regard to composition or crystallinity; the term clay minerals has referred to the specific phyllosilicates (the term for sheet silicate structures) that are layered, hydrous, magnesium or aluminum silicates in such a fraction (Auerbach et al., 2004). Layered structure clays are broadly classified into cationic and anionic. Cationic clays have negatively charged layers with cations in the inter layer. Structurally, anionic clays are the mirror images of the cationic clays and contain positively charged layers and anions in the layers.

1.2.1 Cationic Clays

The cationic clays are commonly in the same general family of 2:1 layered or phyllosilicates. Their crystal structure consists of layers composed of two silica tetrahedra fused to an edge-shared octahedral sheet of either aluminum or magnesium hydroxide. The layer thickness is ~1 nm and the lateral dimensions of these layers may vary from 30 nm to several microns or even larger, depending on the particular layered silicate. Stacking of the layers leads to a regular van der Waal's gap between them, called the interlayer or gallery. Isomorphic substitution within the layers (for example, Al^{3+} replaced by Mg^{2+} or by Fe^{2+}, or Mg^{2+} replaced by Li^{1+}) generates negative charges that

are counterbalanced by alkali and alkaline earth cations situated inside the galleries (see Figure 1.7). There are three main groups of clays: kaolinite-serpentine, illite, and smectite (Ray and Bousmina, 2005).

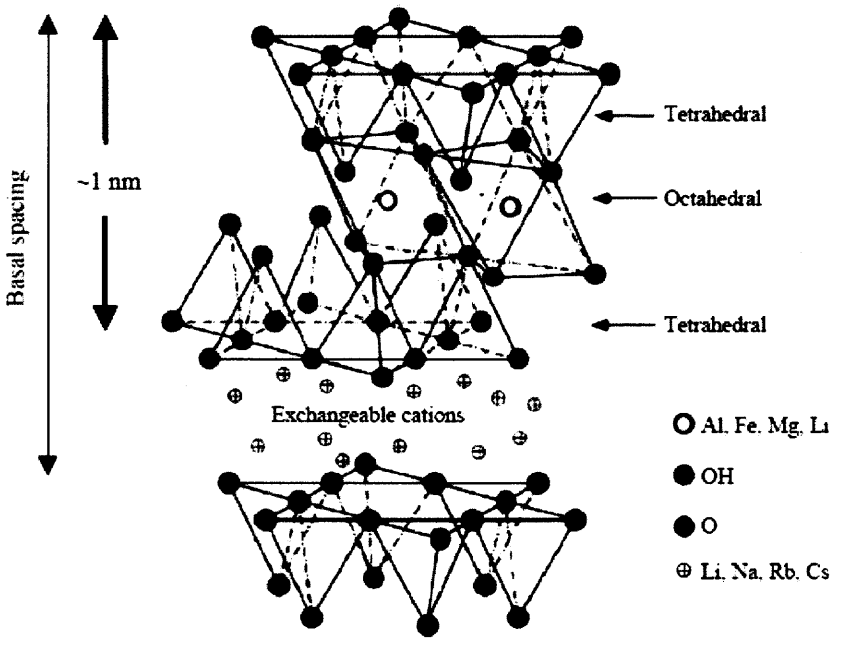

Figure 1.7 Structure of cationic clays.
(Ray and Bousmina, 2005)

Montmorillonite (MMT), a smectite cationic clay, may be used as a microfiller in various polymers. It is a very soft phyllosilicate clay. In such minerals the anionic charge of the aluminosilicate layer is neutralized by the intercalation of compensating, exchangeable cations (e.g., Na^+, Ca^{2+} and Mg^{2+}) and their coordinated water molecules (Kim et al., 2006). The particles are plate-shaped with an average diameter of approximately 1 μm (Ray and Bousmina, 2005). MMT-Na^+ is a natural montmorillonite with a chemical formula of $(Na,Ca)_{0.33}(Al,Mg)_2Si_4O_{10}(OH)_2 \cdot nH_2O$. When montmorillonite experiences high temperatures, such thermal treatment can affect properties such as strength, swelling and adsorption, and these are reflected in changes in

cation exchange capacity, pore structure, surface acidity and catalytic activity. For example, calcination of MMT-Na^+ at 500°C decreases its interlayer space and at 800°C its layer structure collapses. By calcination above 500°C, the MMT particle size and cation exchange capacity are reduced and its surface acidity and acid strength are increased by removing partial surface hydroxyl groups. Calcined MMT with highly porous fused structure is physically and chemically stable (Noyan et al., 2006) (Grimshaw et al., 1971) (Chorom and Rengasamy, 1996).

1.2.2 Anionic Clays

Layered double hydroxides (LDH), also known as anionic clays, can be structurally described as the stacking of positively charged layers with anions in the interlamellar space. The general formula of these materials is $[M(II)_{1-x}M(III)_x(OH)_2]^{X+}\ A^n{}_{x/n}\ mH_2O$, where M(II) is a divalent cation (Mg^{2+} and/or Ni^{2+}, Zn^{2+} ,Co^{2-}), M(III) is a trivalent cation (Al^{3+} and/or Fe^{3+} ,Ga^{3+} ,Cr^{3+}) and A is an anion with charge n (HO^-, CO_3^{2-} ,NO^{3-} , Cl^-, SO_4^{2-}) (Figure 1.8)

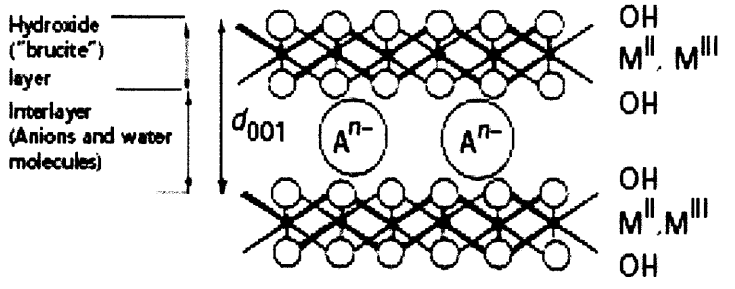

Figure 1.8 Interlayer of anionic clays.
(Erickson et al., 2004)

In contrast to smectites, hydrotalcites (HT) are referred to as anionic clays with a two layer structure (Erickson et al., 2004), similar to that of brucite ($Mg(OH)_2$), where

each Mg^{2+} ion is octahedrally surrounded by six OH^- ions and the different octahedra share edges to form infinite sheets. The sheets are stacked one on top of the other and are held together by weak interactions through hydrogen bonding. If some Mg^{2+} ions are replaced isomorphously by cations with higher charge, but similar radius, the brucite-type sheets become positively charged and the electrical neutrality is maintained by the interlayers composed of anions and water molecules. Usually, HT exchange capacities vary in the range 200–470 mequiv/100 g and are higher than the corresponding cation exchange capacity (CEC) of silicate clays like MMT-Na^+ (exchange capacity 80–145 mequiv/100 g) (Column et al., 2002). A typical chemical formula of hydrotalcite is $Mg_4A_{l2}(OH)_{12}CO_3.3H_2O$ (Mg/Al ratio 4.0/5.0) (Ray et al., 2003). Usually, the calcination process removes the interlayer water, interlayer anions and the hydroxyls of hydrotalcite to produce a mixture of metal oxides; the layer structure and crystallinity of hydrotalcite is destroyed at 500°C. The most interesting properties of the metal oxides obtained by calcination are: 1) High surface area. 2) Basic properties. 3) Stability to thermal treatment, 4) "Memory effect" (Cavani et al., 1991) leading to regeneration of the structure by exposure in suitable aqueous media.

1.3 Biopolymer-Clay Composites

Micrometer or nanometer scale fillers in organic–inorganic composites, called micro- or nanocomposites, respectively, have attracted the interest of many researchers since they may lead to high performance materials at a lower cost. Polymer layered silicate (PLS) nanocomposites were reported in the patent literature as early as 1950 (Carter et al., 1950). However, it was not until Toyota researchers began a detailed examination of

polymer layered silicate clay mineral composites that nanocomposites became more widely studied in academic, government and industrial laboratories (Usuki et al., 1995). Various nano reinforcements currently being developed are nanoclays (layered silicates), cellulose nanowhiskers, ultra fine layered titanate and carbon nanotubes. Of particular interest are polymer and organically modified layered silicate (OMLS) nanocomposites because of their demonstrated significant enhancement, relative to an unmodified polymer resin, of a large number of physical properties, including barrier, flammability resistance, thermal and environmental stability, solvent uptake and rate of biodegradability of biodegradable polymers (Sinha and Okamoto, 2003).

Intercalation of polymers in layered silicates has proven to be a successful approach to synthesize polymer nanocomposites. These polymers containing polar groups capable of associative interactions, such as Lewis-acid/base interactions or hydrogen bonding, lead to intercalation. The greater the polarizability or hydrophilicity of the polymer, the more favorable the interactions should be between the clay and the polymer (Vaia and Giannelis, 1997).

However, it is difficult for nonpolar polymers to penetrate into the gallery of the clay due to lack of compatibility. To render the layered silicates compatible with some biodegradable polymer matrices, one must convert the normally hydrophilic silicate surface to an organophilic one, to facilitate intercalation. Generally, this can be done by ion-exchange reactions with cationic surfactants including primary, secondary, tertiary, and quaternary alkylammonium or alkylphosphonium cations. Such cations lower the surface energy of the inorganic host, improve the wetting characteristics of the polymer matrix, and result in a larger interlayer spacing. Additionally, the alkylammonium or

alkylphosphonium cations can provide functional groups that can react with the polymer matrix, or in some cases initiate the polymerization of monomers to improve adhesion between the inorganic and the polymer matrix (Blumstein, 1965) (Messersmith and Giammelis, 1995). Preparation methods of nanocomposites are divided into three main groups:

1. Intercalation of polymer and pre-polymer from solution

This is based on a solvent system in which the polymer or pre-polymer is soluble and the silicate layers are swellable. The layered silicate is first swollen in a solvent, such as water, chloroform, or toluene. When the polymer and clay solution/suspension are mixed, the polymer chains intercalate and displace the solvent within the interlayers of the silicate. Upon solvent removal, the intercalated structure remains, resulting in polymer/layered silicate nanocomposite (Ray and Bousmina, 2005).

2. In situ intercalative polymerization

In this method, the layered silicate is swollen within the liquid monomer or a monomer solution so polymer formation can occur between the intercalated sheets. Polymerization can be initiated either by heat or radiation, by the diffusion of a suitable initiator, or by an organic initiator or catalyst fixed through cation exchange inside the interlayer before the swelling step (Ray and Bousmina, 2005).

3. Melt intercalation technique

Recently, the melt intercalation technique has become the standard for the preparation of PLS-nanocomposites. This process involves melting a mixture of the polymer and OMLS above the softening point of the polymer, statically or under shear. During melt blending, the polymer chains diffuse into the galleries between the silicate layers. A range of

nanocomposites with structures from intercalated to exfoliated can be obtained, depending on the degree of penetration of the polymer chains. A schematic illustration of this terminology is shown in Figure 1.9 (Dennis et al. 2001) and explained below:

MMT can be delaminated and dispersed into individual layers of only 10 Å thicknesses. Unseparated MMT layers, after introduction into the polymer, are often referred to as tactoids (Lan et al. 1995 and 1966). The term intercalation describes the case where a small amount of polymer moves into the gallery spacing between the clay platelets, but causes less than 20-30 Å separation between the platelets. Exfoliation or delamination occurs when polymer further separates the clay platelets, e.g., by 80-100 Å or more. A well-delaminated and dispersed nanocomposite consists of delaminated platelets distributed homogeneously in the polymer.

Usually, the degree of delamination and dispersion of layered silicated nanocomposites by melt compounding is affected by the clay chemical treatment, the type of extruder and its screw design as well as processing conditions. Compared to single extruder, the twin screw extruders yielded the best delamination and dispersion. It is believed that excellent delamination and dispersion can be achieved by extruders when a fully optimized screw configuration is used. Examples of the importance of clay chemical treatment and processing conditions on clay dispersion are as follows:

Organic modification of the clay is required to overcome the cohesive forces between neighboring platelets so that polymer intercalation and platelet exfoliation can occur during melt processing. For example, Fornes et al. (2002) mentioned three distinct surfactant structural effects on the extent of exfoliation for nanocomposites based on a high molecular weight polyamide: (1) One long alkyl tail on the ammonium ion rather

than two, (2) methyl groups on the amine rather than 2-hydroxy-ethyl groups, and (3) an equivalent amount of amine surfactant on the clay as opposed to an excess amount. Similar trends, but lower extent of exfoliation, were seen for a low molecular weight grade polymer. It was proposed that alkyl ammonium ions that cover a larger percentage of the silicate surface, shield desirable polar polyamide–polar clay interactions and ultimately lead to less platelet exfoliation. Also, the higher molecular weight polyamide consistently led to better exfoliation and greater reinforcement than lower molecular weight polyamides (Fornes et al., 2001 and 2002).

With respect to processing conditions, increasing the mean residence time in the extruder generally improves the delamination and dispersion. However, there appears to be an optimum extent of back mixing, as judged by the broadness of the residence time distribution and an optimum shear intensity; excessive shear intensity apparently causes poorer delamination and dispersion. Shear intensity is required to start the dispersion process, by shearing particles apart into tactoids or intercalants. Residence time in a low shearing or mildly shearing environment is required to allow polymer to enter the clay galleries and peel the platelets apart (Dennis et al., 2001).

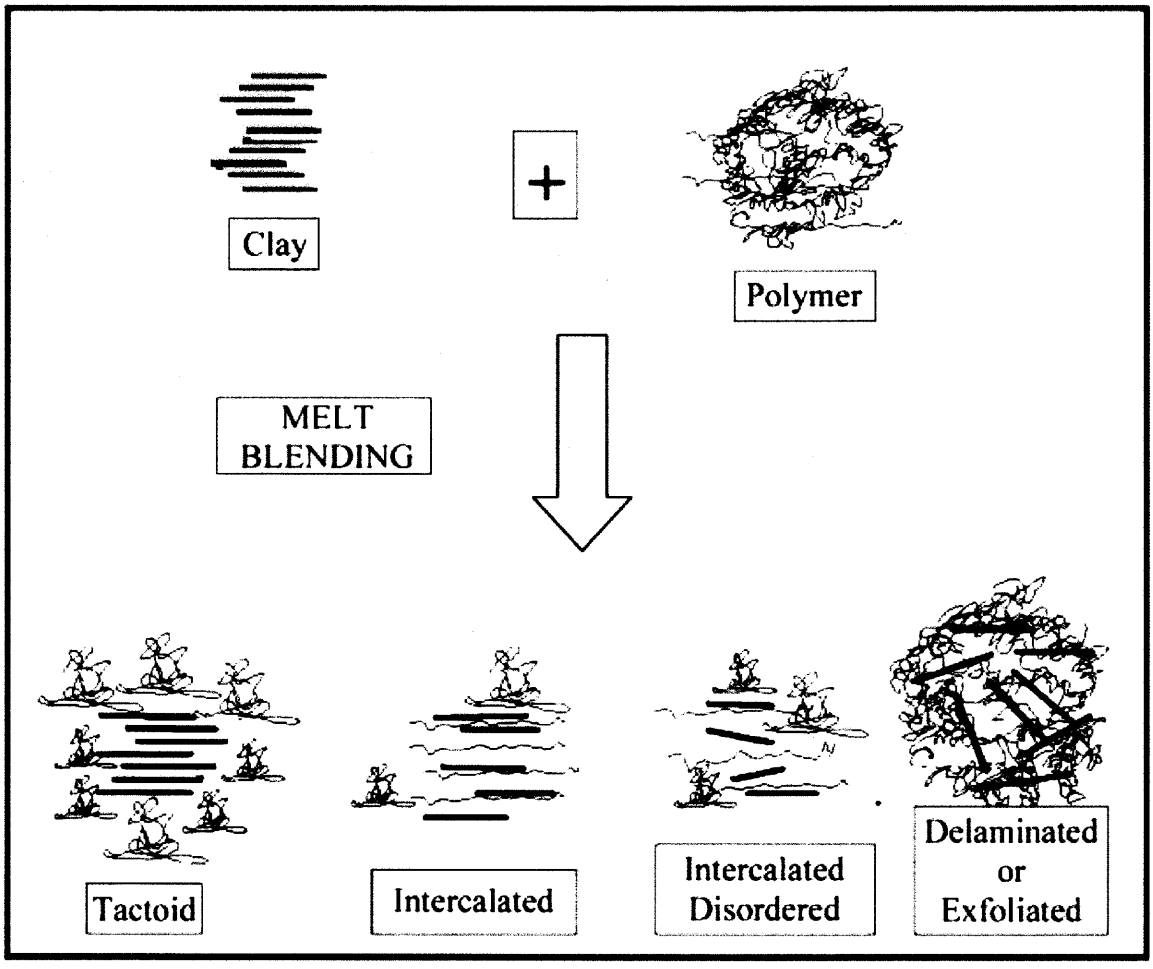

Figure 1.9 Schematic illustration of terminology used to describe nanocomposites formed from organoclays.
(Dennis et al., 2001)

CHAPTER 2

DEGRADATION OF ALIPHATIC POLYESTERS

Degradation is generally looked upon as a deleterious process. In general, to degrade a substance is to impair it in respect to some physical property or to reduce its complexity. (Reich et al., 1971). Polymer degradation could be classified into thermal degradation, oxidative degradation, radiative degradation, mechanical degradation, chemical degradation, biological degradation, hydrolytic degradation and so on. Since hydrolytic and thermal degradation (including thermal oxidative degradation) are major degradation routes for aliphatic polyesters, their mechanisms are reviewed in this chapter.

2.1 Thermal Degradation

Thermal degradation of polymers can be defined as 'molecular deterioration as a result of overheating' (Reich et al., 1971). At high temperatures the components of the long chain backbone of the polymer can begin to separate (molecular scission) and react with another molecule to change the polymer properties.

Several factors can affect the thermal stability of polymers: (1) Additives: water, catalysts and oxygen (2) Polymer morphology: crystallinity and amorphicity. (3) Polymer chain structure: backbone rigidity, branched versus linear structures, crosslinking effects, weak links and end groups, presence of reactive groups. (4) Energy factors affecting: intramolecular forces and intermolecular forces. (5) Some other factors; sample size, sample impurities, molecular weight and molecular weight distribution, temperature and oxygen concentration (Reich et al., 1971).

2.1.1 Mechanism

Research work on the mechanism of thermal degradation of PLA can be summarized as follows: (1) Intra- and intermolecular ester exchange, which leads to the appearance of lactide and cyclic oligomers, is the dominant reaction pathway (Wachsen et al., 1997) (Fan et al., 2003). (2) The cis-elimination for polyesters, which results in small amount (<5%) of acrylic acid and acrylic oligomers, is occurring, but is not at all a dominant reaction even at high pyrolysis temperatures (Kopinke et al., 1996 and 1997). (3) Unzipping depolymerization (backbiting degradation) is also observed. The lower the molecular weight, the more concentrated are the terminal hydroxyl groups, which accelerate the unzipping depolymerization and the intermolecular ester exchange (Liu et al., 2006). (4) Pyrolytic elimination of poly(lactic acid) results in species containing conjugated double bonds due to the carbonyl group (Wang et al., 2008)

Jamshidi et al (1988) suggested that the main thermal degradation of polylactides under nitrogen from 160°C to 240°C is as shown in Figure 2.1; they also considered that oxidative degradation seems unlikely to play an important role in this temperature range.

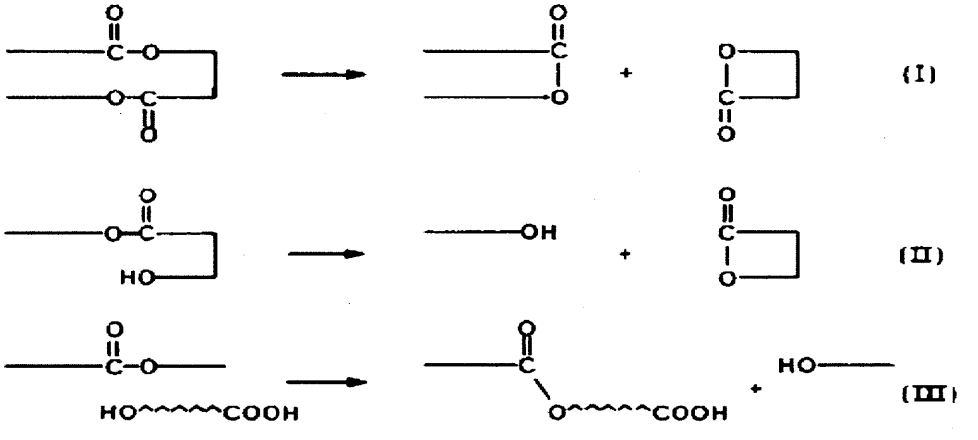

Figure 2.1 Thermal degradation mechanism for PLA (I).
(Jamshidi et al., 1988)

Reaction I, resulting in the formation of monomer and cyclic oligomers, is catalyzed by the residual polymerization catalyst. Reactions II and III are brought about by the terminal hydroxyl groups of the same chain or of monomeric and oligomeric acids produced by eventual hydrolysis of their precursors since PLA may easily to absorb water. Reactions I and II lead to the production of low MW compounds which will evaporate at high temperatures. Therefore, a reduction in weight of the polymer should be easily observed. On the other hand, the random scission nature of reaction III suggests that a sharp drop in MW will occur. Removal of the low MW compounds, as well as the polymerization catalyst in reaction I, will most likely suppress these degradation reactions.

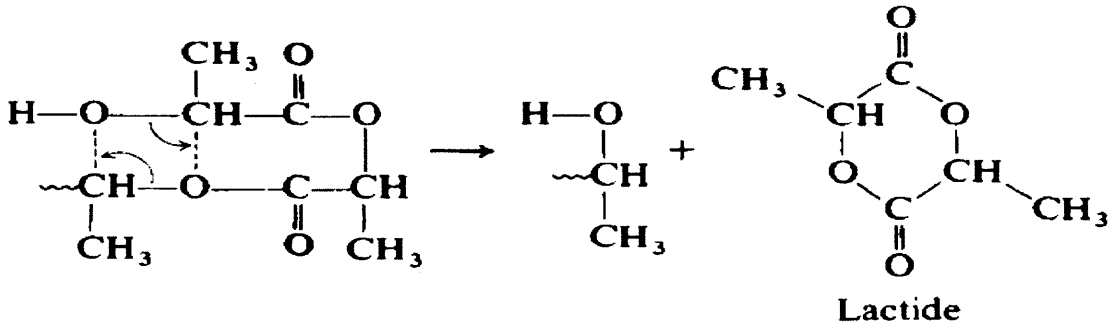

(a)

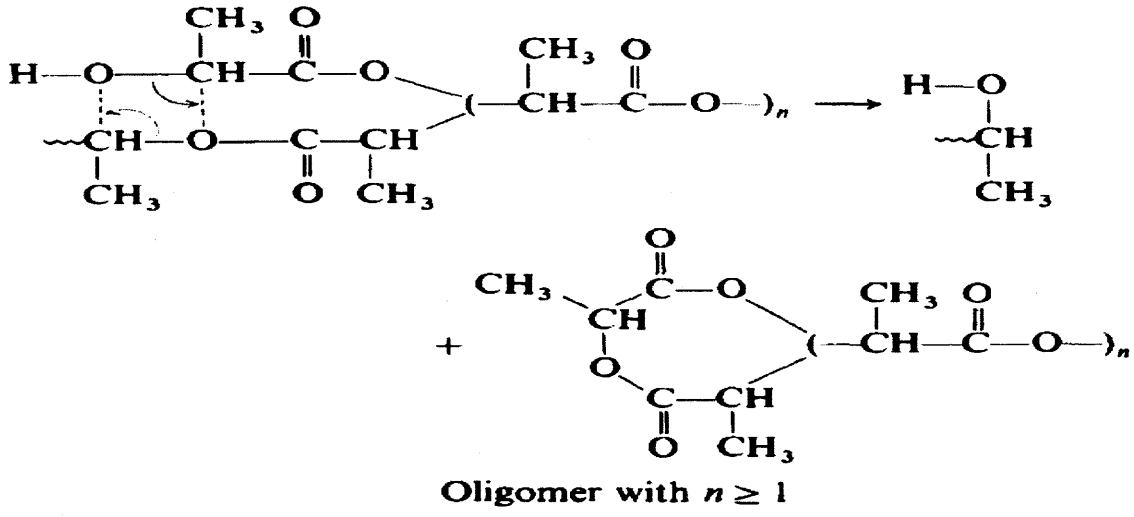

(b)

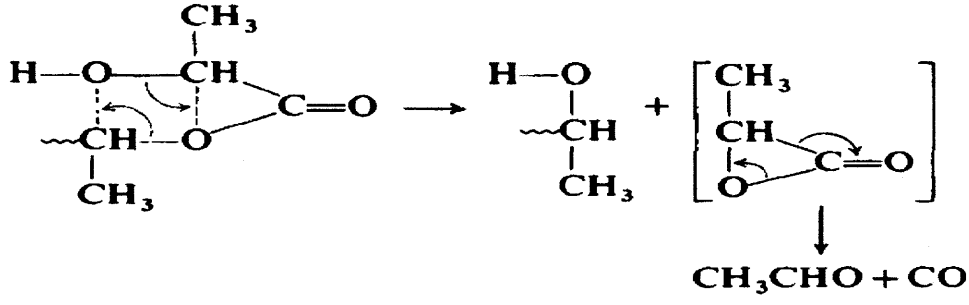

(c)

Figure 2.2 Thermal degradation mechanism for PLA (II).
(McNeill and Leiper, 1985)

McNeill & Leiper (1985) proposed that the main thermal degradation process in polylactide is a non-radical, backbiting ester interchange reaction involving the OH chain ends, proceeding with comparatively low activation energy at all temperatures in the range studied (230-440°C) under vacuum because of the ease of formation of the transition state involved. Depending upon the site in the backbone at which this reaction occurs, the product can be a lactide molecule (Figure 2.2 (a)), an oligomeric ring with more than two repeat units (Figure 2.2(b)), or acetaldehyde plus carbon monoxide (Figure 2.2 (c)). Reaction (Figure 2.2(c)) accounts for the appearance of these two volatile products at lower temperatures than the other volatile materials, which can result only by homolysis of the chain. These reactions do not occur to any significant extent, however, until temperatures in excess of 270°C are reached.

Arraiza et al. (2007) proposed an additional degradation mechanism of PLLA consisting of the carbon-oxygen bond breakage to obtain an acid functionality and an unsaturated ester (Figure 2.3).

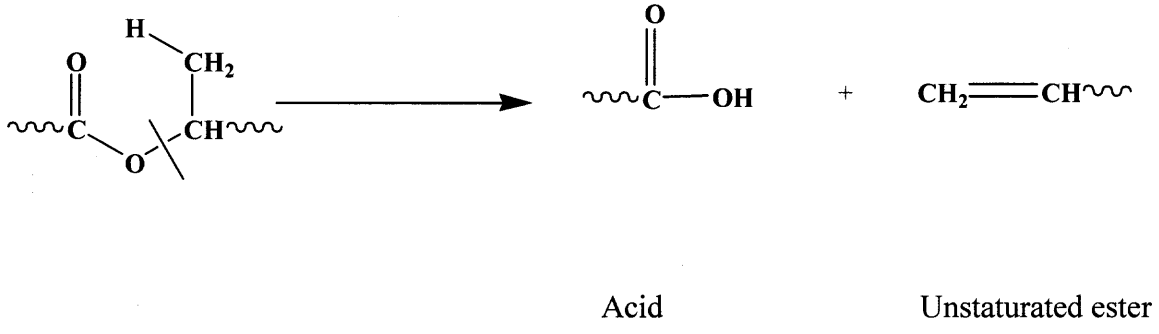

Figure 2.3 Thermal degradation mechanism for PLA (III).
(Arraiza et al., 2007)

2.1.2 Kinetics

The simplest possible degradation occurs when a polymer sample formed by random polymerization is subjected to non-specific degradation, so that bonds are broken at random. Tanford (1961) gave the kinetics of thermal degradation based on the statistics of random scission.as equation 2.1

$$\frac{1}{X_t} - \frac{1}{X_0} = kt \qquad (2.1)$$

where

X_t = the number-average degree of polymerization at any time

X_0 = the number-average degree of polymerization before degradation

k = thermal degradation rate constant

t = thermal degradation time

2.2 Hydrolytic Degradation

Hydrolysis is a type of "Solvolysis", i.e., cleavage of C-X bonds by water. The degradation of semi-crystalline aliphatic polyester matrices is more complicated than for amorphous ones. It was reported by Fischer et al. (1973) that hydrolytic degradation occurs in two stages. In the first stage, water diffuses into the amorphous regions resulting in random hydrolytic scission of ester bonds. The degree of crystallinity can even increase as degradation proceeds. The second stage starts when most of the amorphous regions have been degraded. The hydrolytic attack then progresses from the edge towards the center of crystalline domains. A retardation in degradation has been observed during the degradation of intrinsically amorphous aliphatic polyesters by the

formation of a crystalline phase of an oligomeric stereocomplex as intermediate. This intermediate stereocomplex is highly resistant to hydrolysis (Vert et al. 1994).

Certain factors can affect the extent of hydrolysis, e.g., film thickness, morphology, relative humidity, concentration of acid catalyst, dielectric constant of the polymer, autocatalysis by functional groups within the polymer, molecular orientation without formation of crystallinity, type and number of ionizable or functional groups, electrostatic and steric effects, adsorption of water on the polymer, and chain conformation (Reich et al., 1971). The presence of a crystalline phase, the T_g of the amorphous phase as well as the hydrophobicity also affect the degradation rate (Jong et al., 2001).

It should be mentioned here that there are some conflicting views of the effect of some of the above parameters. For example, there are conflicting reports on the effect of crystallinity and glass transition temperature on the degradation. Although most researchers believe that an increase in polymer crystallinity will reduce polymer degradation, still other researchers (Tsuji and Ikada, 2000) (Chye et al., 2005) (Hurrell et al., 2002) reported an accelerating degradation with increasing polymer crystallinity. It is well known that higher temperature accelerates the degradation process. However, only very limited reports of the T_g effect on polymer degradation are available. Weir et al. (2004) studied the accelerated degradation of PLLA with increasing temperature and suggested that above or below the PLA T_g degradation proceeded by the same mechanism. However, Agrawal et al. (1997) found that the activation energies for the degradation reaction at temperatures below and above T_g were distinctly different for

PLGA. Thus, they recommended that tests performed at T > T_g should not be used to predict degradation behavior at T < T_g .

2.2.1 Mechanism

Hydrolytic degradation studies can be conducted under neutral, acidic, or alkaline conditions. Generally, neutral and acidic hydrolyses are similar, whereas alkaline hydrolysis can be quite different. Most hydrolytic studies are heterogeneous, though in most neutral and acid hydrolyses the reaction within the polymer network is homogeneous. Hydrolytic studies may be conducted on polymers in the bulk phase (generally as films) over a wide range of pH. Hydrolytic degradation can involve main-chain scission because of functional inter units in condensation polymers and /or side groups.

2.2.1.1 Neutral and Acid Hydrolysis. At pH ≤ 7, hydrolysis is initiated by a protonation process which is followed by the addition of H_2O and the cleavage of the ester linkage. This is illustrated in a simplified manner by the following reactions (Schnabel, 1981) (Figure 2.4).

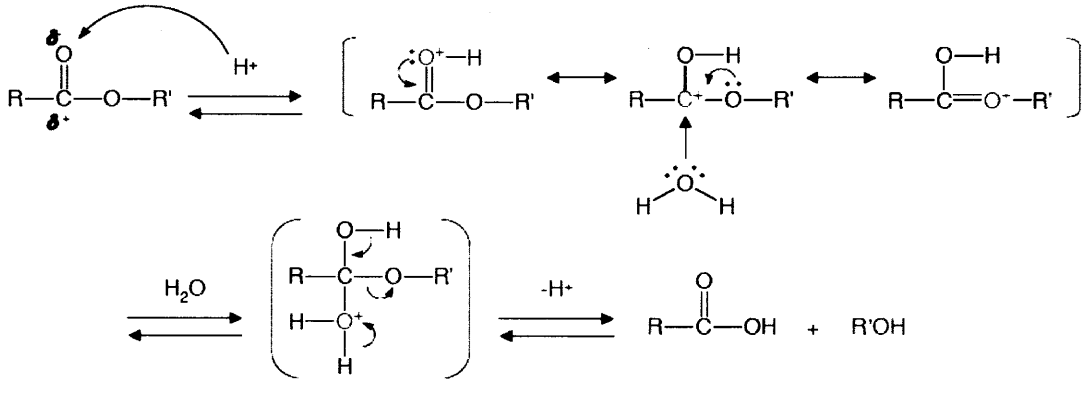

Figure 2.4. Hydrolytic degradation mechanism at pH ≤ 7.
(Albertsson and Karlsson, 1994)

In the acid hydrolysis of polyesters, it was found that the rate increased rapidly since acid acts as a catalyst. In general, the acid produced during hydrolysis moves with difficulty to the aqueous phase; it rather stays in the polymer itself assuming that, the polymer has a low dielectric constant. Furthermore, it was found that the hydrolysis rate can increase as the reaction proceeds, which is due to the autocatalytic effect of the formed carboxyl acid groups. (Reich et al., 1971)

2.2.1.2 Alkaline Hydrolysis. In alkaline media, hydroxyl ions are attached to the carbonyl carbons. Subsequently ester linkages are ruptured, as illustrated by the following reactions: (Schnabel, 1981) (Figure 2.5)

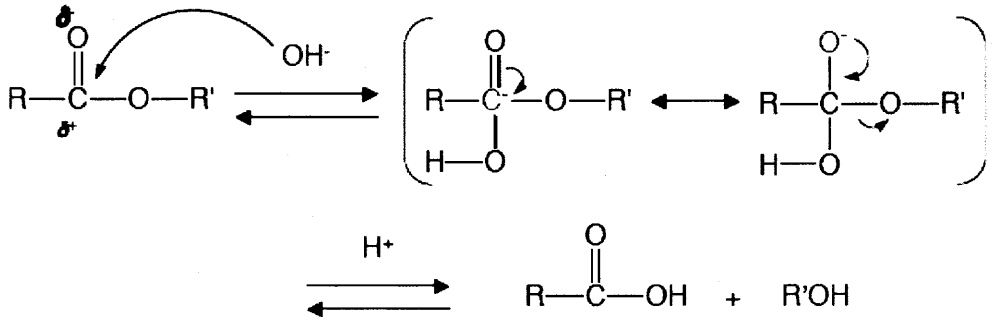

Figure 2.5 Hydrolytic degradation mechanism at alkaline conditions.
(Albertsson and Karlsson, 1994)

In the alkaline hydrolysis, the reaction is heterogeneous with respect to the polymer, and not homogeneous as in neutral or acidic hydrolysis. The alkaline attack is primarily a surface reaction resulting in weight loss as some oligomers are removed into the solution. This was explained on the basis that perhaps the OH^- ions cannot penetrate the polymer structure because of the lower dielectric constant of the polymer, and that the

resulting carboxylate ions might be repelling the attacking hydroxyl ion (Reich et al., 1971).

In the alkaline hydrolysis of a simple ester, the absence of acid catalysis is offset by a stronger nucleophilic reagent, OH^- instead of H_2O. Alkaline and acidic hydrolysis involve cleavage of the bond between the oxygen and acyl group, forming alcohol and acid salt in the former and acid in the latter (Reich et al., 1971).

According to Shih (1995), base-catalyzed hydrolysis of polyesters proceeds by a random scission mechanism whereas in acid-catalyzed hydrolysis of PLA, chain-end scission is faster. Belbella et al. (1996) came to the opposite conclusion: a sequential cleavage from the chain end in alkaline medium and random scission at acidic pH values.

2.2.1.3 Types of Degradation. To classify degradable polymers a distinction is made between surface (or heterogeneous) and bulk (or homogeneous) eroding materials, as shown in Figure. 2.6

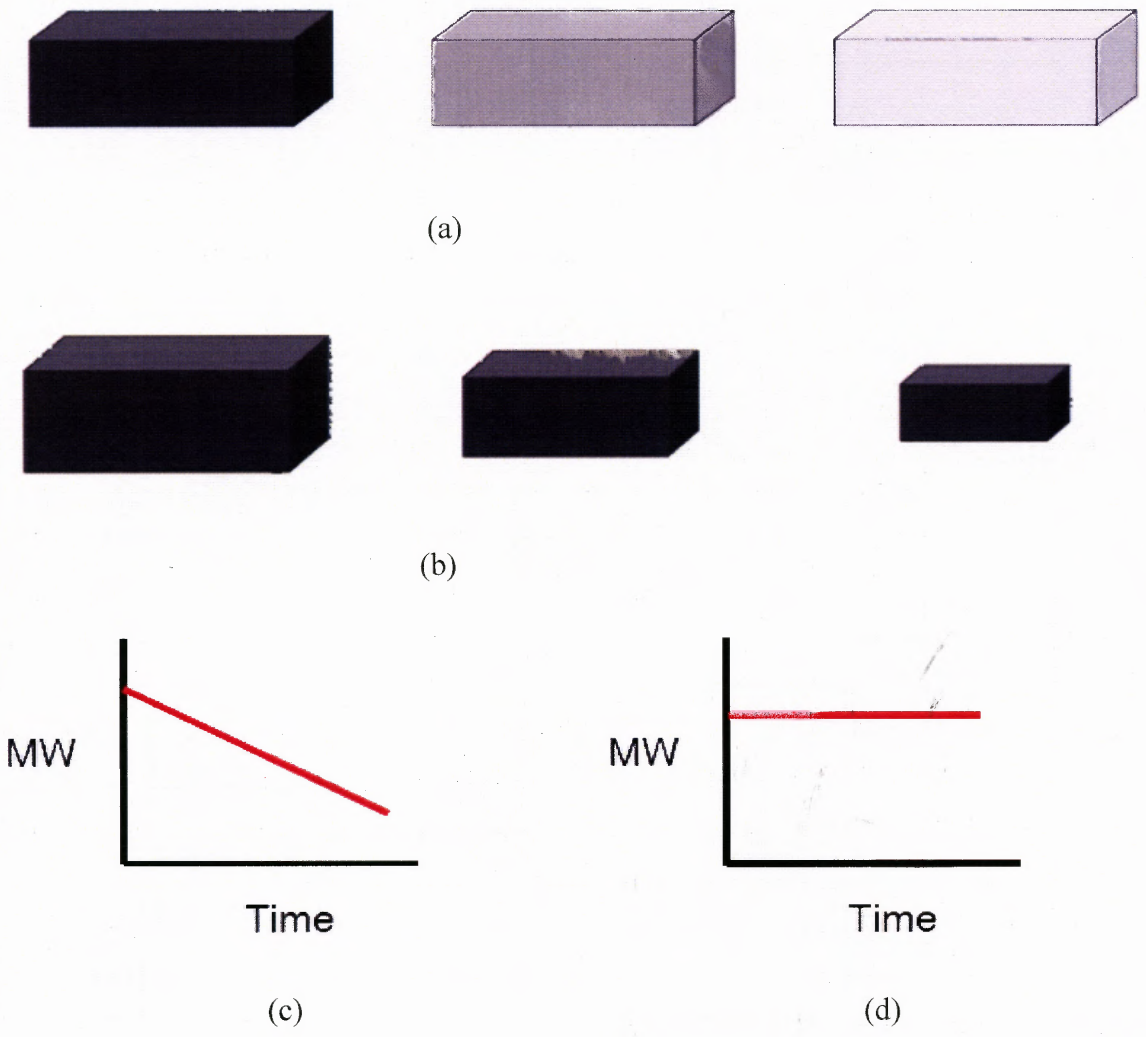

Figure 2.6 (a) Bulk Degradation; (b) Surface Degradation; (c) Molecular Weight Change vs Time for bulk degradation; (d) Molecular Weight Change vs time for surface degradation.
(Albertsson and Karlsson, 1994)

In homogeneous or bulk degradation, hydrolysis occurs simultaneously throughout the entire specimen. Hence, the decrease in molecular weight, the reduction in mechanical properties, and the loss of mass also occur throughout the entire specimen at

the same pace. Polymers containing ester, ether, and amide groups, such as poly(lactic acid) (PLA), poly(glycolic acid), poly(α-caprolactone), polyamide, proteins, and cellulose (and its derivatives), generally exhibit this type of degradation (Pitt et al., 1981). These reactions can sometimes be catalyzed by the polymers' own hydrolysis products. In heterogeneous or surface degradation, hydrolysis mainly occurs in the region near the surface, whereas the bulk material is only slightly or not at all hydrolyzed. As the surface is eroded and removed, the hydrolysis front marches through the material core. This leads to a moving boundary or surface. The rate of boundary movement is very often nearly constant (Heller et al., 2002). Polymers such as poly(ortho ester)s (POEs), PAHs, and some polycarbonates tend to undergo surface degradation. Pure surface or bulk degradation are ideal cases that most polymers do not follow. Assuming that the polymer degradation velocity is uniform inside a polymer matrix, one can hypothesize that two major processes have an impact on the degradation kinetics: (Göpferch and Tessmar, 2002).

1. the diffusion of water into the polymer bulk,
2. the degradation rate of the polymer backbone.

If the diffusion of water into the polymer is faster than the degradation of the polymer bonds, the polymer will undergo bulk degradation, because degradation is not confined to the polymer surface. If, however, the degradation of the polymer bonds is faster than the diffusion of water, it will be consumed by the hydrolysis of bonds on the polymer surface and will thus be prevented from diffusion into the bulk. Degradation processes are then strictly confined to the matrix surface resulting to the ideal case of a surface eroding polymer (Partini, 2006).

2.2.2 Kinetics

It is generally accepted that the hydrolysis of most polyesters, proceeds according to the reaction shown in Figure 2.7. (Chye et al., 2005)

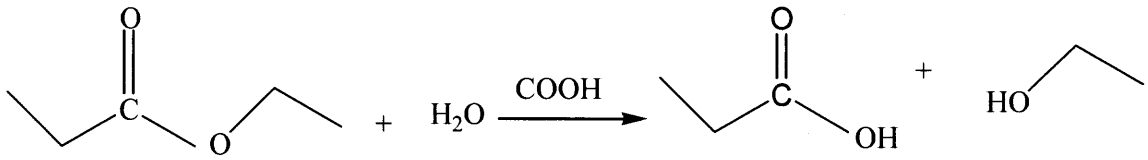

Figure 2.7 Hydrolysis of ester bonds in biodegradable polyesters.
(Chye et al., 2005)

Neglecting the contribution of uncatalyzed hydrolysis, the rate of chain scission of an aliphatic polyester autocatalyzed by the generated carboxylic acid end groups is given by equation (2.2)

$$\frac{d[COOH]}{dt} = k_1[COOH][ester][H_2O] \tag{2.2}$$

This equation assumes that the carboxylic acid group is not ionized in the hydrophobic polymer bulk and functions by hydrogen bonding to the ester links. For a small number of chain scissions, the ester concentration as well as the water concentration can be considered constant, and equation (2.2) simplifies to equation (2.3)

$$\frac{d[COOH]}{dt} = k_2[COOH] \tag{2.3}$$

where $k_2 = k_1[ester][H_2O]$ (2.4)

Integration results in

$$\frac{[COOH]}{[COOH]_0} = \exp(k_2 t) \tag{2.5}$$

where [COOH] and $[COOH]_0$ are the carboxylic end group concentrations at times t and zero, respectively. This expression will hold until loss of oligomers reduces the carboxylic acid end group concentration in the polymer bulk. Provided that

$$[COOH] = 1/\overline{M_n} \quad , \tag{2.6}$$

where $\overline{M_n}$ is the number average molecular weight

Equation (2.5) can be rewritten as

$$\overline{M_{nt}} = \overline{M_{n0}} \exp(-k_2 t) \tag{2.7}$$

if changes in the form and width of the molecular weight distribution can be neglected. Substitution of the Mark-Houwink equation (2.8)

$$IV = [\eta] = B(\overline{M_v})^{\nu} \tag{2.8}$$

into equation (2.7) leads to equation (2.9),

$$\ln(\frac{IV}{IV_0}) = -k_2^* t \tag{2.9}$$

where, $k_2^* = \nu k_2$

and the values of B and ν, the Mark-Houwink parameters, are respectively, 5.45 x 10^{-4} and 0.73 for PLLA and 2.21 x 10^{-4} and 0.77 for PDLLA (Hyon et al., 1997). Derivation of equation 2.9 is based on the assumption that the value of the viscosity average molecular weight, $\overline{M_v}$, is closer to that of the weight average molecular weight, $\overline{M_w}$ which in turn is proportional to $\overline{M_n}$. As will be shown below, IV ratios were used to calculate the hydrolytic degradation constants.

If the hydrolysis of the ester linkage is not autocatalytic, chain cleavage will be following equation (equation 2.10):

$$\frac{d[COOH]}{dt} = k_3[ester][H_2O] \quad (2.10)$$

Provided the degree of polymerization is high, the concentration terms in equation (2.10) may be treated as constants during the initial stage of hydrolysis, and integration leads to equation 2.11 (Pitt et al., 1987).

$[COOH] - [COOH]_0 = k_3 [ester][H_2O]$, and (2.11)

$$\frac{1}{M_{nt}} = \frac{1}{M_{no}} + k_3 t \quad (2.12)$$

Based on the different assumptions used to derive the autocatalyzed first-order reactions (equations 2.2 and 2.7) and the non-autocatalyzed zero-order reactions (equations 2.10 and 2.12) a higher degradation rate constant would correspond to equation (2.7) compared to equation (2.12) for the same material and at same degradation conditions.

2.3. Degradation of Aliphatic Polyester Composites - A Review

This section consists of two parts referring to the hydrolytic and thermal degradation, respectively, of aliphatic polyester composites containing cationic and anionic clays.

2.3.1 Thermal Degradation

Nanocomposites based on layered silicate clays and biodegradable polylactide matrices have already been extensively studied in terms of mechanical, fire retardancy or gas permeability behaviors. Although much more work has been reported on their thermal stability, most methods focus on measuring weight loss by TGA. Examples of recent

related work on nanocomposites based on various aliphatic polyesters, including PLA, are given below:

Pluta et al. (2002) investigated the thermal stability of PLA nanocomposites (modified MMT at 3%) and microcomposites (MMT- Na^+ at 3%) and compared them with unfilled PLA by TGA under helium and oxygen respectively. All samples were obtained through melt blending and quench processing. Under both gases, MMT-Na^+ did not significantly affect the polymer thermal degradation. Compared with unfilled PLA and its microcomposites, the thermal stability for the nanocomposite significantly increased under thermooxidative conditions.

Paul et al. (2003) studied the thermal properties of nanocomposites obtained by direct melt blending of polyethylene glycol plasticized poly(L-lactide) filled with different types of MMTs, organo-modified (Cloisite 25A, Cloisite 20A and Cloisite30B) and unmodified (Cloisite Na^+). An increase of the thermal stability of the polymer matrix was observed under air when filled with 3% fillers. Depending on the nature of the different modifiers, this effect was more or less pronounced, the greater thermal stability improvement triggered by Cloisite 30B. They also studied the influence of different modified clay (Cloisite 30B) contents on the polymer thermal stability. An increase in thermal stability with increasing content was observed by TGA, with a maximum obtained for a clay loading of 5 wt%. Further increase of the filler content, resulted in a decrease in thermal stability.

Marras et al. (2007) prepared nano- and micro-composites of PLLA with various loadings of natural and hexadecylamine modified MMT by solvent casting. TGA analysis under air and nitrogen revealed that the introduction of a small amount of organo-

modified silicate in the polymer matrix significantly improve its thermal stability and the nanocomposites displayed a better thermal stability compared to microcomposites and pure polymer, especially in oxidative atmosphere

Chang et al (2003) prepared hexadecylamine–montmorillonite (C_{16}–MMT), dodecyltrimethyl ammonium bromide–montmorillonite (DTA-MMT), and Cloisite 25A PLA nanocomposites by solution casting. The TGAs of the hybrids were carried out at a heating rate of 20 °C/min under N_2 flow. When C_{16}–MMT and Cloisite 25A hybrids were compared with pure PLA, the thermal stability decreased linearly with an increasing amount of organoclay from 2 to 8 wt %. In the hybrid with DTA–MMT, temperature at a 2% weight loss had nearly constant values, regardless of the clay loading.

Other authors (Lepoittevin et al., 2002) (Chrissafis et al., 2007) reported on the thermal degradation of PCL containing a variety of micro and nanofillers. Chrissafis et al. (2007) showed by TGA under nitrogen that organo modified MMT and nanosilica accelerated the decomposition of PCL. However, unmodified monmorillonite and multi-walled carbon nanotubes inhibited the thermal degradation of PCL. The activation energies of all the prepared samples were estimated using the Ozawa, Flynn and Wall (OFW) and Friedman methods. It was verified that neat PCL degrades by two consecutive mechanisms: the first one corresponding to small mass loss and the second to the main decomposition mechanism. Nanoparticles did not affect the decomposition mechanism

Malinconico et al (2007) succeeded in incorporating a hydrotalcite-like solid constituted of magnesium-aluminum hydroxide layers into a chemically modified PCL that was chemically modified by grafting maleic anhydride and a second unsaturated

comonomer such as glycidyl methacrylate (GMA). The presence of LDH lowered the decomposition temperature of the composite compared to pure PCL. By increasing the inorganic content, a further decrease of the decomposition temperature was observed.

It appears that, at least for PLA, organomodified MMT enhances thermal stability under oxidative conditions acting as a heat barrier. There are conflicting reports on the effect of unmodified MMT and hydrotalcites on the polymer thermal stability. Still, few reports on PLA/clay thermal stability kinetics and modeling as well as molecular weight change under isothermal degradation condition are found, particularly as related to: a) the comparison of cationic clay vs anionic clays, b) the comparison of calcined vs noncalcined clays c) the effects of polymer crystallinity, and d) the effect of different processing temperatures.

2.3.2 Hydrolytic Degradation

Often an unfavorable hydrolytic degradation rate will limit the PLA applications. Considerable efforts have been made to control the hydrolytic degradation rate (usually accelerate) so that PLA can have wider biomedical or ecological applications without a compromise of the product properties prior to the onset of degradation. Degradation rates can be controlled by blending PLA with additives, plasticizers and often micro- or nanofillers

Ray et al (2003) and Paul et al. (2005) widely studied the biodegradation and hydrolytic degradation of PLA/organoclay nanocomposites and PLA/microcomposites respectively.

In the work of Ray et al. (2003) on biodegradation by composting at 58°C four factors were examined: 1) initial degree of polymer crystallinity, 2) presence of terminal hydroxylated edge groups of the clay, 3) dispersion of the intercalated modified clay in the matrix, 4) initial molecular weight, MW, of polymer. The authors showed that biodegradation of the nanocomposites took place more rapidly than that of the unfilled PLA.

Paul et al. (2005) reported the controlled hydrolytic degradation (phosphate buffer solution (PBS), pH 7.4, 37 °C), of micro- and nanocomposites based on an amorphous polylactide and three different types of unmodified and organomodified MMTs. Composites were prepared by melt blending PLA with 3 wt% of unmodified MMT (Cloisite Na^{+}) or modified MMTs (Cloisite 25A and Cloisite 30B), respectively. The authors concluded that the relative hydrophilicity of the clay plays a determining role in the hydrolytic degradation process with more hydrophilic fillers, promoting faster degradation.

Wu et al. (2006) prepared nanocomposites by solution mixing PLA with a MMT organoclay, which was first treated with n-hexadecyl trimethylammonium cations and then with a biocompatible/biodegradable chitosan in an aqueous solution containing 1wt% of lactic acid to improve the chemical affinity between PLA and MMT. Degradation carried out in PBS at pH 7.2 showed that the reaction rates for the nanocomposites were slower than that of the unfilled matrix. Also, the crystallinity of the unfilled PLA and that of the PLA in the nanocomposites increased after 7 weeks degradation.

Maiti et al. (2003) reported the biodegradation of melt mixed polyhydroxybutyrate (PHB) composites containing MMT treated with an octadecylammonium salt, or fluoromica treated with a dimethyl ditallow ammonium salt. The experiments were performed on sheets covered with compost manure at 60°C and 90% humidity in a closed chamber by following weight loss. In the PHB/MMT composites, the degradation level was initially higher than that of the pure PHB probably because of the presence of Al Lewis acid sites, which would catalyze the hydrolysis of the ester linkages. Fluoromica contains Mg and as a result the biodegradation paralleled that of unfilled PHB. Interestingly, after 4.5 weeks the rates for both PHB/MMT and PHB/fluoromica were much slower than that of the unfilled PHB, apparently due to the enhanced barrier properties of the nanocomposites.

He et al. (2004) reported the hydrolytic degradation of poly (lactic-co-glycolic acid) (PLGA) modified with 5% of either of two additives: a surfactant and an organoclay, Cloisite 30B. The major component of this surfactant is a polyethylene oxide/polypropylene oxide tri-block polymer. Hydrolytic degradation experiments carried out by following weight loss in pH 7.3 buffer solutions showed that both modifiers can increase the degradation rate of PLGA.

Ratto et al. (1999) reported a series of polycaprolactone (PCL)/clay nanocomposites prepared by either *in situ* polymerization or by twin screw extrusion. Biodegradation of films in soil was investigated by a respirometric method, which measures polymer mineralization representing polymeric carbon converted to CO_2. Weight loss experiments in a marine environment were carried out in laboratory flasks at

22°C and aquarium incubations of continuously flowing seawater. Experimental results showed that in all cases the clay promotes biodegradation.

Lee et al (2002) investigated the biodegradability of aliphatic copolyester (APES)/clay hybrids. Thin films were buried in activated soil at 60°C and relative humidity of 60 ± 5%. Compared to pure APES, the lower biodegradability of APES nanocomposites may originate from the presence of dispersed silicate layers with large aspect ratio, which forces the microorganisms diffusing in the bulk of the film to follow more tortuous paths.

Chouzouri and Xanthos (2003) studied composites produced by solution mixing of a biodegradable thermoplastic polyester based on butylene adipate / succinate, as well as a commercial polylactic acid, with surface coated and uncoated hydrotalcite inorganic minerals. Materials were also melt-mixed in a twin screw extruder for comparison. They found that the significant structural and morphological differences depend on the materials and the processing methods. Biodegradability and biocompatibility were evaluated by performing tests "in vitro" in the presence of a phosphate buffered saline solution.

In their subsequent report (2004), two types of these synthetic magnesium/aluminum carbonate/hydroxide minerals, at 30wt% filler level, were mixed with poly(L-lactic acid): surface coated and uncoated. Polymer composites showed significant differences in structure and morphology through the addition of the filler. The composites were exposed to a phosphate buffer saline solution, at 37°C, to study the "in vitro" degradation of the polymer, and also to simulated physiological solution to detect

bioactivity by the formation of an apatite type structure layer. They found that these novel composites could have a potential use in tissue engineering applications.

Tammaro et al. (2007) studied Poly(ε-caprolactone) (PCL)/modified Mg-Al hydrotalcite nanocomposites prepared by solution mixing. Different amounts of the fillers were incorporated in PCL and processed as films of 0.15mm thickness. Their mechanical properties were better than those of the pristine polymer. The release process of antibiotic molecules was found to be promising for tuneable drug delivery. The total release time was linearly dependent on the nanofiller loaded in the polymer, and it was much higher than the time needed for complete release of the drug directly incorporated into the polymer.

Layered silicate fillers can accelerate polymer biodegradation acting catalytically, or can suppress biodegradation due to the enhanced barrier properties of the nanocomposites. Still, our present knowledge of the hydrolytic degradation (a major element of the biodegradation process) of PLA/ layered silicates, is relatively limited, particularly as related to: a) the comparison of organoclays vs the unmodified clay, b) the comparison of organoclays containing different modifiers, c) the effects of polymer crystallinity, and d) the effect of increasing temperature of the degradation medium.

Also, few studies on the hydrolytic degradation (a major element of the biodegradation process) of PLA/clay composites were found in the literature, particularly as related to: a) the comparison of cationic vs anionic clays and b) the comparison of calcined vs. non calcined clays.

CHAPTER 3

OBJECTIVES

There are two major objectives in this research related to the hydrolytic and thermal degradation of PLA composites.

As mentioned in Section 2.3.1, no consistent conclusions are available on the effects of unmodified MMT and hydrotalcites on the polymer thermal stability. It is important to point out that reports on PLA/clay thermal stability kinetics and modeling can not be found in the literature. Also, no published articles report molecular weight changes under isothermal degradation conditions, which are important to control final material properties, particularly as related to: a) the comparison of cationic vs anionic clays, b) the comparison of calcined vs noncalcined clays c) the effects of polymer crystallinity, and d) the effect of different processing temperatures.

Therefore, the objective of the thermal degradation research is to report on the effects of micro- and nanofillers with different modifiers on the kinetics of the thermal degradation of PLA composites based on amorphous and semicrystalline polymers and the effects of cationic clay and anionic clays as well as their calcination products on the kinetics of the thermal degradation, and modeling of the thermal degradation of PLA and its composites. Consideration is given to the effect of testing at elevated temperatures, near or above the polymer processing temperature, on the isothermal degradation mechanism followed by molecular weight changes.

Hydrolytic degradation is a major element of biodegradation. However, our present knowledge of the hydrolytic degradation of PLA/ layered silicates, is relatively limited, particularly as related to: a) the comparison of organoclays vs the unmodified

clay, b) the comparison of organoclays containing different modifiers, c) the comparison of cationic vs anionic clays and d) the comparison of calcined vs. non calcined clays. e) the effects of polymer crystallinity, and f) the effect of increasing temperature of the degradation medium.

Thus, the objective of the hydrolytic degradation research is to report on the effects of micro- and nanofillers with different modifiers on the kinetics of the hydrolytic degradation of PLA resins having different crystallinity, the effects of cationic and anionic clays as well as their calcination products and model the degradation at different temperatures. Consideration is given to the effect of testing at elevated temperatures, near or above the polymer glass transition temperature, on the autocatalytic heterogeneous degradation mechanism.

CHAPTER 4

EXPERIMENTAL

4.1 Materials

4.1.1 Polymers

Two commercial polylactic acid grades and their 50:50 blend were chosen and used in this research. Both are biodegradable and can be processed as conventional thermoplastic polyesters. They are as follows:

PLLA: PLLA is a semicrystalline polymer from Biomer (Biomer L9000) with T_g of about 60° C and a T_m of about 160° C as reported by the manufacture.

PDLLA: PDLLA (amorphous) obtained from NatureWorks LLC (PLA Polymer 4060D) was reported to have a T_g of 58°C and no T_m. The resin is in a form of clear pellets and starts becoming tacky at 45°C.

PLAB: A polymer blend, PLAB was made by melt mixing PLLA and PDLLA at 1:1wt. ratio in a Brabender mixer at 180°C and 50 rpm for 12 minutes under nitrogen.

4.1.2 Clays

Four different cationic and three anionic clays were used in this work.

4.1.2.1 Cationic Clays. Three clays were obtained from Southern Clay Products directly and a fourth was produced by calcination in our laboratory. They are as follows:

- Cloisite ® Na^+ ($MMT\text{-}Na^+$) is a natural montmorillonite with a chemical formula of $(Na,Ca)_{0.33}(Al,Mg)_2Si_4O_{10}(OH)_2 \cdot nH_2O$ (Figure 4.1). It is typically formed as a weathering product of low silica rocks. Manufacturer's data are shown in Table 4.1.

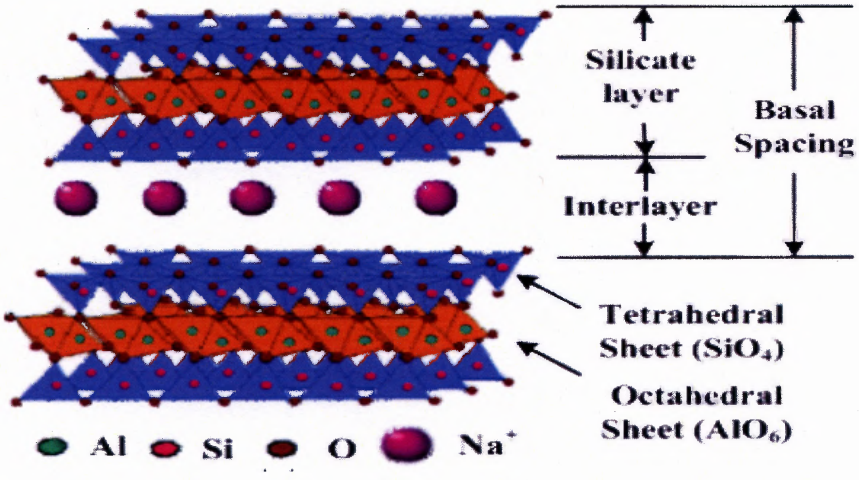

Figure 4.1 Montmorillonite (MMT-Na^+) Structure.
(Kim et al., 2006)

- Cloisite® 30B (30B) is a natural montmorillonite (Cloisite® Na^+) modified with a quaternary ammonium salt (Figure 4.2). Cloisite® 30B is used as an additive for plastics to improve various physical properties. Manufacturer's data are shown in Table 4.1

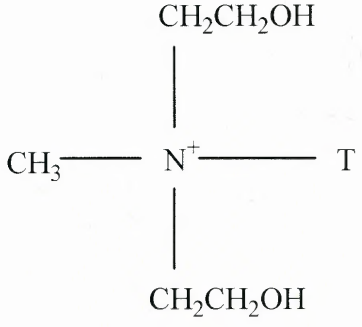

Figure 4.2 Chemical structure of the modifier for Cloisite® 30B. MT2EtOH: methyl, tallow, bis-2-hydroxyethyl, quaternary ammonium. Where T is Tallow (~65% C18; ~30% C16; ~5% C14) and the anion is Chloride

- Cloisite® 15A (15A) is a natural montmorillonite (Cloisite ® Na^+) modified with a quaternary ammonium salt (Figure 4.3). Cloisite® 15A is also used as an additive for plastics to improve various plastic physical properties. Manufacturer's data are shown in Table 4.1.

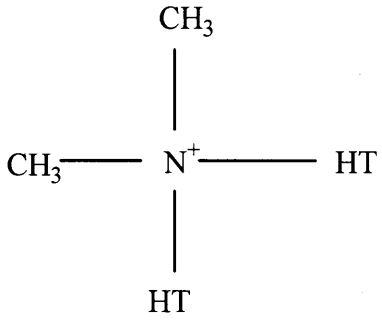

Figure 4.3 Chemical structure of the modifier for Cloisite® 15A. 2MT2HT: dimethyl, dehydrogenated tallow, quaternary ammonium. Where HT is dehydrogenated Tallow (~65% C18; ~30% C16; ~5% C14) and the anion is chloride

- MMT-Na^+(C) was made through calcination of MMT-Na^+ to remove water and partially remove surface hydroxyl groups. The calcination was carried out in a furnace (3031 SOLA BASIC LINDBERG) at 500 °C for 2 hours under air. The partial or complete removal of surface hydroxyls was expected to provide a corresponding decrease in the interlayer space and surface activity. Its pH value is about 10~11.

Table 4.1 Properties of Cationic MMT Clays [1]

	Closite® Na^+	Closite® 30B	Closite® 15A
Organic Modifier	None	MT2EtOH [2]	2MT2HT[3]
Modifier Concentration	None	90meq/100gclay	125meq/100gclay
% Moisture	4-9	≤2	≤2
% Weight Loss on ignition	7	30	43
Density, g/cc	2.66	1.98	1.66
Bulk Density, lbs/ft^3			
Loose	12.45	14.25	10.79
Packed	20.95	22.71	18.64
X-Ray Results, d_{001}, Å	11.7	18.5	31.5
Particle Size, μm			
10% less than	2	2	2
50% less than	6	6	6
90% less than	13	13	13
pH value (4)	9~10	8.1~8.6	7.2~7.6

(1) Manufacture's Data
(2) MT2EtOH: methyl, tallow, bis-2-hydroxyethyl, quaternary ammonium
(3) 2M2HT: dimethyl, dehydrogenated tallow, quaternary ammonium
(4) Measured in our laboratories

4.1.2.2 Anionic Clays. One commercial anionic clay was obtained from Doobon Yubwa, C. Ltd, S. Korea directly and a third one was made by calcination. They are as follows:

- Hydrotalcite (HT) (trade name CLC-120) is a synthetic aluminum-magnesium-hydroxycarbonate, belonging to the group of layered double hydroxides. The ratio of Mg/Al in the hydrotalcite used is 4.0~5.0. Properties and characteristics of the hydrotalcites are listed in Table 4.2 and Figure 4.4.

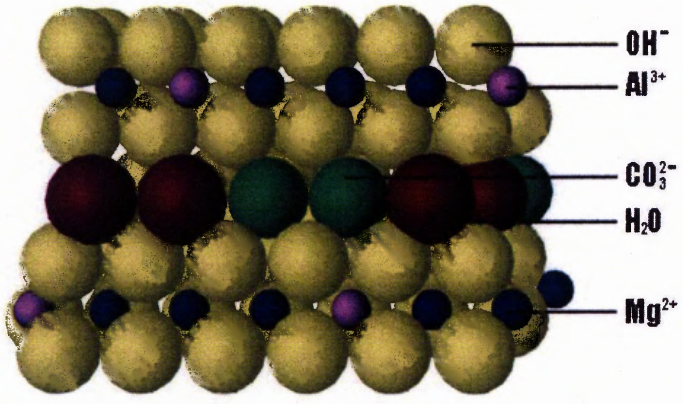

Figure 4.4 Molecular structure of hydrotalcite (HT) platelet.
(Gopakumar et al., 2006)

Table 4.2 Properties and Characteristics of Hydrotalcite

Designation	**Chemical Structure**	**Form**	**Supplier**	**Trade Name**	**Measured pH in Water**
HT	$Mg_4Al_2(OH)_{12}CO_3.3H_2O$	White Powder (Average Particle Size of 0.4~0.5μm)	Doobon Yubwa., Co.Ltd, S.Korea	CLC-120	8.51-8.99 (1wt%~ 10wt%)

- Calcined Hydrotalcite (HT(C)) was made by calcination of HT to partially remove hydroxyl and carbonate groups. During this process the layer structure is destroyed (Figure 4.5). The calcination was carried out in a furnace (3031 SOLA BASIC LINDBERG) at 500 °C for 2 hours under air. Firstly, the interlayer water is released at 150–250 °C. Then by heating at 350–600 °C, the hydroxyl and carbonate groups are simultaneously transformed into water and carbon dioxide, respectively. The layered crystal structure of hydrotalcite collapses to form a predominantly amorphous mixture of Mg and Al oxides. (Kovanda et al., 1999) The measured pH value of the calcination products is about 10~11

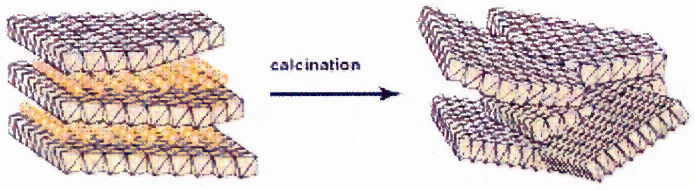

Figure 4.5 Hydrotalcite structure before and after calcination.
(Tichit et al., 2003)

4.2 Sample Preparation

Predried polymer pellets (12 hours, 40°C under vacuum) were first dry mixed with 5wt% predried clays (4 hours, 100°C under vacuum), and compounded in a Brabender counter-rotating batch mixer at 50 rpm for 12 min under nitrogen at a processing temperature of 180°C. Unfilled PLLA, PDLLA and PLAB polymers were also processed as controls at the same conditions. The melt mixed compounds were cut into small chips, pressed into 0.5mm thick films under about 45 kN force for one min. at 190°C and then cooled down. In order to eliminate air bubbles, the chips were preheated at 190 °C for 40 seconds before applying force. Two 4x4 cm^2 or 3x4 cm^2 specimens were cut from each film for duplicate hydrolytic degradation experiments. Annealing of the unfilled PLLA and its composites was carried out at 100°C for 90 min followed by slow cooling to room temperature.

4.3 Thermal Degradation

Four 1.5x 1.5 cm^2 specimens for each polymer or polymer composite were cut from each film. Each specimen was then placed in a glass vial and the uncovered vial was placed in an oven under air at 180°C or 200°C. At predetermined times, a specimen was removed from the oven and the intrinsic viscosity of the polymer was measured (see section 4.5.6) after removal of the filler by filtration.

4.4 Hydrolytic Degradation

Two preweighted 4x4 cm^2 or 3x4 cm^2 specimens were placed in a jar containing 100 ml of a NaOH solution at pH 10.5. The jars were placed in an oven set at the degradation temperature (50°C, 60°C or 70°C). At predetermined immersion periods, a specimen was removed from the solution and rinsed several times with distilled water. At the same time, the pH value of the solution was measured with a pH meter. The residual water was wiped off from the sample surface. One smaller 1x4 cm^2 piece was cut from each specimen. The smaller sample was weighed after wiping off the surface water (W_w). These small samples were then placed in a vacuum oven under reduced pressure at room temperature for one week and then weighed again (W_d).

$$\text{Water Uptake} = \frac{W_w - W_d}{W_d} * 100\% \qquad (4.1)$$

4.5 Characterization

4.5.1 Dynamic Differential Scanning Calorimetry (DSC)

Glass transition (T_g), melting (T_m), crystallization (T_c) and cold crystallization (T_{cc}) temperatures were determined by differential scanning calorimetry (DSC) (DSC Q100 TA Instruments). Heating and cooling rates were 10° C/min at predetermined temperature range under nitrogen flow (40 cm^3/min). Values were recorded during the first and second heating scans and during the cooling scan. All test samples were 0.5mm thick films.

4.5.2 Dynamic Thermogravimetric Analysis TGA

Thermogravimetric analysis (TGA) was performed using a TGA Q50 thermogravimetric analyzer (TA Instruments). The kinetics experiments were performed at heating ramps of 10°C/min, 20 °C/min, 30°C/min and 40°C/min under air or nitrogen flow (60 cm^3/min) from room temperature to 500 °C. Initial sample weight was set as 10~13 mg with thickness 0.5 mm for each operation.

4.5.3 Wide-angle X-ray diffraction (XRD)

Wide-angle X-ray diffraction (WAXD) analyses were performed for different types of pure clay powders and corresponding polymer composites on Philips PW3040 diffractometer (Cu Ka radiation wavelength λ=0.154 nm), operated at 45 kV/40 mA. Samples were scanned in a fixed time mode with a counting time of 2 s under diffraction angle 2θ in the range of 2°–10°.

4.5.4 Scanning Electron Microscopy (SEM)

Morphology of the samples was observed by a scanning electron microscope (SEM) (LEO Field Emission Gun Digital SEM) at 2kV of working voltage. The unfilled polymers and polymer composites samples were prepared by fracturing at liquid nitrogen temperature. The pure clay particles were also characterized by SEM.

4.5.5 Energy Dispersive X-ray Analysis (EDX)

In order to quantitatively analyze the filler dispersion in the polymer, Energy Dispersive X-ray Analysis (EDX) (2400 Perkin-Elmer CHN Elemental Mapping), was used to determine the concentration of some elements present in the fillers and their dispersion in the polymers. By selecting characteristic elemental peaks mapping is possible by analyzing the sample point by point. The working voltage was 8kV and the mapping time was 1100 seconds for the MMT polymer composites and 1500 seconds for the HT polymer composites.

4.5.6 Intrinsic Viscosity

The intrinsic viscosities (*IV*) $[\eta]$ of the polymers, either neat or present in the polymer composites after removing the filler or impurities by using disposable Teflon filters, were measured in an Ubbelohde viscometer at 25°C in chloroform by a single point measurement in an approximately 1% polymer solution. The following equation was used:

$$[\eta]=\frac{\sqrt{2(\eta_{sp}-\ln\eta_r)}}{c} \qquad (4.2)$$

where η_r is relative viscosity, $\eta_{sp} = \eta_r - 1$ is specific viscosity and c is polymer solution concentration (Solomon et al., 1962). The intrinsic viscosity of each polymer sample was measured three times and the results were within +/- 0.01 dl/g. A duplicate sample was also measured three times and the average of six determinations was the reported final intrinsic viscosity of the material. Intrinsic viscosity can be related to viscosity molecular weight ($\overline{M_v}$) through equation (2.8).

4.5.7 Melt Flow Index (MFI)

The melt flow index (MFI) was measured in a Tinius-Olsen plastometer at 190°C and 2.16kg load for all unfilled polymers and polymer composites. The final MFI value was based on an average value of three samples.

CHAPTER 5

RESULTS AND DISCUSSION

5.1 Dispersion of Fillers in Polymer Matrix

5.1.1 Cationic Micro- and Nanofillers

The type of filler dispersion in the polymer matrix was determined by WAXD. The diffraction pattern of the MMT-Na^+ clay powder shows a weak peak around $2\theta = 6.5°$, corresponding to a basal spacing of 12.1 Å which is close to the manufacturer's data of 11.7 Å. This peak is not evident in the melt mixed PLLA/MMT-Na^+ composites possibly because of the low filler loading (5 wt%) (Figure 5.1(a)); note that a weak peak was evident when 10wt% MMT-Na^+ was added in the PDLLA matrix in other experiments (not reported here). Thus, PLLA/MMT-Na^+ composites can be considered as microcomposites in which the lamellae have not been fully separated, in agreement with data by Paul et al. (2005). The mean interlayer spacing for the MMT-Na^+(C) powder is 9.68Å corresponding to $2\theta = 9.13°$ (Figure 5.1 (a)). The reduction in the interlayer spacing is due to water removal (Grimshaw, 1971). In the case of PLLA/MMT-Na^+(C) and PDLLA/MMT-Na^+(C), small shifted weak peaks are observed at $2\theta=9.5°$ (interlayer spacing of 9.3 Å Figure 5.1(a)) corresponding to their microcomposites. EDX will be used to further identify their microcomposite structures.

The mean interlayer spacing for the 30B powder organoclay is 18.22 Å corresponding to $2\theta = 4.85°$ (Figure 5.1 (b)) which is very close to the manufacturer's data (18.5 Å). In the case of PLLA/30B, a shifted small peak is observed at $2\theta = 2.66°$ (interlayer spacing of 31.18 Å) (Figure 5.1(b)), corresponding to a mixture of exfoliated and intercalated silicate layers dispersed in the PLLA matrix. Thus, PLLA containing

5 wt% 30B may be considered as a nanocomposite. The PDLLA/30B sample in Figure 5.1(b) is also a nanocomposite showing a slightly stronger peak at 2.88°, corresponding to an increase in the number of intercalated silicate layers (less exfoliation) dispersed in the amorphous PDLLA matrix. This may be due to the higher melt viscosities of the PLLA vs. PDLLA leading to higher shear forces during melt mixing, known to be beneficial for the exfoliation process (Loyens et al., 2005) (Zhu and Xanthos, 2004). The mean interlayer spacing for the 15A powder is 31.82Å at $2\theta = 2.77°$ (Figure 5.1 (c)) which is close the manufacturer's data (31.5 Å). In the case of PLLA/15A, no significant peak shift was observed (Figure 5.1(c)). By contrast, a slight shift and a stronger peak is observed at $2\theta = 2.88°$ (30.68 Å) for PDLLA/15A (Figure 5.1 (c)) suggesting a more intercalated structure. Thus, both PLLA/15A and PDLLA/15A may be considered as nanocomposites with higher degree of intercalation than the equivalent 30B composites. This is in agreement with the conclusions of Lee et al. (2003).

Further morphological analyses by SEM and EDX were carried out to determine the extent of the clay dispersion. By mapping the silicon distribution in the PDLLA, it can be shown that the overall clay particle distribution is much finer and uniform for the 30B (Figures 5.2 (e) and (f)) and 15A (Figures 5.2 (g) and (h)) clays than for the MMT-Na^+ where much more agglomeration is observed (Figures 5.2 (a) and (b)). The agglomeration of MMT-Na^+(C) in PDLLA (Figures 5.2 (c) and (d)) decreased as compared with that of MMT-Na^+ since the removal of water resulted in a shrinkage of the clay particle thickness (Brownell, 1976). EDX results further confirmed PDLLA/MMT-Na^+(C) as a microcomposite.

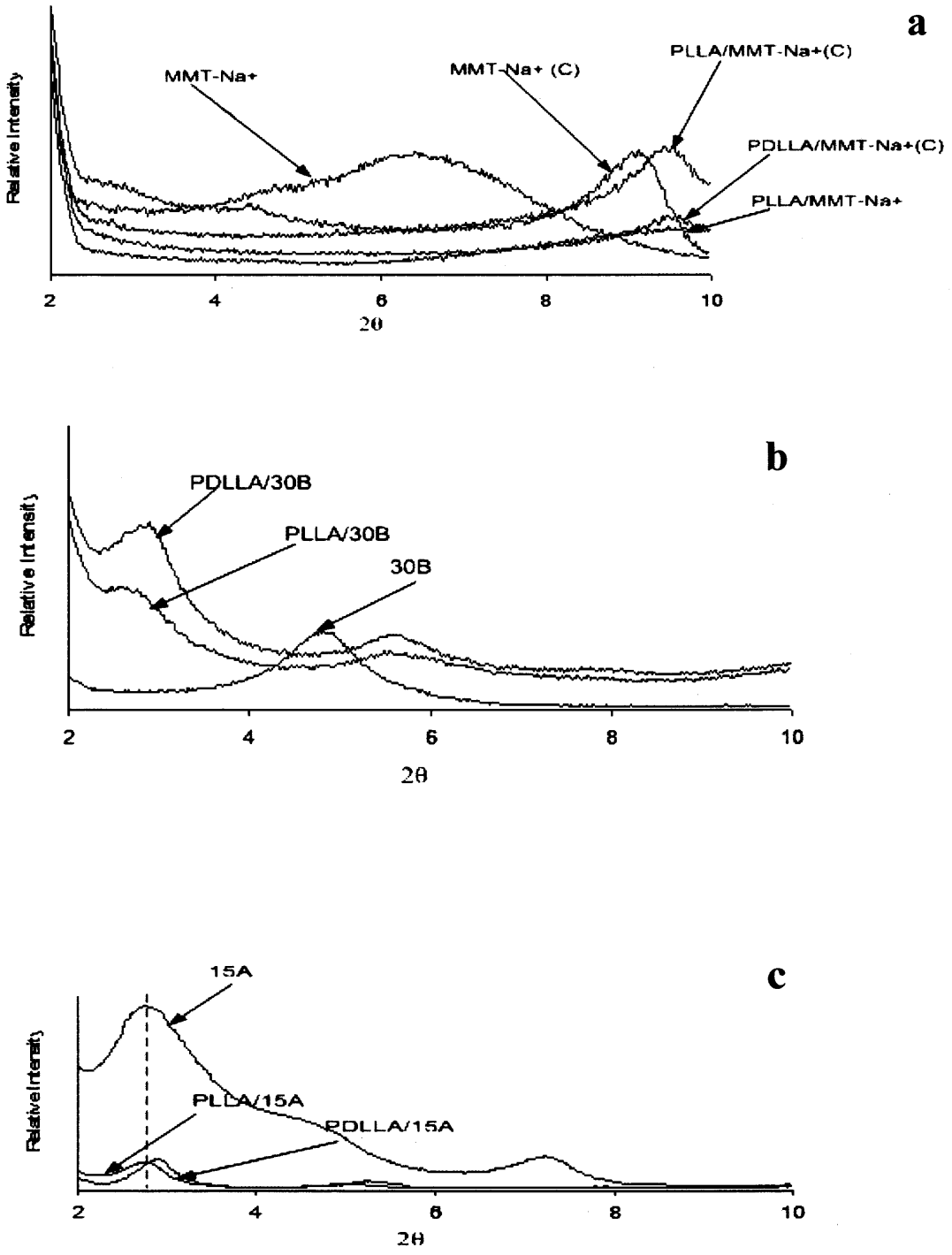

Figure 5.1 WAXD patterns: (a) MMT-Na^+ and MMT-Na^+ (C) and their composites; (b) 30B, PLLA/30B and PDLLA/30B; (c) 15A, PLLA/15A and PDLLA/15A.

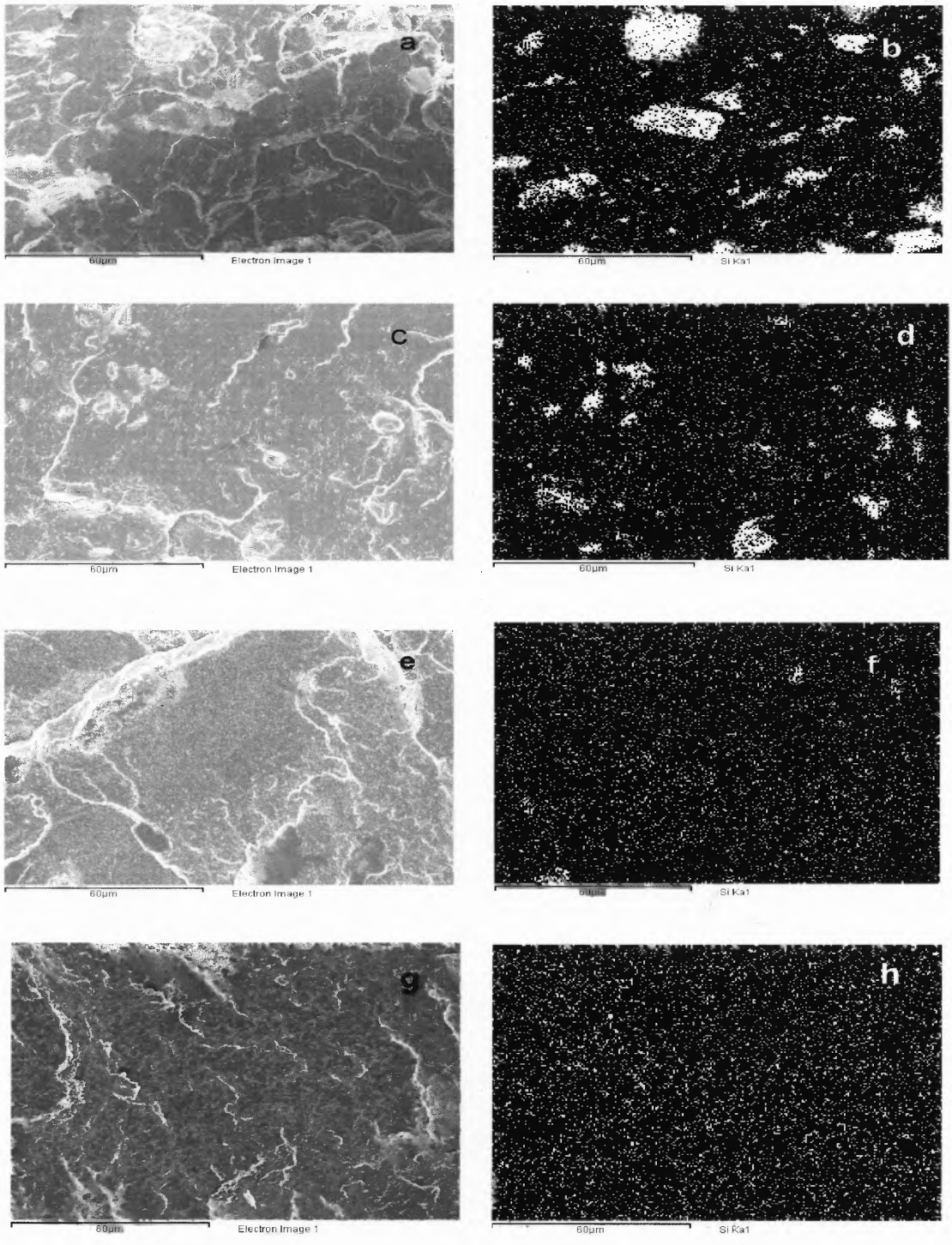

Figure 5.2 SEM and EDX of film cross-section patterns: (a) PDLLA/MMT-Na^+ (SEM); (b) PDLLA/MMT-Na^+ (EDX); (c) PDLLA/MMT-Na^+(C) (SEM); (d) PDLLA/MMT-Na^+(C) (EDX); (e) PDLLA/30B (SEM); (f) PDLLA/30B (EDX); (g) PDLLA/15A(SEM); (h) PDLLA/15A(EDX).

5.1.2 Anionic Clays and their Calcined Products

Filler dispersion in the polymer matrix was also determined by WAXD. The mean interlayer spacing for the HT powder is 7.61 Å at $2\theta = 11.62°$ (Figure 5.3(a)). After blending with PLLA, its interlayer distance increased from 7.61 Å to 13.62 Å at $2\theta = 6.48°$ (Figure 5.3(b)). The mechanism of the layer expansion is not fully understood in the literature, although oligomers may be more easily intercalated into the interlayer space of the HT during melt processing compared to the higher MW chains. This is in agreement with the conclusions of Tian et al (2007). In the case of HT(C) and PLLA/HT(C), no peaks were observed (Figures 5.3 (a) and (b)) since in the HT(C) the layer structure was destroyed. Note that both the XRD lines of PLLA/HT and PLLA/HT(C) in Figure 5.3 are tilted due to the rise of the XRD line of the PLLA to a peak located beyond $2\theta=15°$. The thickness of HT is only 1.5 nm. (Khan and O'Hare, 2002). Thus, PLA/HT composites may be considered as nanocomposites.

Further morphological analyses by SEM and EDX were carried out to determine the extent of the clay dispersion. By mapping the silicon or magnesium distribution in the PDLLA, it can be shown that the overall clay particle distribution is much better for the HT and HT(C) (Figures. 5.4(a),(b),(c) and (d)) than for the MMT-Na^+ and MMT-Na^+(C) where much more agglomeration is observed (Figures. 5.2 (a),(b),(c) and (d)).

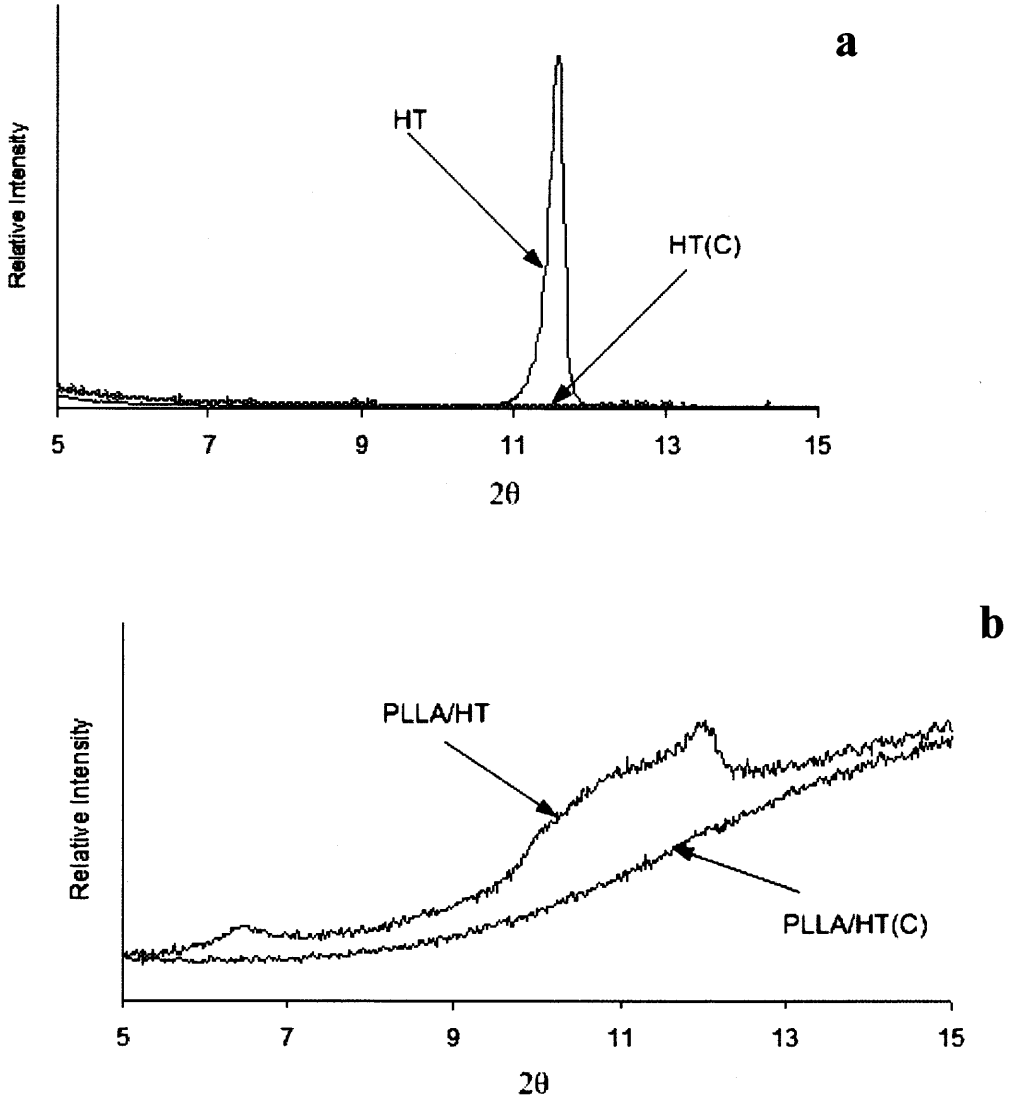

Figure 5.3 WAXD patterns: (a) HT and HT (C); (b) PLLA/HT ; PLLA/HT(C).

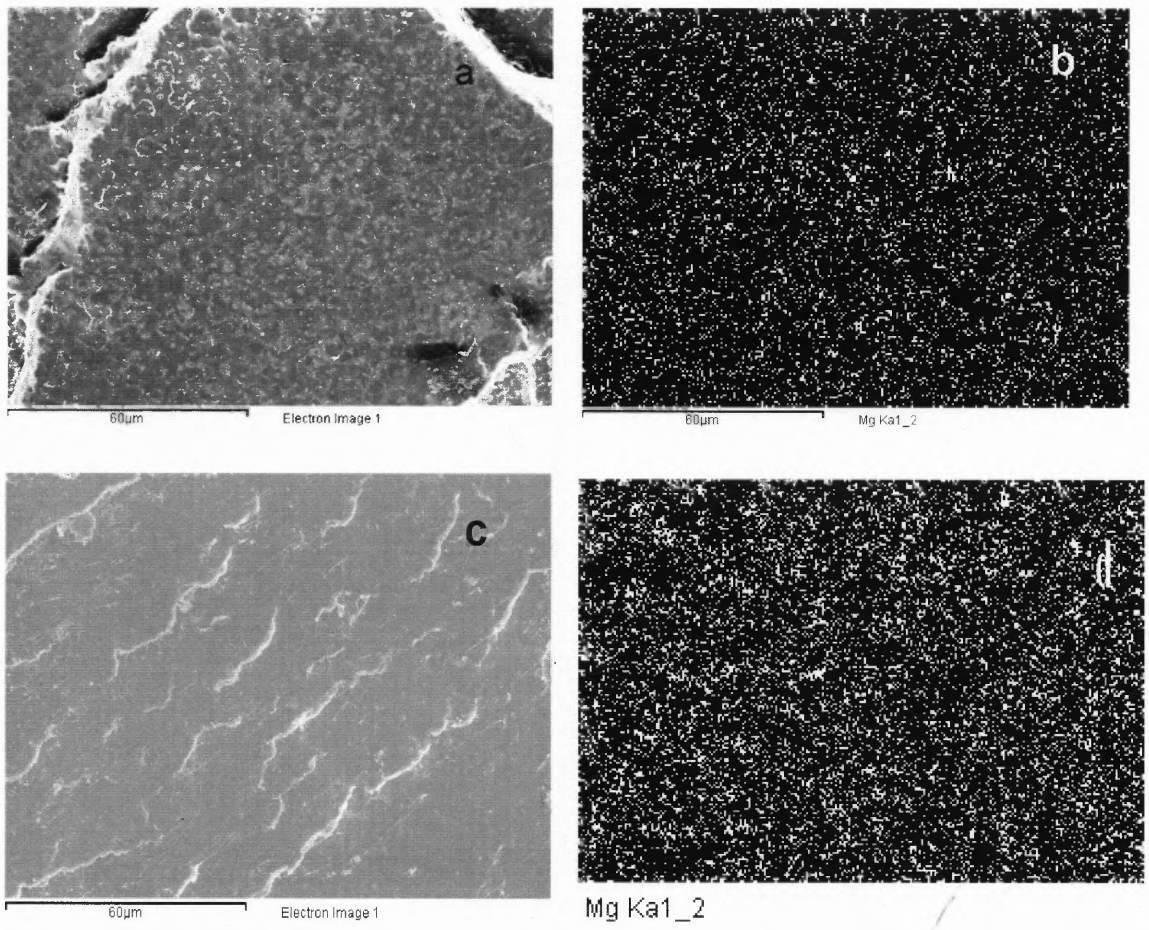

Figure 5.4 SEM and EDX patterns: (a) PDLLA/HT(SEM); (b) PDLLA/HT(EDX);(c) PDLLA/HT(C)(SEM); (d) PDLLA/HT(C)(EDX).

Table 5.1 summerizes the classification of the different composites as nano- or micro- based on XRD and SEM/EDX information

Table 5.1 Polymer Composites Information

Nanocomposites		Microcomposites
Cationic	Anionic	Cationic
PLLA/30B	PLLA/HT	PLLA/MMT-Na^+
PDLLA/30B	PDLLA/HT	PDLLA/MMT-Na^+
PLLA/15A	PLLA/HT(C)	PLLA/MMT-Na^+ (C)
PDLLA/15A	PDLLA/HT(C)	PDLLA/MMT-Na^+(C)

5.2 Thermal Degradation

5.2.1 Degradation during Melt Processing

5.2.1.1 Intrinsic Viscosity Change. Unfilled PLA is known to rapidly degrade at high temperatures, losing up to 80% of its initial MW on melt processing (Degee et al., 1997). It was, therefore, of interest to investigate the effect of fillers on the polymer MW during processing. Table 5.2 shows the *IV* change of unfilled polymers and polymer in their composites after melt processing vs. the unprocessed polymer pellets. The decrease in *IV* is in the following order: both cationic microcomposites and anionic HT nanocrocomposites > nanocomposites (except for PLLA/15A) > anionic HT(C) nanocomposites >unfilled polymers. The mechanism that causes *IV* changes involves shear and thermal hydrolytic degradation. Considering that the different moisture contents after drying were in the order: both cationic microfiller and anionic nanofiller (0.8%) > cationic nanofiller (0.31%~0.36%) > unfilled polymers (0.04%~0.05%), it is reasonable to explain the differences in the *IV* changes. Note that the moisture of HT(C) and MMT-Na^+ are not measured. The experimental results of cationic nano- and microcomposites are in general agreement with those of Pluta et al (2005). Note that as expected, the decrease in *IV* for composites containing calcined clays (MMT-Na^+(C) and HT(C)) is less than that of their non-calcined counterparts. It is of interest that the *IV* changes of unfilled PDLLA and its corresponding polymer in the composites are lower than those in the unfilled PLLA and its composites. This may be explained by the higher melt viscosities (lower MFI) of the unfilled PLLA and its composites compared to the corresponding unfilled PDLLA and its composites (Figures 5.5 and 5.6), leading to higher shear forces that may speed up degradation during melt mixing.

Table 5.2 Intrinsic Viscosity Changes after Melt Processing Comparison with Unprocessed Polymer Pellets

Samples	IV_0 (dl/g) *	ΔIV (%) **	M_{v0} ***
PLLA (pellet)	1.92	0	72240
PLLA	1.51	21	51980
PLLA/MMT-Na^+	1.27	34	41010
PLLA/MMT-Na^+ (C)	1.3	32	42340
PLLA/30B	1.36	29	45040
PLLA/15A	1.14	41	35370
PLLA/HT	1.05	45	31600
PLLA/HT(C)	1.39	28	46410
PDLLA (pellet)	1.34	0	81770
PDLLA	1.2	10	68430
PDLLA/MMT-Na^+	0.93	31	49150
PDLLA/MMT-Na^+(C)	1.04	22	56830
PDLLA/30B	1.15	14	64750
PDLLA/15A	1.07	20	58970
PDLLA/HT	0.9	33	47100
PDLLA/HT(C)	1.08	13	59680

* Polymer IV after melt processing

** $\Delta IV(\%) = \frac{IV_{polymerpellet} - IV_0}{IV_{polymerpellet}}$

*** Calculated viscosity average molecular weight based on IV_0

5.2.1.2. Melt Flow Index. Figure 5.5 shows the dependence of *IV* values (proportional to polymer MW) of : a) "as received" polymer pellets, b) processed neat polymers and c) processed polymers present in the MMT composites, on the MFI of the same samples. For neat polymers, MFI is a direct indication of melt viscosity and, hence, polymer MW. For composites, in addition to the contribution of the polymer MW, MFI is also dependent on the effects of filler/polymer interactions on viscosity. It is evident that melt processing of the unfilled polymers results in MW reduction as shown by the decreasing *IVs* and the increases in MFI vs. the unprocessed pellets. However, thermomechanical degradation is more pronounced (to different degrees) in the presence of all fillers, an indication of their considerable catalytic effect. Compared to microcomposites, the lower MFI of the nanocomposites suggests stronger interaction forces between the nanofiller and the polymer matrix. In the case of nanocomposites, the lower MFI of the 30B composites vs. the 15A composites may be due to differences in interactions and dispersion as a result of the polar modifier present in 30B.

The data for MMT nanocomposites and microcomposites (PLA/MMT-Na^+) (Figure 5.5) are in good agreement with those of other authors who observed the susceptibility of PLA to degradation upon melt processing (Pluta et al., 2005 and 2007). However, the effects of the clays appear to depend on processing conditions and types of clays. In the experiments of Pluta et al. (2005) PLA was mixed with MMT-Na^+ clays in the presence of 0.3 wt % stabilizer in a counter rotating mixer (180°C, 60 rpm, 10 min, apparently under air atmosphere). As expected, PLA degraded on melt processing by 41.2% compared to the native PLA. However, the addition of either MMT-Na^+ or the organomodified clay strongly limited this degradation to only 22.1 or 19.6%,

respectively. In subsequent melt blending experiments by Pluta et al (2007) (180°C, 50 rpm, 20 min under nitrogen) the presence of the nanoclay Cloisite 30B contributed to further decrease of the MW of PLA, possibly through catalytic reactions with the organic modifier. It should be noted that a particular acid treated MMT (K10) promotes significant thermal degradation of PLA (toluene, 100°C, 6 hours) (Okamoto et al., 2005) to linear-type oligomers; this was attributed to the catalytic effects of the Lewis acid sites of the aluminosilicate layers.

Figure 5.6 compares the *IV* values vs the MFI for the unfilled polymers and two cationic and one anionic clay microcomposite. Again, these results are in good agreement with the observed pronounced thermomechanical degradation in the presence of fillers whose extent depends on the filler type. Compared to unmodified clay composites, the MFI of calcined clay composites are lower since the *IVs* of the polymers in the calcined clay composites are higher.

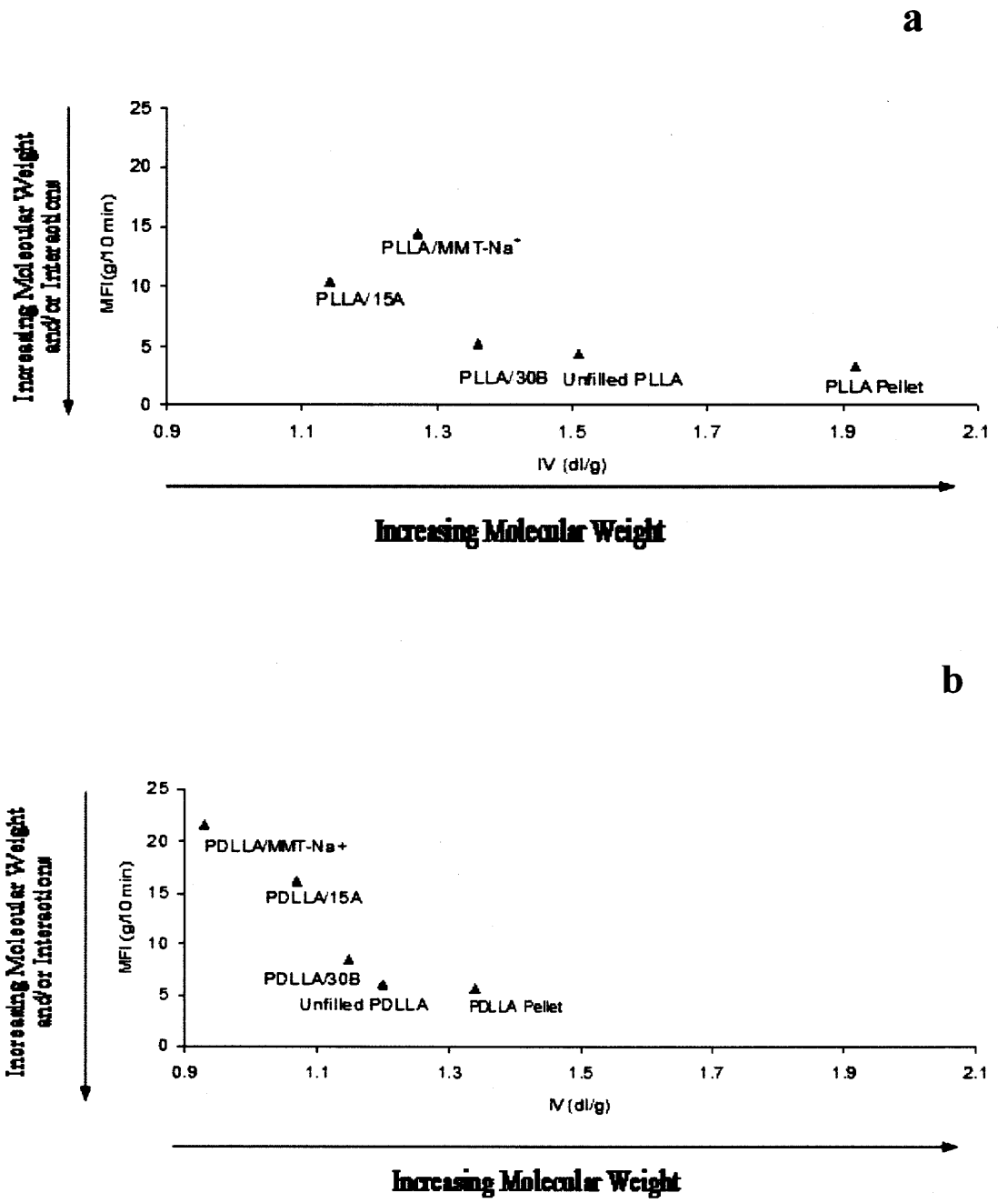

Figure 5.5 Melt flow index vs. intrinsic viscosity after melt processing (a) PLLA and its MMT composites, (b) PDLLA and its MMT composites. Values for unprocessed pellets are also shown for comparison.

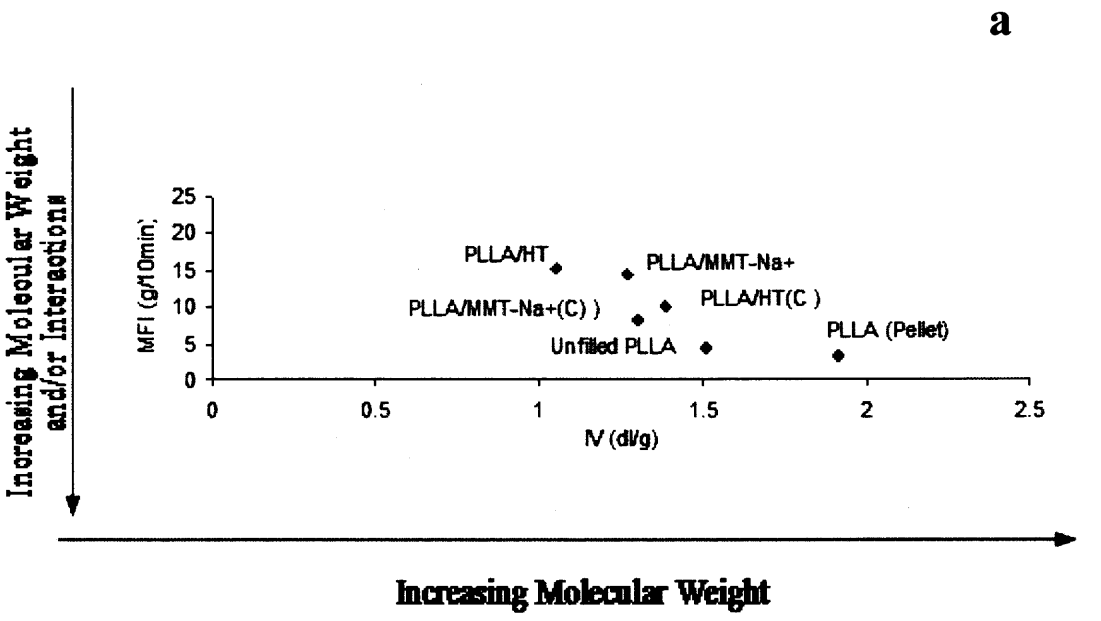

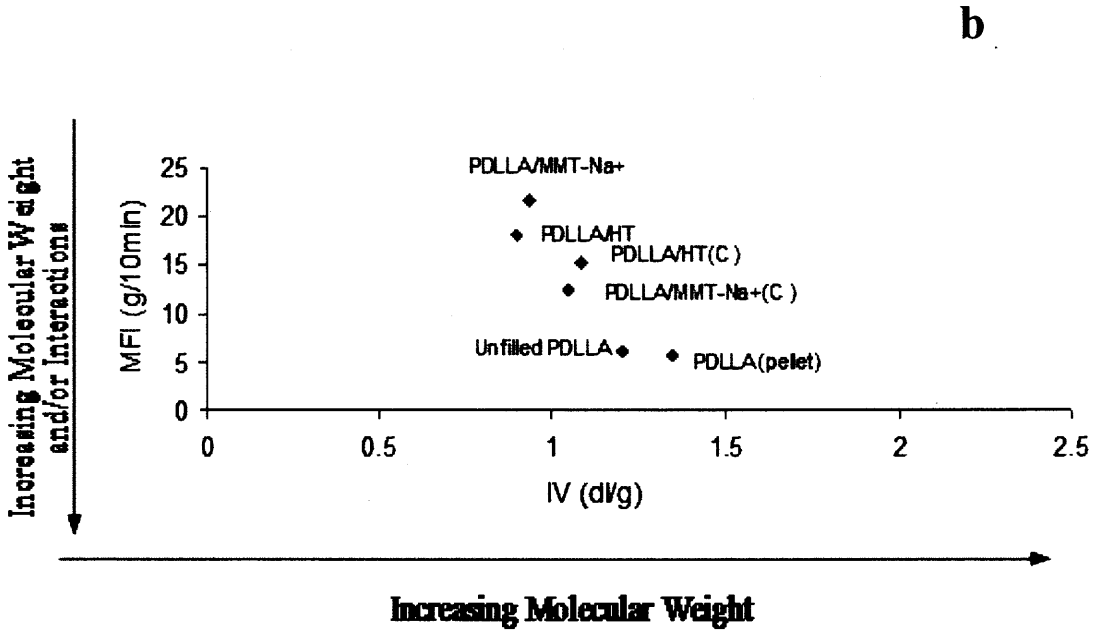

Figure 5.6 Melt flow index vs. intrinsic viscosity after melt processing (a) PLLA and its MMT/HT composites, (b) PDLLA and its MMT/HT composites. Values for unprocessed pellets are also shown for comparison.

5.2.1.3 Thermal Properties. Focusing on the thermal transitions and crystallization behavior of the unfilled PLLA and its MMT nano- and microcomposites (PLLA/MMT-Na^+) after melt processing (Figure 5.7), it can be firstly noted that the PLLA T_g in the composites appear to very slightly increase compared to unfilled PLLA. This behavior has been ascribed to the restricted segmental motions at the organic–inorganic interface neighborhood of intercalated compositions. A similar increase in T_g for nanocomposites has been reported by Ray et al. (2003). In-depth analysis of these thermograms revealed a sharp endothermic peak associated with T_g in PLLA/MMT-Na^+ and PLLA/15A, typically attributed to their structural relaxation during the first heating scan. Compared to the unfilled PLLA, the T_{cc} of the PLLA composites shifted to lower temperature, especially for PLLA/30B since this filler appears to act as an effective nucleating agent to speed up PLLA crystallization. The nanosized layered platelets with large surface area, especially for the 30B composite having an exfoliated structure enhance this crystallization ability.

The melting peaks of the PLLA composites slightly shift to lower temperature. Except for PLLA/30B, unfilled PLLA and its composites show two melting peaks due to two lamellar populations with different perfection that are observed in their heating scans (Liu and Petermann, 2001). The presence of one melting peak in the 30B nanocomposites may be due to either the strong H-bonding between nanofiller modifier and polymer matrix inhibiting a crystal reorganization process, or to the presence of only one lamellar population. A small endothermic peak observed just before melting commenced in the PLLA nanocomoposites is attributed to additional polymer crystallization since near the polymer melting temperature chain mobility would have increased, allowing some of the amorphous segments to reorder themselves.

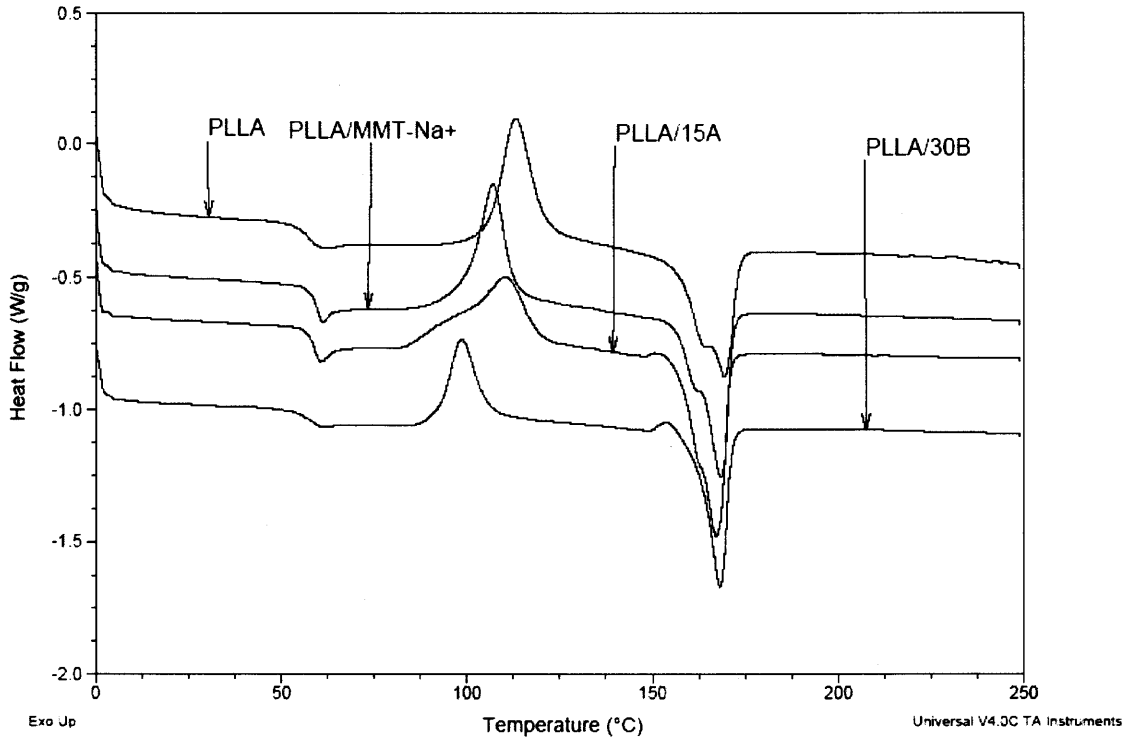

Figure 5.7 DSC curves after melt processing for PLLA and its MMT composites (first heating scan).

The thermal transitions and crystallization behavior of PLLA containing MMT-Na^+, HT and their calcined products are compared in Figure 5.8. Curves follow the same trends as before with all fillers acting as efficient nucleators, with the exception of HT(C). For HT(C) two T_{cc} peaks, apparently corresponding to the two different oxides formed by calcination, and a broad melting temperature range are observed.

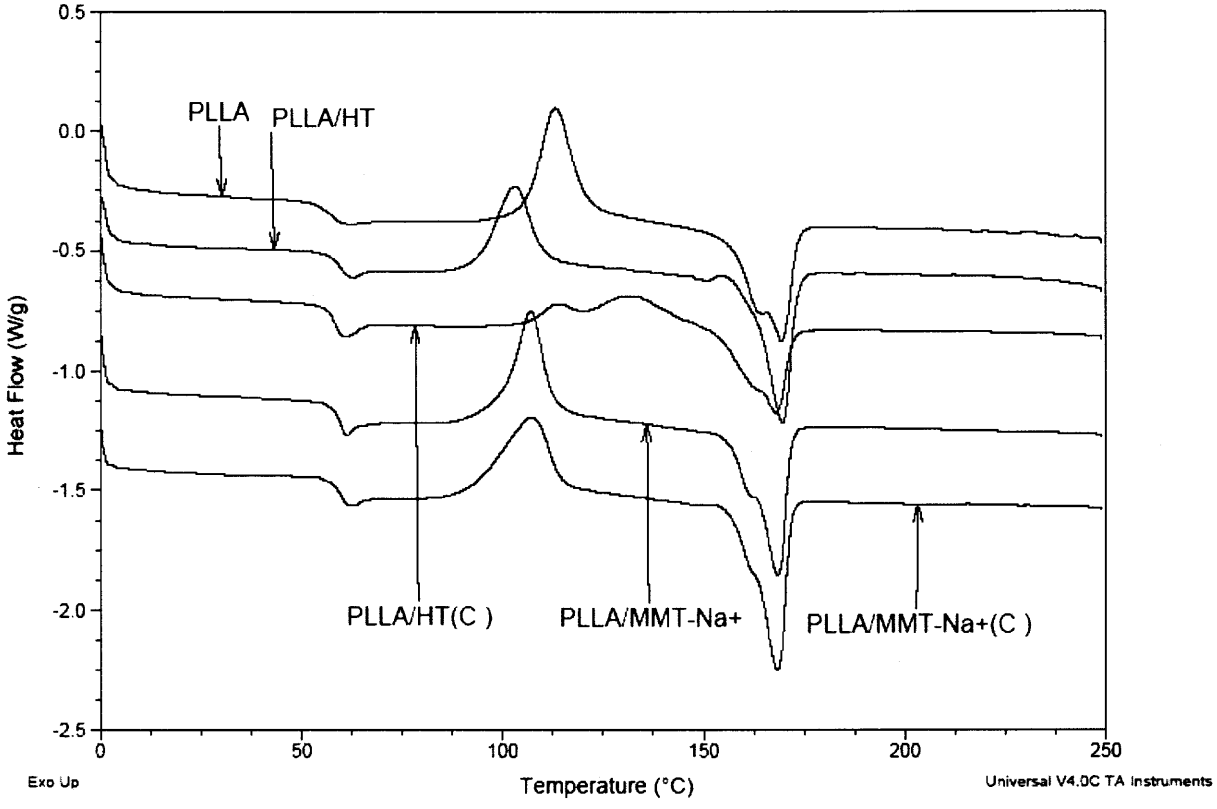

Figure 5.8 DSC curves after melt processing for PLLA and its MMT and HT composites (first heating scan).

5.2.2 Isothermal Degradation

5.2.2.1 Theory. Assuming that degradation takes place by random scission obeying (equation 2.1) two new degradation equations (equations 5.1 and 5.2)

$$\frac{1}{IV_t} - \frac{1}{IV_0} = k_{iv}t \tag{5.1}$$

$$\text{where } k_{iv} = \frac{k_v \nu}{B} \tag{5.2}$$

based on *IV* changes can be derived as shown in Appendix.

5.2.2.2 Effect of Polymer Type. The rate constants k_{iv} at 180°C and 200°C designated as k_{iv1} and k_{iv2}, respectively, for the random scission model (equation 5.1) were determined by linear regression from plots of $1/IV_t$ versus time at 180 °C (Figures 5.9, 5.10, 5.11) and 200°C (Figure not shown). The $1/IVs$ of the unfilled polymers and all their composites (except for PDLLA/HT) increase with degradation time throughout the experimental time period. The apparent degradation rate constants and the corresponding r^2 correlation coefficients are shown in Tables 5.3 and 5.4 . The high correlation coefficients (except for, PDLLA/15A and PDLLA/HT at 180°C) support the validity of the random scission degradation mechanism. Since PDLLA and PLLA have different ν and B values (see equation 2.8), equation (5.2) was used to change k_{iv} into k_v (see equations. A6 and A7) to compare our degradation rate constants based on viscosity average MW. According to the data in Tables 5.3 and 5.4, the degradation rate constants (k_v) of unfilled PDLLA and its composites are lower than those of the unfilled PLLA and its composites. These results are supported from data of Tables 5.3 and 5.4 indicating that the final/initial IV ratios for the PDLLA and its composites are higher than those of the PLLA and its corresponding composites at the degradation temperature of 180°C. This is accounted for by the fact that the average initial molecular weights M_{v0} of PDLLA in the unfilled polymer and its composites are higher than that of the PLLA and its corresponding composites (Tables 5.3 and 5.4).

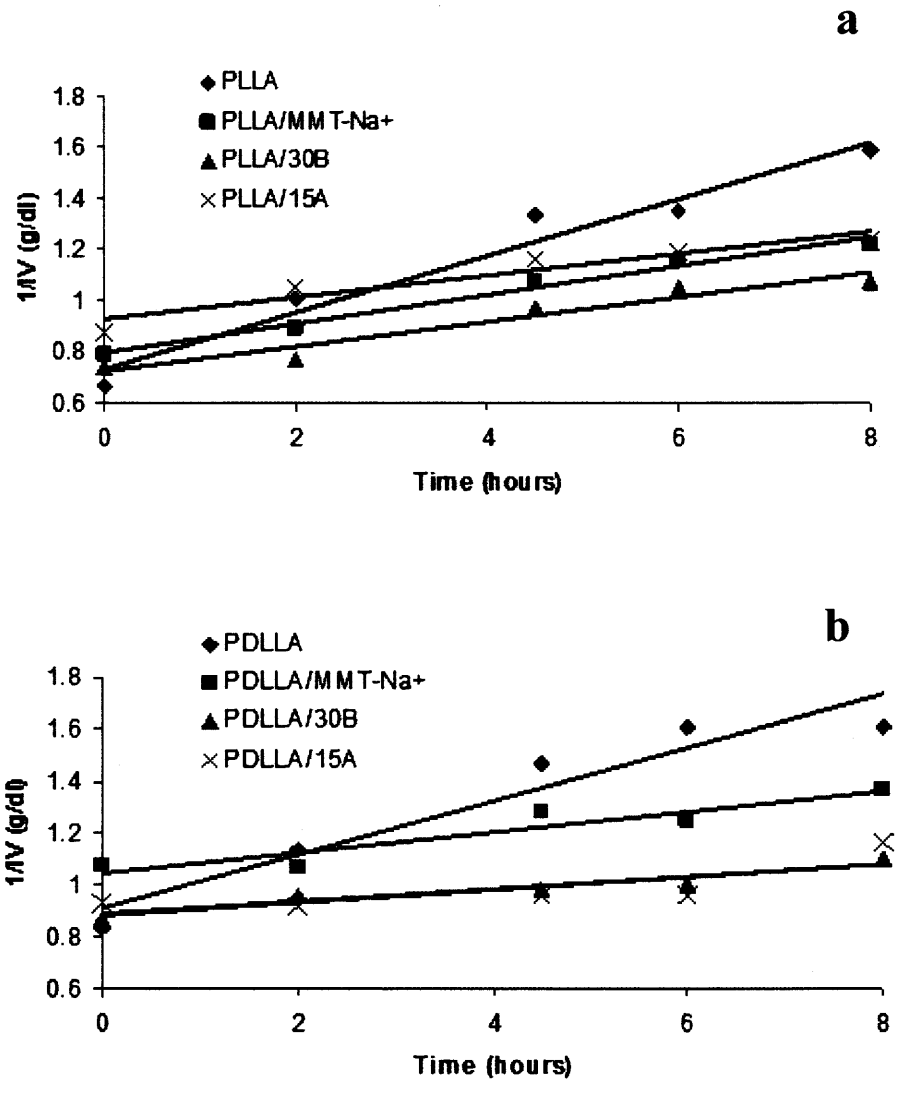

Figure 5.9 Random thermal scission model at 180°C: (a) PLLA and its MMT composites (b) PDLLA and its MMT composites. Data fitted according to equation (5.1).

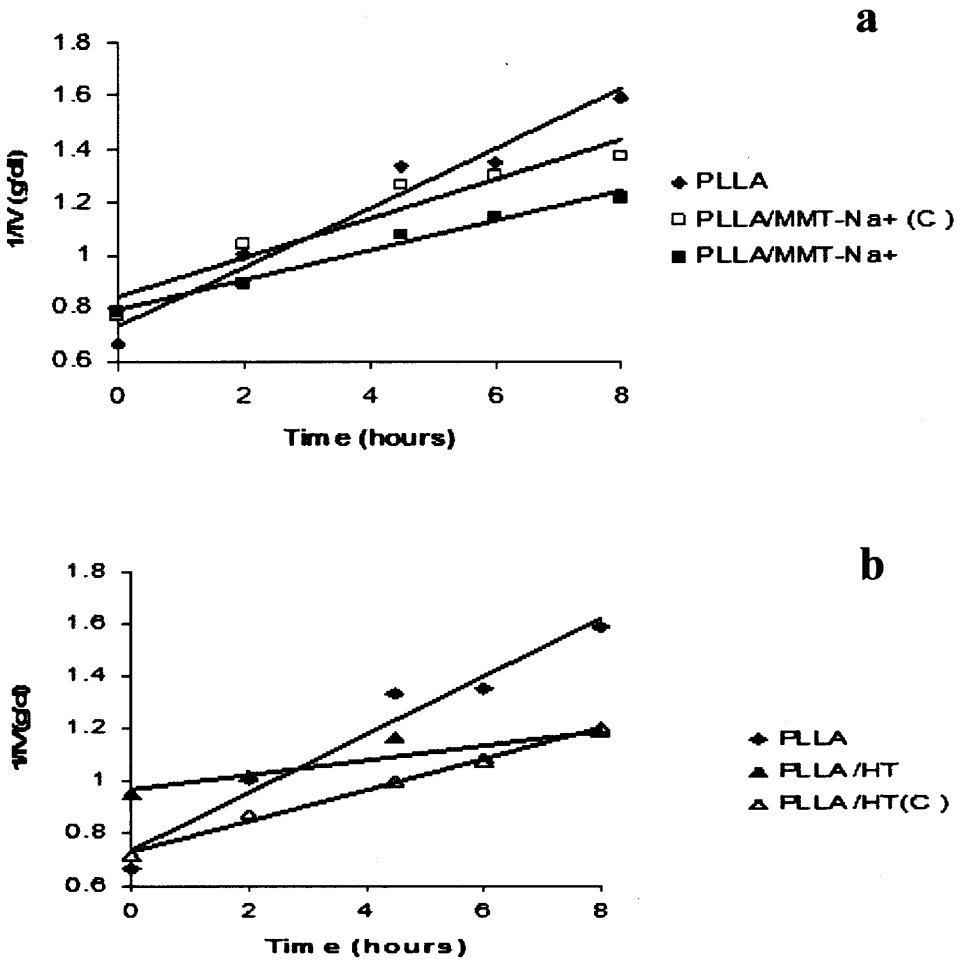

Figure 5.10 Random thermal scission model at 180°C: (a) PLLA and its untreated and calcined MMT-Na^+ composites (b) PLLA and its untreated and calcined HT composites Data fitted according to equation (5.1).

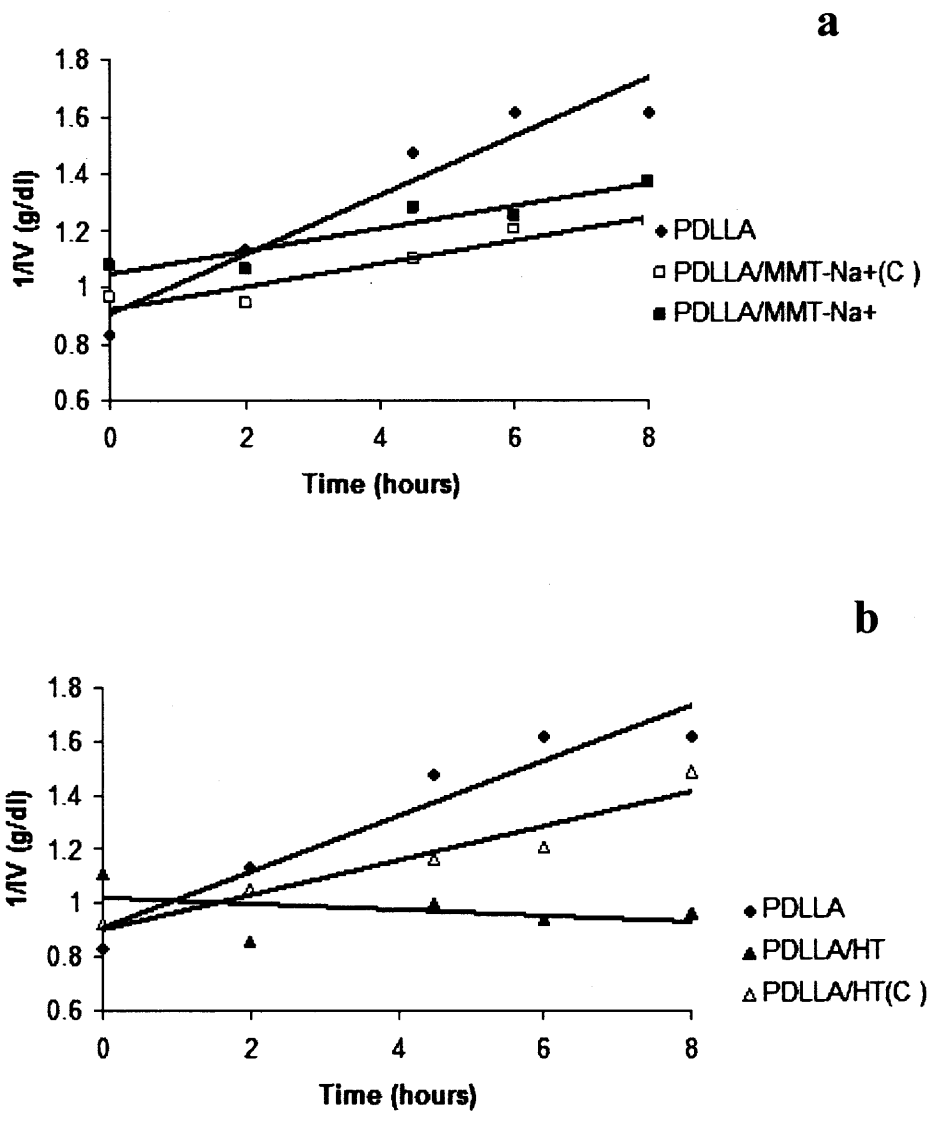

Figure 5.11 Random thermal scission model at 180°C (a) PDLLA and its untreated and calcined MMT composites and (b) PDLLA and its untreated and calcined HT composites. Data fitted according to equation (5.1).

Table 5.3 Summary of Isothermal Degradation Results for Unfilled Polymer and their MMT Micro- and Nanocomposites at 180°C and 200°C

Samples	PLLA	PLLA/ MMT-Na^+	PLLA/30B	PLLA/15A	PDLLA	PDLLA/ MMT-Na^+	PDLLA/30B	PDLLA/15A
180°C								
Degradation Rate Constant, k_{iv1} (g/dl.hour)	0.11	0.056	0.049	0.043	0.1	0.04	0.025	0.025
r^2	0.959	0.987	0.937	0.912	0.919	0.873	0.908	0.61
IV_8/IV_0	0.42	0.65	0.68	0.71	0.52	0.78	0.79	0.8
Degradation Rate Constant, k_v (g/dl.hour) (10^5)	8.3	4	4	3	3	1	0.7	0.7
200°C								
Degradation Rate Constant, k_{iv2} (g/dl.hour)	0.17	0.21	0.077	0.086	N/A	N/A	N/A	N/A
r^2	0.899	0.85	0.967	0.881	N/A	N/A	N/A	N/A
IV_8/IV_0	0.32	0.3	0.52	0.53	N/A	N/A	N/A	N/A

Table 5.4 Summary of Isothermal Degradation Results for Unfilled Polymers and Untreated and Calcined Cationic and Anionic Clay Composites at 180°C and 200°C

Samples	PLLA	PLLA/ MMT-Na^+	PLLA/ MMT-Na^+ (C)	PLLA/ HT	PLLA/ HT(C)	PDLLA	PDLLA/ MMT-Na^+	PDLLA/ MMT-Na^+(C)	PDLLA/ HT	PDLLA/ HT(C)
180°C										
Degradation Rate Constant, k_{iv1}, (g/dl.hour)	0.11	0.056	0.074	0.028	0.059	0.1	0.04	0.04	0.011	0.064
r^2	0.958	0.987	0.915	0.81	0.995	0.919	0.873	0.905	0.138	0.918
IV_8/IV_0	0.42	0.65	0.56	0.76	0.6	0.52	0.78	0.79	1.16	0.62
Degradation Rate Constant, k_v (g/dl.hour) , (10^5)	8	4	5.5	2	4	3	1	1	0.3	2
200°C										
Degradation Rate Constant, k_{iv2} (g/dl.hour)	0.17	0.21	0.23	0.12	0.13	N/A	N/A	N/A	N/A	N/A
r^2	0.899	0.85	0.883	0.853	0.884	N/A	N/A	N/A	N/A	N/A
IV_8/IV_0	0.32	0.3	0.26	0.46	0.37	N/A	N/A	N/A	N/A	N/A

5.2.2.2 Effects of Filler Type. Data in Figure 5.9 and Table 5.3 show that the *IV* changes and the degradation rate constants of the MMT micro- and nanocomposites are significantly lower than those of the unfilled polymers at 180°C. Thus, both microfiller and nanofillers hinder polymer degradation, in agreement with the ratios of final/initial *IVs* at 180°C. Since the surface water of the fillers has been removed during melt processing, at this temperature the major function of the silicate platelets is to act as an additional barrier, which most likely works against oxygen diffusion towards the bulk of the polymer (Zanetti et al., 2001). The degradation rate constants of the nanocomposites are lower than those of the microcomposites presumably due to the good dispersion of the nanofillers in the polymer matrix. As 30B and 15A composites have very close degradation rate constants (Table 5.3), it can be concluded that the extent of nanofiller dispersion (exfoliation vs. intercalation) has the same effect on rate of polymer degradation at this temperature.

Data in Figure 5.10 and 5.11 and Table 5.4 also show that the *IV* changes and the degradation rate constants of the MMT and HT composites are significantly lower than those of the unfilled polymers at 180°C. Thus, both cationic and anionic clays (unmodified or calcined) hinder polymer degradation, in agreement with the ratios of final/initial *IV*s at 180°C. In contrast to polymer/ cationic clay composites, the degradation rate constants of polymer/anionic clay composites are lower than those of polymer/cationic clay composites due to the good dispersion of the anionic clays in the polymer matrix (Figure 5.4) compared to the cationic ones (Figure 5.2). Also, at this temperature, anionic clays may act catalytically promoting condensation polymerization

(El-Toufaili et al., 2006), particularly for the PDLLA/HT, where molecular weight slightly increases with heating time (Note lack of fit and low r^2 in Table 5.3). The presence of the calcined clay in the polymer yields a higher or slightly higher degradation rate constant than for the non-calcined clay since air diffusion is easier due to the presence of mesopores or macropores in the calcined clay (Noyan et al., 2006) (Grimsaw, 1971) (Auerbach et al., 2004).

5.2.2.3 Effects of Temperature. Table 5.3 shows results of accelerated isothermal degradation at 180°C and 200°C for unfilled PLA's and their MMT composites. The degradation rate constant increases with increasing temperature. At 200°C, the degradation rate constant of the cationic microcomposites is higher than those of the unfilled polymer and nanocomposites. It is reasonable to consider that Brønsted and Lewis acid sites and interlayer water release in the microfillers promote more polymer degradation at 200°C (Figures 5.12 and 5.13) since the interlayer water has already started to be released from the clay at 200°C to create strong acidic sites (Auerbach et al., 2004). Figures 5.12 and 5.13 show the PLA degradation mechanism catalyzed by those Brønsted and Lewis acid sites present in MMT-Na^+. By constrast, nanofillers significantly suppress polymer degradation since their modifiers are adsorbed on the surfaces of the clay via cation exchange (Xu and Boyd, 1995) and weaken the acid sites. Another reason is that nanofillers having good dispersion in the polymer matrix can act as strong barriers to greatly retard degradation. This retarded degradation can also be attributed to the formation of a carbonaceous-silicate char structure from a small amount of nanofillers, which is produced on the surface of the nanocomposite during burning

(Gilman et al., 2000) since the organic modifier starts to decompose at about 200°C (Xie et al., 2001).

In the presence of oxygen, the intimate contact between the clay platelets and the polymer favors this char formation (Berta et al., 2006), which acts as an excellent insulator and mass transport barrier delaying the diffusion of oxygen to the polymer mass, thus, reducing degradation. Comparison of the effects of 30B and 15A on the degradation rate constants at 200°C, based on filler dispersion differences, can explain the lower rate constants observed for the PLLA/30B vs. the equivalent composites containing 15A (Table 5.3) since the nanostructure effect can be more pronounced in the exfoliated nanocomposite than in the intercalated one (Chen and Yoon, 2005).

Table 5.4 contains results of accelerated isothermal degradation at 180°C and 200°C for unfilled PLA's and their unmodified and calcined cationic and anionic composites. At 200°C, the degradation rate constants of the PLLA/MMT-Na^+ composites are not only higher than that of the unfilled polymer but also of the HT composites. Calcination of MMT-Na^+ and HT appears to increase the degradation rates of PLLA at both temperature with less pronounced effects for the PDLLA/MMT-Na^+(C) composites. At high temperature, the degradation rate constants of all composites approach that of unfilled polymer.

Overall, it is evident that PLA thermal degradation in the presence of clays is a complex phenomenon depending on clay dispersion, clay and polymer types, clay heat treatment history and degradation temperature.

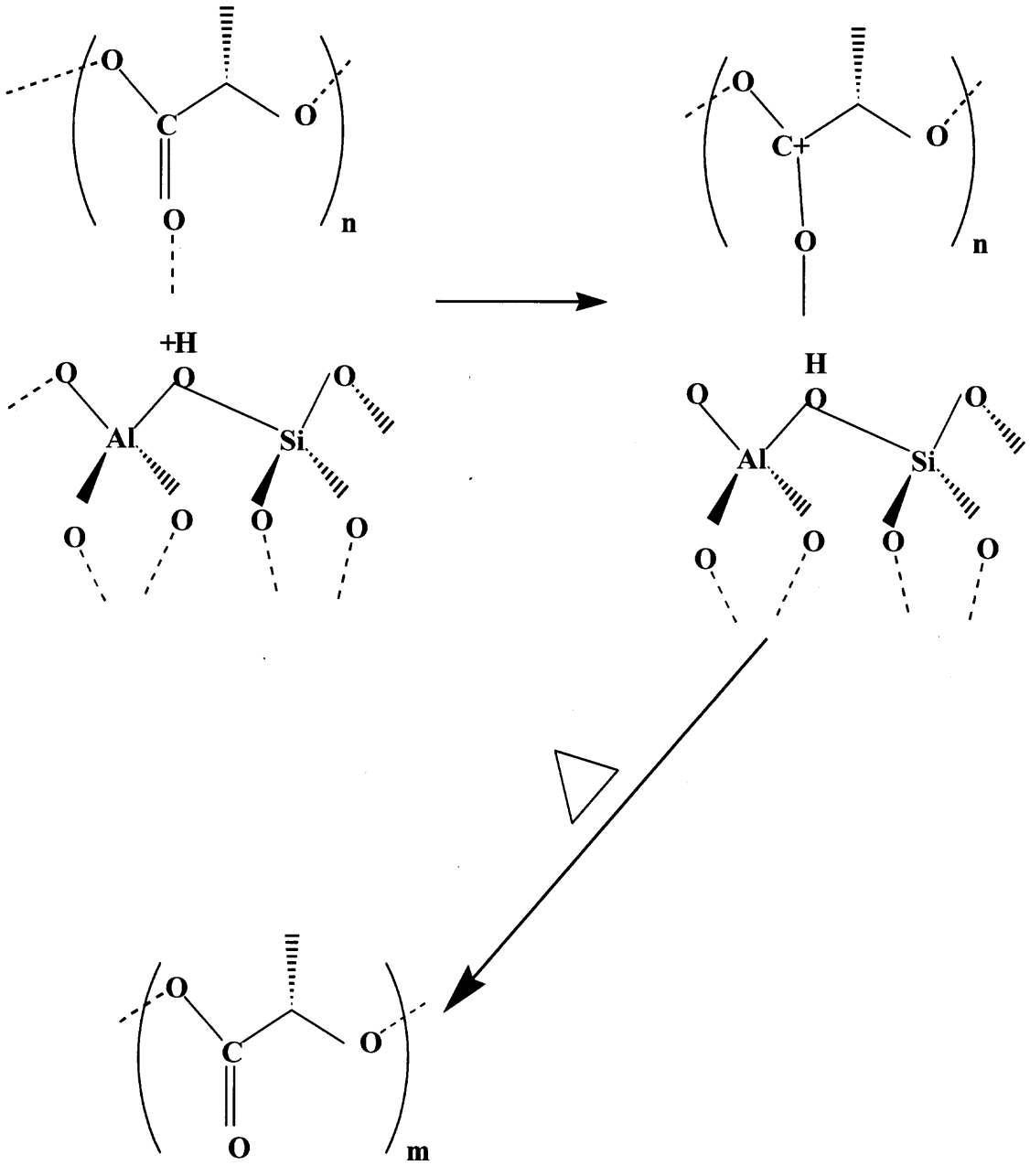

Figure 5.12 Structure of MMT-Na^+ proposed to catalyze degradation of PLA showing Brønsted acid sites; Note that m<n schematic based on reference.
(Okamoto et al., 2005)

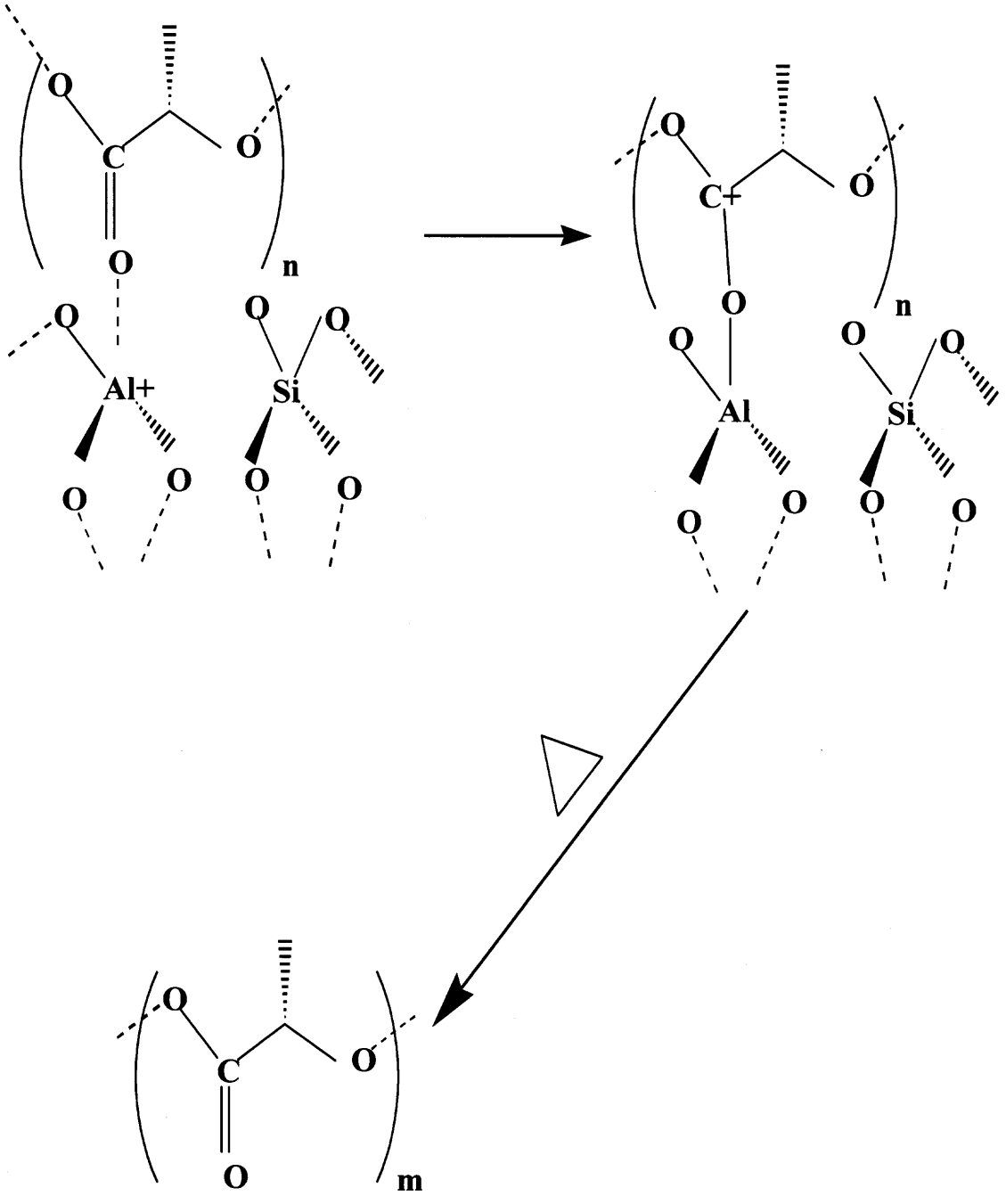

Figure 5.13 Structure of MMT-Na^+ proposed to catalyze degradation of PLA showing Lewis acid sites; Note that m<n schematic based on reference.
(Okamoto et al., 2005)

5.3 TGA Thermal Stability

5.3.1 Weight Loss

5.3.1.1 Fillers. The thermal stability of MMT micro- and nanofillers was recorded by TGA under nitrogen and air at 20°C/min (Figure 5.14). Below 200°C, the weight loss of the nanofillers is lower than that of the microfiller since the latter is more hydrophilic than the nanofillers which contain 30~43wt% hydrophobic modifiers (Figure 5.14). Above 200°C, the weight loss of the nanofillers significantly increase and a higher weight loss is observed above 250°C due to the beginning of the modifiers decomposition which follows a Hofmann elimination reaction (Xie et al., 2001) as follows (Qin et al., 2005):

$$MMT^{-}{}^{+}[NR_1R_2R_3R_4] \xrightarrow{\Delta} MMT^{-+}H + NR_1R_2R_3 + R_4'$$

where R_4'is olefin.

As shown in figure 5.14, nanofillers are more stable in air than nitrogen above 350°C. The oxidative stability of a molecule may increase due to the role of a confining morphology in modifying oxygen transport compared to nonoxidative decomposition (Xie et al., 2001) . This result agrees with those in the study of Marazzato et al (2007).

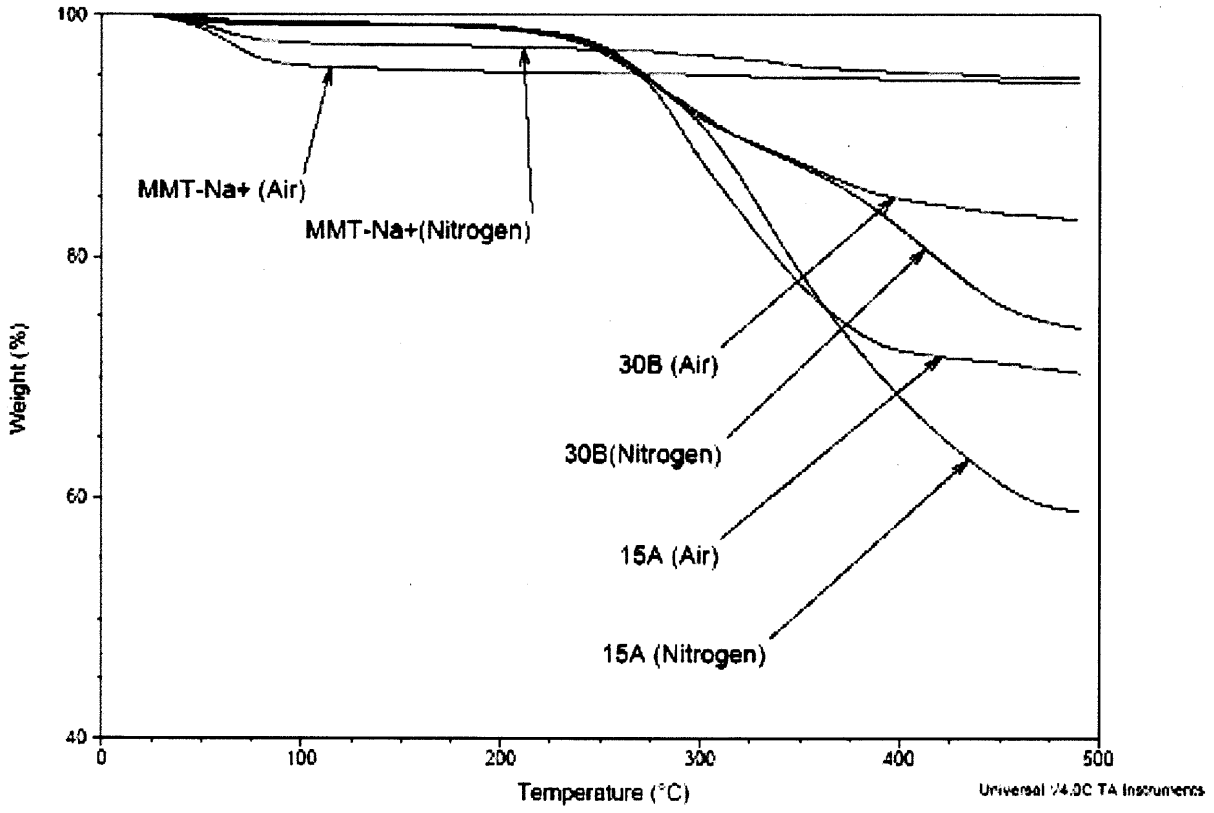

Figure 5.14 TGA curves recorded at 20°C/min for micro- and nano- MMT fillers under nitrogen and air.

The thermal stability of untreated and calcined cationic and anionic fillers was also recorded by TGA under nitrogen and air at 20°C/min (figure 5.15). In general, the thermal stability of the various fillers is in following order: MMT-Na^+(C) >MMT-Na^+ >HT(C) >>HT. With the exception of HT clay, calcined or non-calcined, retain more than 95% of their weight regardless of the testing atmosphere. The thermal stability of the cationic clays is, in general, higher than that of the anionic clays. Calcined clays are much more stable than non-calcined clays since interlayer and/or surface water, part of hydroxyl groups, or carbon dioxide were removed after calcination. Except for HT(C), the thermal stabilities of the cationic fillers appear to be higher under nitrogen than air. The HT thermal decomposition is characterized by two stages under nitrogen and three

stages under air. Dehydration below 200°C is followed by the collapse of the lamellar structure and loss of CO_2 giving rise to mixed oxides between 200°C and 400°C (Bellotto et al., 1996).

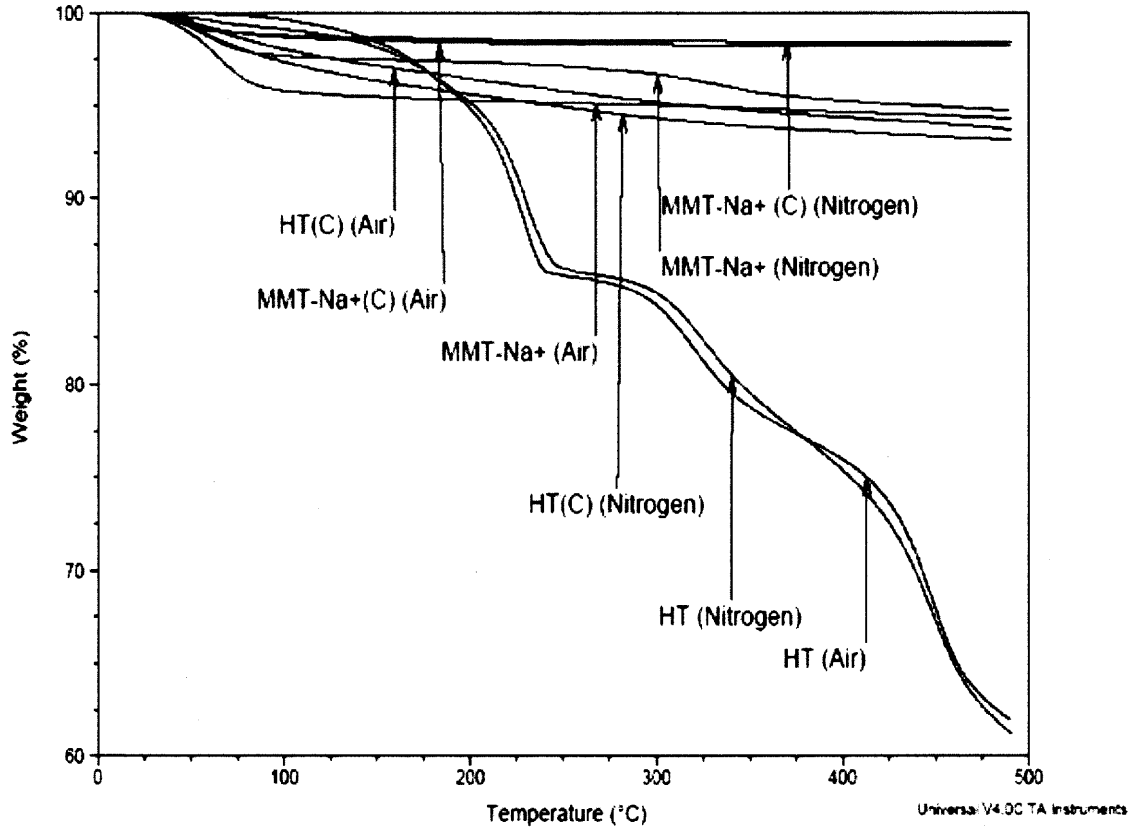

Figure 5.15 TGA curves recorded at 20°C/min for untreated and calcined MMT and HT fillers under nitrogen and air.

5.3.1.2 Unfilled Polymers and their Composites. Figures 5.16(a) and (b) show TGA traces and their derivatives [differential thermogravimetry (DTG)] for unfilled PLLA and its micro and nanocomposites obtained under nitrogen and air, respectively. In both cases, MMT-Na^+ significantly reduces the polymer thermal stability above 300°C. To explain this behavior, it must be reminded that the Na^+ cations present in the interlayer spaces are highly hydrated. At high temperatures, some inside water release could be

responsible for the PLLA chain degradation by hydrolysis (Paul et al., 2003). Other factors are the Brønsted and Lewis acid sites in the microfiller that promote polymer degradation at higher temperatures (Figures 5.12 and 5.13). In general, organoclays did not enhance the polymer thermal stability under nitrogen (Figure 5.16(a)); however, they enhanced thermal stability under air (Figure 5.16 (b)) since the stability of nanofillers is higher under air than under nitrogen as shown in Figure 5.14. Oxygen initiates depolymerization leading to the formation of hydroperoxides which can yield char (Bourbigot et al., 2004). Thus, reaction of oxygen with the polymeric matrix initiates earlier degradation of the material and, then, yielding more char in a particular temperature range. The role of the nanofiller is to promote char (transient char) during the thermo-oxidative degradation of the polymer (Bourbigot et al., 2004). This charring has been reported to be partially responsible for the limited diffusion of the combustion gases and could be at the origin of the fire retardant properties of polymer layered silicate nanocomposites (Gilman, 1999). Our experimental results agree with those of Paul et al. (2003) and Pluta et al. (2002).

The shape of the curves in Figure 5.16 may be explained by considering that in the early stages of thermal decomposition, the nanoclay would shift the decomposition to higher temperature as barrier. After that, this heat barrier effect would result in a reverse thermal stability. The stacked silicate layers could then hold accumulated heat that could be used as a heat source to accelerate the decomposition process, in conjunction with the heat flow supplied by the outside heat source (Ray and Bousmina, 2005).

The data on the temperatures corresponding to weight loss of 10% (T_{10}), 50% (T_{50}) and T_p (peak temperature determined at the DTG maximum peak) (Table 5.5) show

that the thermal stability of unfilled PLLA is slightly higher under nitrogen than air. By contrast to PLLA, the thermal stability of 30B composites is slightly higher under air than nitrogen. Also, these data show that the thermal stability of 30B and 15A nanocomposites is higher than that of the MMT-Na^+ microcomposites. In the case of thermal stability at the initial stages the data at T_{10} show that the thermal stabilities of PLLA and its composites are lower than those of PDLLA and its composites whereas the thermal stabilities of the nanocomposites are higher than those of the unfilled polymers and their microcomposites.

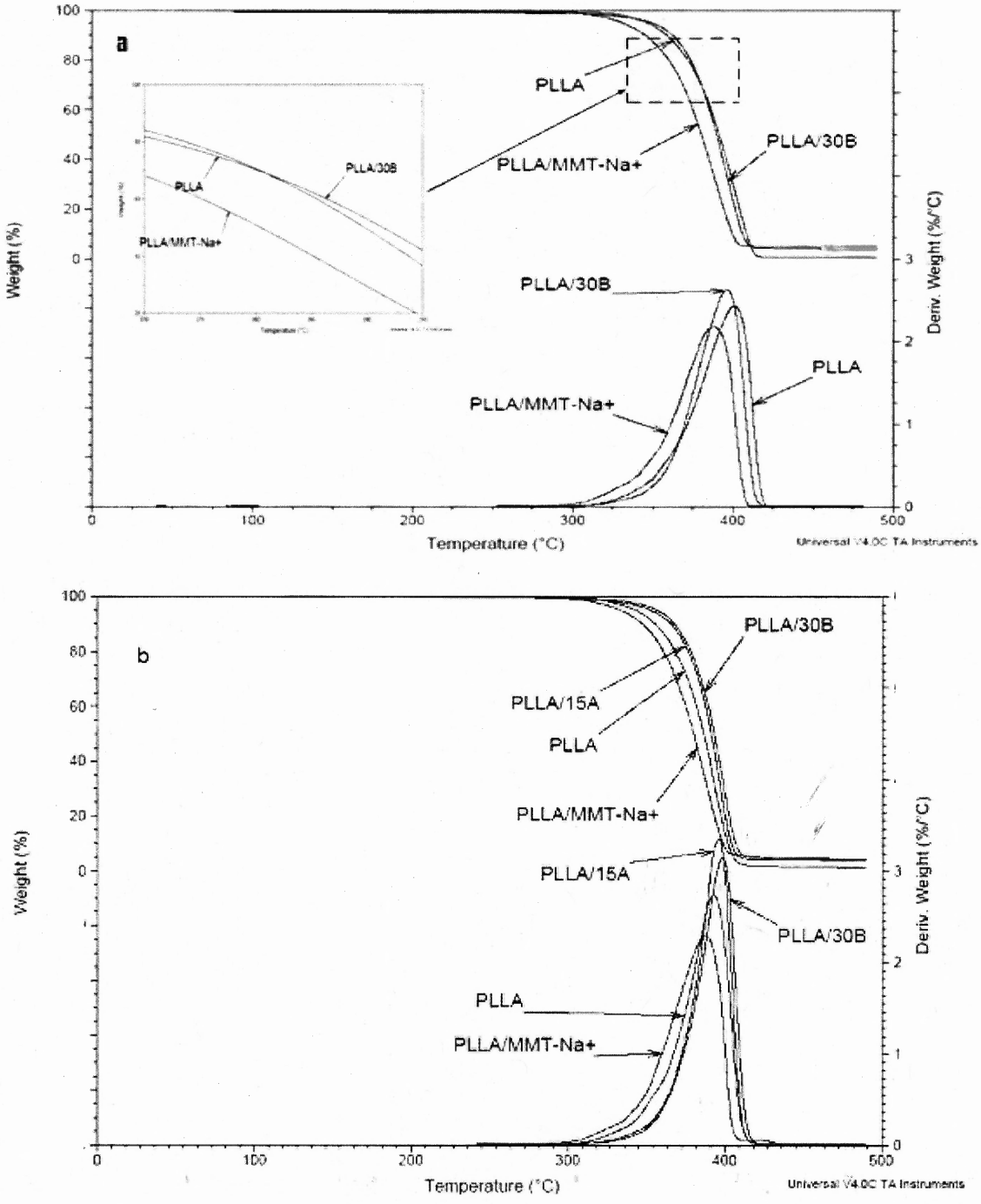

Figure 5.16 TGA traces recorded at 20°C/min: (a) PLLA and its composites under nitrogen; (b) PLLA and its composites under air.

Table 5.5 Weight Loss of Unfilled Polymers and their Micro- and Nano Composites at a heating rate of 20°C/min

Sample	Nitrogen Atmosphere		
	% Weight Loss Temperature (°C)		
	T_{10} (°C)	T_{50} (°C)	T_p (°C)
PLLA	358	391	401
PLLA/MMT-Na^+	345	380	388
PLLA/30B	363	390	397
PLLA/15A	364	392	398
PDLLA	363	390	399
PDLLA/MMT-Na^+	349	381	389
PDLLA/30B	367	392	398
PDLLA/15A	369	393	400
Sample	Air Atmosphere		
	% Weight Loss Temperature (°C)		
	T_{10} (°C)	T_{50} (°C)	T_p (°C)
PLLA	355	387	394
PLLA/MMT-Na^+	346	379	388
PLLA/30B	367	393	400
PLLA/15A	366	391	397
PDLLA	363	390	395
PDLLA/MMT-Na^+	350	381	387
PDLLA/30B	371	395	400
PDLLA/15A	369	393	397

Figures 5.17 (a) and (b) show TGA traces and their derivatives for unfilled PLLA and its cationic and anionic clay composites obtained under nitrogen and air, respectively. In both cases, the thermal stability order is: unfilled polymers > polymer/MMT-Na^+ (C) > polymer/MMT-Na^+ > polymer/HT(C) > polymer/HT. All fillers reduce the polymer thermal stability. The thermal stability of the calcined clay composites is slightly higher or much higher than that of their noncalcined counterpart since the water content in the calcined clay is much lower than that of noncalcined clay. For HT composites, during decomposition, a great amount of water and carbon dioxide will be released with the

formation of mixtures of metal oxides. In both HT and HT (C), these oxides may further accelerate polymer degradation (Figure 5.14) (Fan et al., 2004) (Motoyama et al., 2007). The thermal stability order among those polymer/clay composites is in good agreement with that of pure fillers.

The data in Table 5.6 and Figure 5.17 for the T_{10}, T_{50} and T_p, indicate that the thermal stabilities of unfilled PDLLA and its composites are higher than those of unfilled PLLA and its composites (except for HT(C) composites) under both nitrogen and air at T_{10}. These results agree with the isothermal degradation results. Please note that the difference in thermal stability between PDLLA/HT and PLLA/HT under air is much higher than that under nitrogen. It has already been found that *IV* increase with time for PDLLA/HT at 180°C isothermal degradation. Thus, it is reasonable to consider an oxidative chain extension/crosslinking reaction takes place between HT and PDLLA under air. The lowest thermal stability among the various fillers in Table 5.6 is observed in the HT composites as a result of the inherent low thermal stability of the filler. Note that the thermal stability of the anionic clay composites is higher under air than nitrogen and overall lower than that of the cationic clay composites since the residue of such combustion is the metallic oxides that impedes the burning process by reducing the oxygen supply to the fresh surface beneath (Miyata et al., 1978).

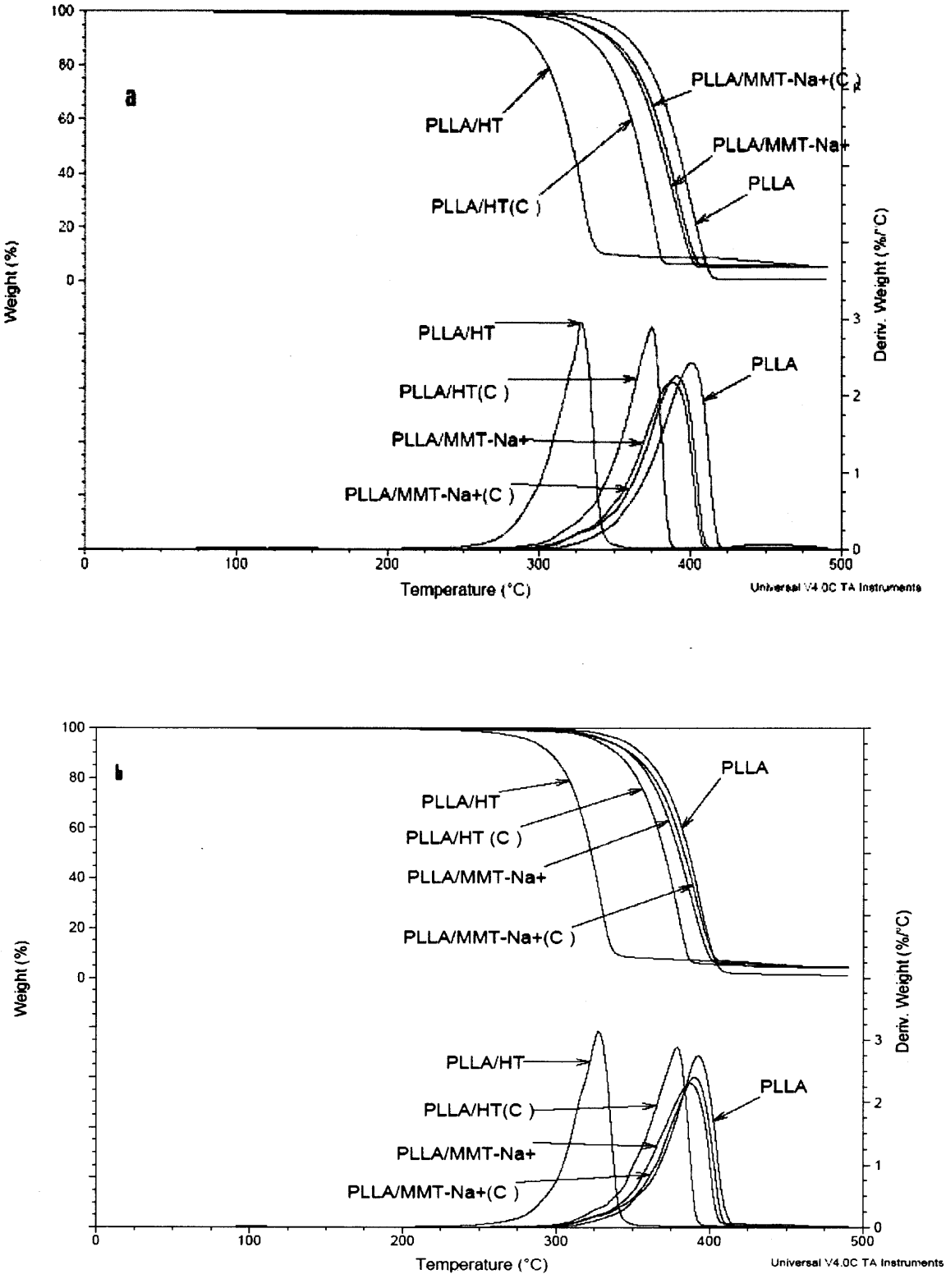

Figure 5.17 TGA and DTG traces recorded at 20°C/min: (a) PLLA and its composites under nitrogen; (b) PLLA and its composites under air.

Table 5.6 Weight Loss of Unfilled Polymers and their Cationic and Anionic Clay Composites at a heating rate at 20°C/min

Sample	Nitrogen Atmosphere		
	Weight Loss Temperature (°C)		
	T_{10} (°C)	T_{50} (°C)	T_p (°C)
PLLA	358	391	401
PLLA/MMT-Na^+ (C)	347	383	391
PLLA/MMT-Na^+	345	380	388
PLLA/HT	293	322	329
PLLA/HT(C)	322	365	376
PDLLA	363	390	399
PDLLA/MMT-Na^+ (C)	355	386	391
PDLLA/MMT-Na^+	349	381	389
PDLLA/HT	294	323	330
PDLLA/HT(C)	327	362	373
Sample	Air Atmosphere		
	Weight Loss Temperature (°C)		
	T_{10} (°C)	T_{50} (°C)	Tp (°C)
PLLA	355	387	394
PLLA/MMT-Na^+ (C)	348	383	392
PLLA/MMT-Na^+	346	379	388
PLLA/HT	296	322	329
PLLA/HT(C)	339	370	379
PDLLA	363	390	395
PDLLA/MMT-Na^+ (C)	353	383	391
PDLLA/MMT-Na^+	350	381	387
PDLLA/HT	309	336	342
PDLLA/HT(C)	333	366	375

5.3.2 Effect of Peak Temperatures

Figure 5.18 shows the peak temperatures change versus heating rate under nitrogen for unfilled PLLA and its micro- and nanocomposites. The peak temperature shifts to higher values with increasing heating rate. As shown by the different shapes of the regression liner in Figure 5.18. The increase in the peak temperatures with heating rate of the nano- and the microcomposite is faster than that of the unfilled polymer, particularly for the

microcomposite. Thus, the thermal stability difference between unfilled polymer and polymer composites decreases with increasing heating rate.

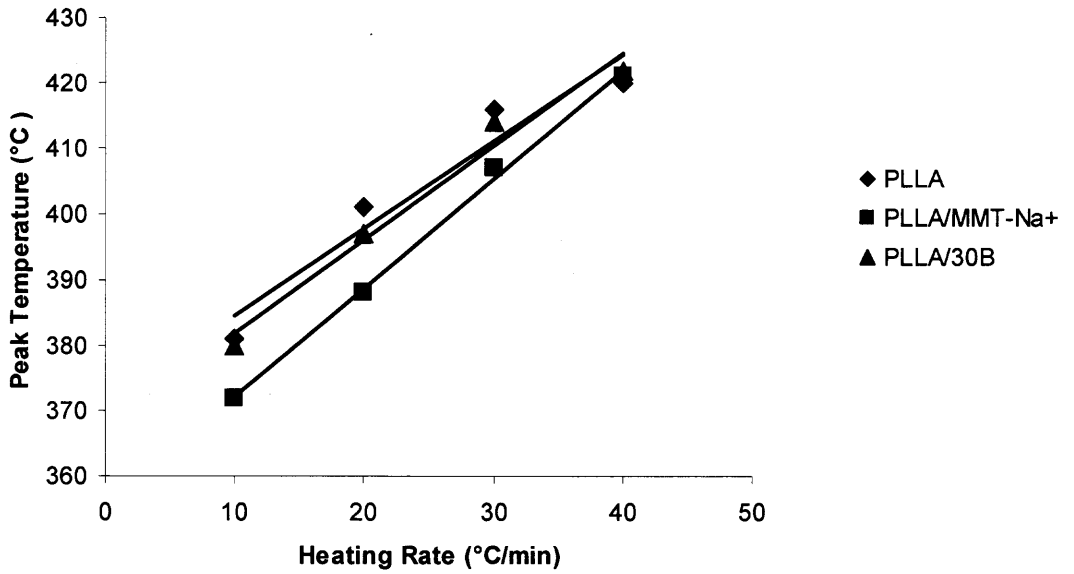

Figure 5.18 Peak temperature change at different heating rates for unfilled polymers PLLA and its micro and nano MMT composites.

Figure 5.19 shows the peak temperature change versus heating rate under nitrogen for unfilled PLLA and its cationic and anionic clay composites. The peak temperatures shift to higher values with increasing heating rate. The increase in the peak temperatures with heating rate for MMT-Na^+(C) and MMT-Na^+ composites is faster than that of the unfilled polymer. On the contrary, the increase in peak temperature of HT and HT (C) is almost the same as that of the unfilled PLLA. Thus, the anionic clays effect on the polymer degradation appears to be independent of the heating rate.

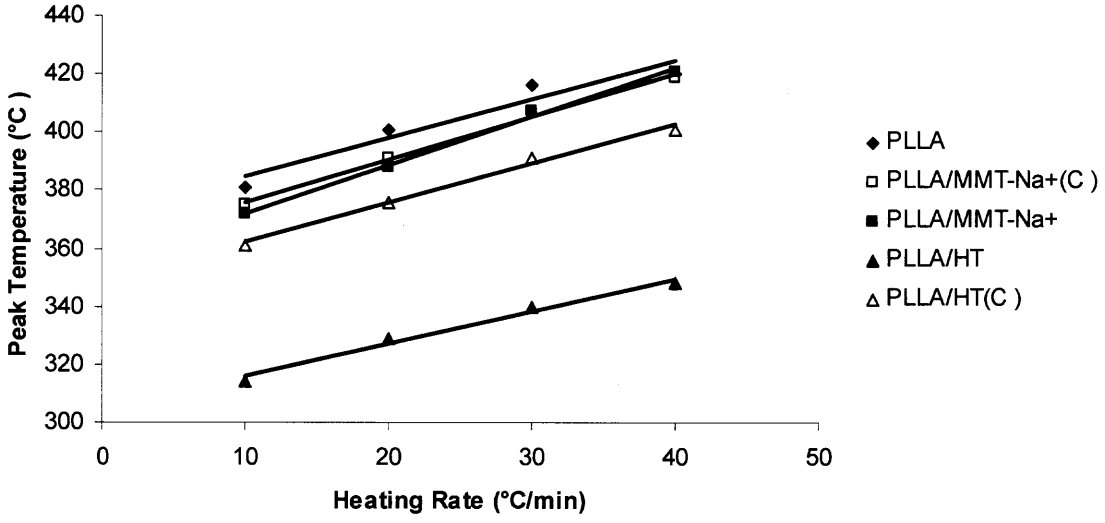

Figure 5.19 Peak temperature change at different heating rate for unfilled PLLA and its cationic and anionic clay composites.

5.3.3 Thermal Kinetic Analysis

In order to further understand the thermal experimental observations, a kinetic analysis may be performed. The Ozawa–Flynn–Wall method (Ozawa, 1965) is one of the integral methods that can determine the activation energy for the thermal degradation reaction without knowledge of the reaction order. It represents a relatively simple method for determining the activation energy directly from data of weight loss versus temperature obtained at several heating rates. Equation (5.3) is the Ozawa–Flynn–Wall equation after taking logarithms:

$$\log\varphi = \log\frac{AE_a}{g(\alpha)R} - 2.315 - \frac{0.4567E_a}{RT} \tag{5.3}$$

where φ is heating rate , A is the frequency factor or pre-exponential factor, R is the ideal gas constant, T is absolute temperature, α is the degree of conversion and E_a is the activation energy of the reaction. g(α) is the integral function of conversion. Thus, at a

given conversion, E_a is obtained by plotting log φ against 1/T. Usually, values of α between 0.1 and 0.9 and φ value from 10°C/min to 40°C/min with an interval of 10°C/min are selected to obtain the average E_a. The average activation energies ($\overline{E_a}$) and the average linear correlation coefficients ($\overline{r^2}$) of the unfilled polymers and polymer composites are listed in Tables 5.7 and 5.8. Activation energy for decomposition, E_a, of the unfilled polymers and their composites can also be calculated from the TGA curves by the integral method proposed by Horowitz and Metzger (Horowitz and Metzger, 1963) using the following equation:

$$\ln(\ln(1-\alpha)^{-1}) = \frac{E_a \theta}{RT_m^2} \qquad (5.4)$$

Where T_m is the temperature at maximum rate of weight loss, θ is (T - T_m). From the plots of $\ln[\ln(1-\alpha)^{-1}]$ versus θ, the activation energy (E_a) for decomposition can be determined from the slope of the straight line. E_a values calculated by this method are listed in Tables 5.7 and 5.8.

The results show that the activation energies of PDLLA and its composites are higher than those of PLLA and its composites. The activation energies of nanocomposites and unfilled polymers are higher than those of the microcomposites. Figure 5.20 shows that the activation energies of the 30B nanocomposites are higher than those of the unfilled polymer at the initial reaction stages (>60% weight remaining) and then become lower. These results support our experimental data listed in Table 5.3, Table 5.5 and Figure 5.16. Figure 5.20 shows that the dependence of E_a on % weight remaining for the microcomposite and the unfilled polymer can be separated in two distinct regions, the first region is the values up to 70% weight remaining, in which E_a shows a rapid increase

and the second (below 70%) in which E_a shows little change. This dependence of E_a on % weight remaining is an indication of a complex reaction with the participation of at least two different mechanisms. The 30B nanocomposite appears to have a different decomposition trend with only one region.

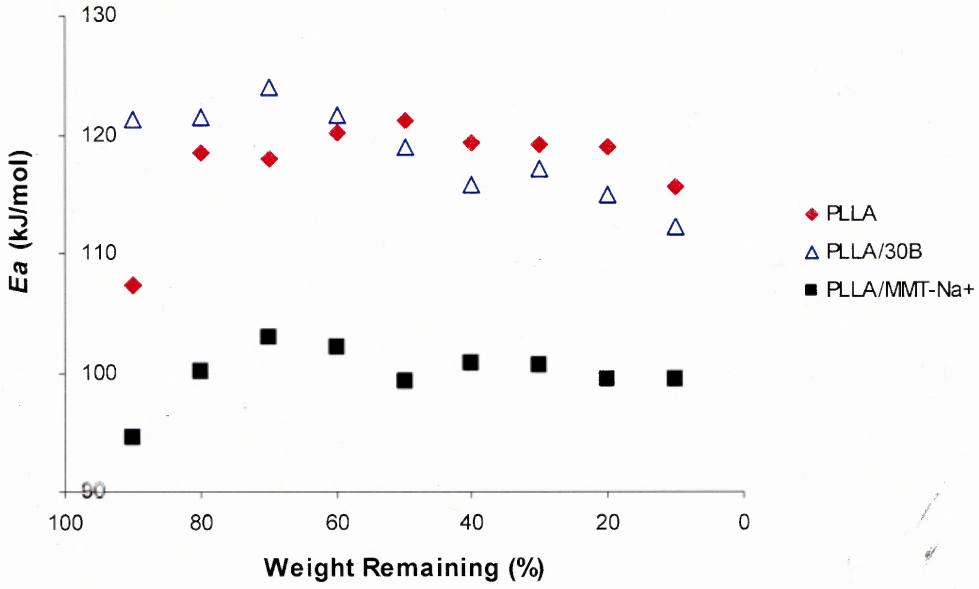

Figure 5.20 Dependence of the activation energy (E_a) on the weight remaining under nitrogen, as calculated by the Ozawa–Flynn–Wall's method for PLLA and different MMT composites.

Table 5.7 Activation Energy for Thermal Degradation of Unfilled Polymers and their Micro- and Nanocomposites

Sample	Nitrogen Atmosphere				
	Horowitz and Metzger*		Ozawa–Flynn–Wall		
	E_a (kJ/mol)	r^2	$\overline{E_a}$ (kJ/mol)	$\overline{r^2}$	$\overline{\ln A}$ (min^{-1})
PLLA	229	0.999	111	0.997	20.67
PLLA/MMT-Na^+	173	0.998	99	0.987	
PLLA/30B	263	0.998	118	0.989	
PLLA/15A	261	0.999	115	0.999	
PDLLA	258	0.999	124	0.991	
PDLLA/MMT-Na^+	205	0.999	114	0.963	
PDLLA/30B	287	0.999	122	0.981	
PDLLA/15A	296	0.999	124	0.990	
Samples	Air Atmosphere				
	Horowitz and Metzger*		Ozawa–Flynn–Wall		
	E_a (kJ/mol)	r^2	$\overline{E_a}$ (kJ/mol)	$\overline{r^2}$	$\overline{\ln A}$ (min^{-1})
PLLA	243	0.995	135	0.999	24.37
PLLA/MMT-Na^+	194	0.998	116	0.973	21.02
PLLA/30B	296	0.998	123	0.996	21.99
PLLA/15A	299	0.995	122	0.972	
PDLLA	283	0.998	149	0.999	
PDLLA/MMT-Na^+	229	0.999	124	0.982	
PDLLA/30B	313	0.999	130	0.998	
PDLLA/15A	324	0.997	130	0.991	

* Experimental results based on the data at heating rate 20°C/min

Table 5.8 also show that the activation energies under nitrogen of PDLLA and its composites are higher than those of PLLA and its composites, except for the HT(C) composites. In general, the activation energies of unfilled polymers are higher than those of polymer composites. These results support isothermal degradation and thermal stability experimental data listed in Tables 5.4 and 5.6. However, the activation energies for unfilled polymer and its polymer composites under air are higher than those of

unfilled polymer and polymer composites under nitrogen. This is in agreement with the TGA stability experimental results of only anionic clay composites. The differences in the activation energy are based on the different assumptions used as also shown in Section 5.3.4.

Table 5.8 Activation Energy for Unfilled Polymers and their Cationic and Anionic Clay Composites

Samples	Nitrogen Atmosphere				
	Horowitz and Metzger*		Ozawa–Flynn–Wall		
	E_a (kJ/mol)	r^2	$\overline{E_a}$ (kJ/mol)	$\overline{r^2}$	$\overline{\ln A}$ (min^{-1})
PLLA	229	0.999	111	0.997	20.67
PLLA/MMT-Na^+	173	0.998	99	0.987	
PLLA/MMT-Na^+ (C)	196	0.996	113	0.978	19.69
PLLA/HT	201	0.996	116	0.980	22.76
PLLA/HT(C)	221	0.987	111	0.976	19.74
PDLLA	258	0.999	124	0.991	21.54
PDLLA/MMT-Na^+	205	0.999	114	0.963	
PDLLA/MMT-Na^+(C)	228	0.998	131	0.991	
PDLLA/HT	248	0.991	107	0.995	
PDLLA/HT(C)	212	0.987	111	0.986	
Samples	Air Atmosphere				
	Horowitz and Metzger*		Ozawa–Flynn–Wall		
	E_a (kJ/mol)	r^2	$\overline{E_a}$ (kJ/mol)	$\overline{r^2}$	$\overline{\ln A}$ (min^{-1})
PLLA	243	0.995	135	0.999	24.37
PLLA/MMT-Na^+	194	0.998	116	0.973	21.02
PLLA/MMT-Na^+(C)	214	0.994			
PLLA/HT	221	0.993			
PLLA/HT(C)	234	0.991			
PDLLA	283	0.998	149	0.999	
PDLLA/MMT-Na^+	229	0.999	124	0.982	
PDLLA/MMT-Na^+ (C)	229	0.999			
PDLLA/HT	249	0.987			
PDLLA/HT(C)	222	0.990			

* Experimental results based on the data at heating rate 20°C/min

5.3.4 Thermal Kinetics Model Fitting

A fitted model benefits us to further understand the thermal stability mechanism. This fitted model can be separated into two stages. In the first stage, a general chemical reaction a(s) $\longrightarrow$ b(s) + d(g) was set up. The chemical reaction rate for b can be determined as follows (Dabrowski et al., 2000):

$$\frac{d[\mathrm{b}]}{dt} = k' f'([\mathrm{a}]) \tag{5.5}$$

$$[\mathrm{b}] = [\mathrm{a}_0](1-\alpha) \tag{5.6}$$

$[a_0]$ is the initial concentration of a, [a] is the concentration of a at time t, $f'([a])$ is a function of a and k' is the rate constant.

$$f'([\mathrm{a}]) = f([\alpha]) \tag{5.7}$$

where α is the fraction of a decomposed at time t, k' is the rate constant, and f(α) is a function of α.

$$\frac{d\alpha}{dt} = kf(\alpha) \tag{5.8}$$

$$\text{where } k = -\frac{k'}{[a_0]} \tag{5.9}$$

k obeys an Arrhenius relationship as:

$$k = A\exp(-E_a / RT) \tag{5.10}$$

where A is frequency factor, and E_a is the activation energy of the reaction.

The heating rate, φ, is defined as:

$$\varphi = \frac{dT}{dt} \tag{5.11}$$

Combining equations (5.8), (5.10) and (5.11) and then separating the variables, rearranging and integrating, we can write the following equation:

$$\int_0^{\alpha} \frac{d\alpha}{f(\alpha)} = \frac{A}{\varphi} \int_0^{T} \exp(-E_a / RT) dT \tag{5.12}$$

Now, we make the following assumption

$$f(\alpha) = (1-\alpha)^n \tag{5.13}$$

Where n is the reaction order. Substituting equation (5.13) into equation (5.12) and based on the Coats–Redfern integral method (Coats and Redfern, 1964), the following equation can be obtained

$$\frac{1-(1-\alpha)^{1-n}}{1-n} = \frac{ART^2}{\varphi E_a}\left(1-\frac{2RT}{E_a}\right)\exp(-E_a / RT) \tag{5.14}$$

Note that this is an approximation of the Arrhenius integral since an analytical expression is not available.

The value of n can be determined by the Kissinger method (Kissinger, 1957):

$$n = 1.26\sqrt{s} \tag{5.15}$$

where s is the shape index of the differential thermal analysis (DTA) curve for nonisothermal dynamic degradation.

According to the Freeman–Carroll (Freeman, 1958) method, the average value $\overline{\ln A}$ is obtained based on the value of $\ln A$ in the interval $0.1<\alpha<0.9$.

$$\ln\frac{d\alpha}{dt} = \ln A + n\ln(1-\alpha) - \frac{E_a}{RT} \tag{5.16}$$

In the second stage, W, the apparent weight fraction remaining after the first stage has been completely used, and:

$$\alpha = 1\text{-}W \tag{5.17}$$

The s value of the shape index of DTA curves is close to 0; then according to the Kissinger method, n is also close to 0. The E_a in equation (5.16) was selected from the average values of Ozawa–Flynn–Wall method (Tables 5.7 and 5.8) and the A value was estimated from the Freeman–Carroll method. Substituting E_a, n and A values (from $\overline{\ln A}$) into equation (5.14), mathematical equations including only α and T are obtained. The final results obtained by using the same kinetic parameters reported in Table 5.7, are shown in Figures 5.21 and 5.22. Model fitting results compare well with experimental data at different heating rates for unfilled PLLA under nitrogen (Figure 5.21 (b)). The model is also good for matching data of unfilled PLLA and its microcomposites under air at 20°C/min in the first stage when $\alpha<0.95$ (weight remaining <0.05) (Figure 5.21 (a) and (b)). However, this model fitting method is unsatisfactory for the nanocomposite (PLLA/30B) at 20°C/min under air (Figure 5.22 (a)). This can be attributed to char that caused heat and/or mass transfer problems affecting temperature control. Another factor of the discrepancy between the experimental data and the model may be attributed to the effect of 30B on the activation energy change (Figure 5.20) that could result in a different kinetic reaction order.

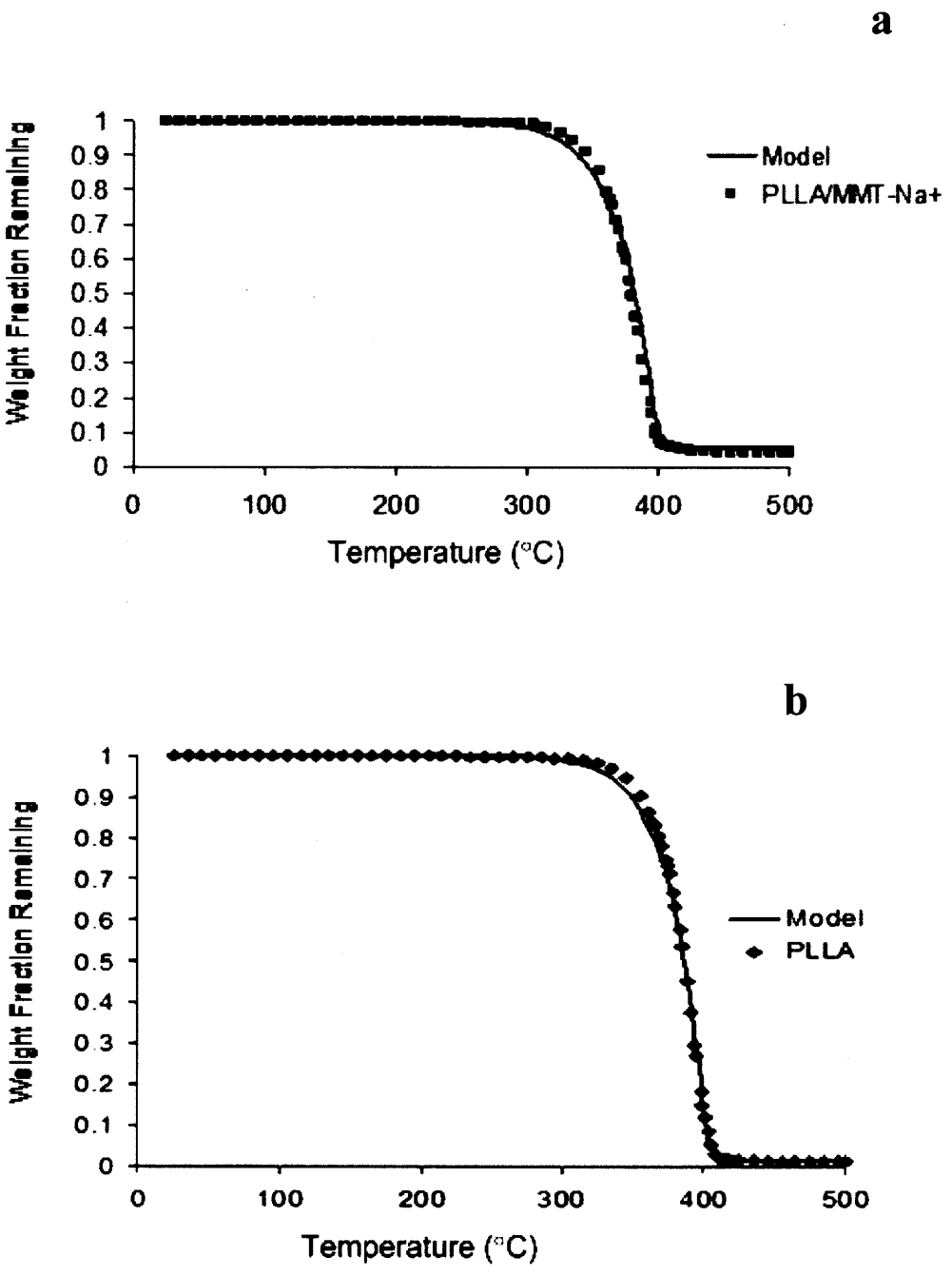

Figure 5.21 TGA Model fitting (a) PLLA/MMT-Na^+ at heating rate 20°C/min under air; (b) PLLA at heating rate 20°C/min under air.

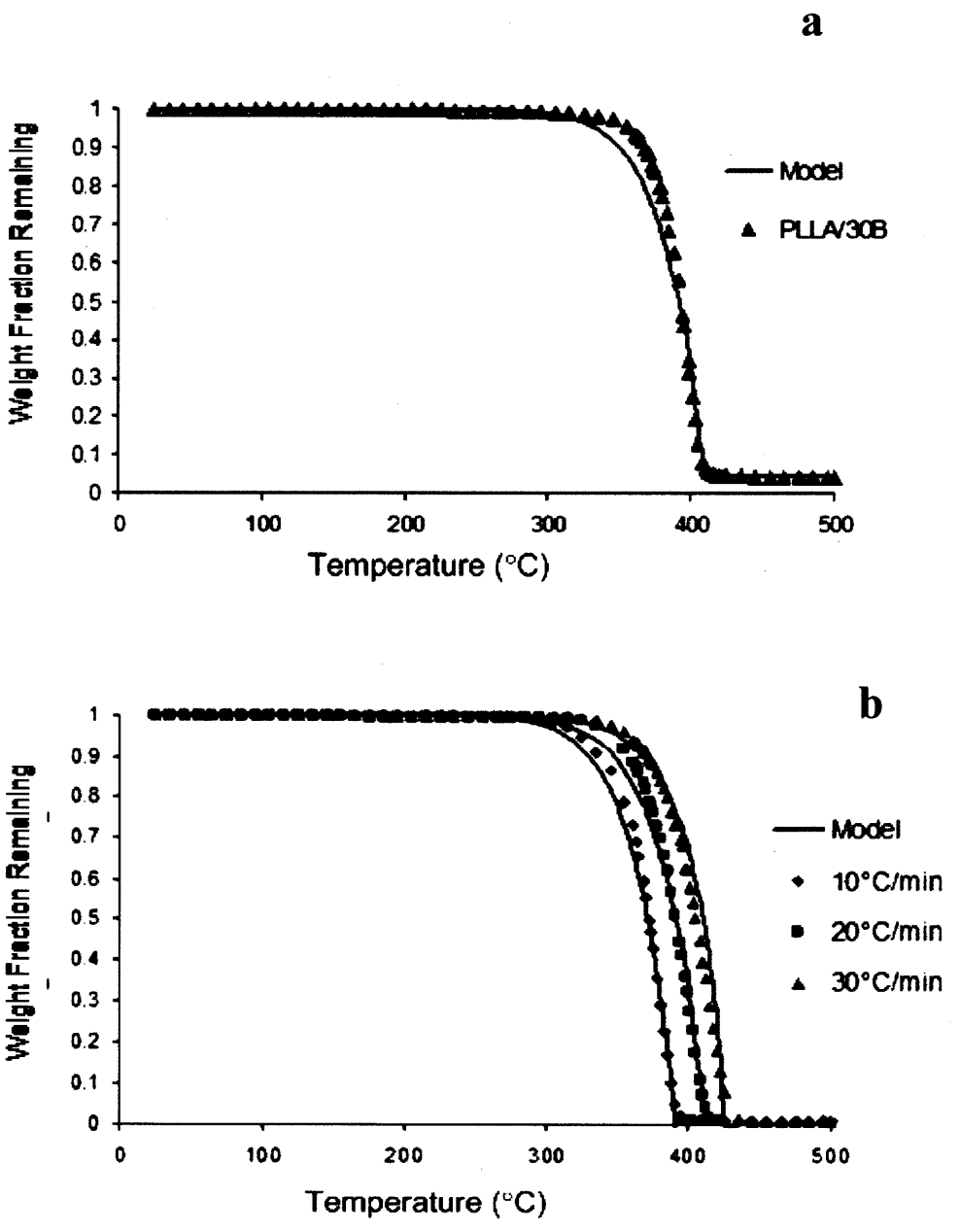

Figure 5.22 TGA Model fitting (a) PLLA/30B at heating rate 20°C/min under air; (b) PLLA at different heating rate (10, 20 and 30°C/min) under nitrogen.

The final results obtained by using the kinetic parameters reported in Table 5.8, are shown in Figure 5.23. Model fitting results compared well with experimental data at different heating rates for unfilled PDLLA under nitrogen (Figure 5.23(a)). The model is

also good for matching data of unfilled PLLA and its microcomposites under nitrogen at 20°C/min in the first stage when $\alpha<0.9$ (weight remaining >0.1) (Figure 5.23 (b)). Thus, it can be concluded that both cationic and anionic clays would not change the polymer degradation reaction order.

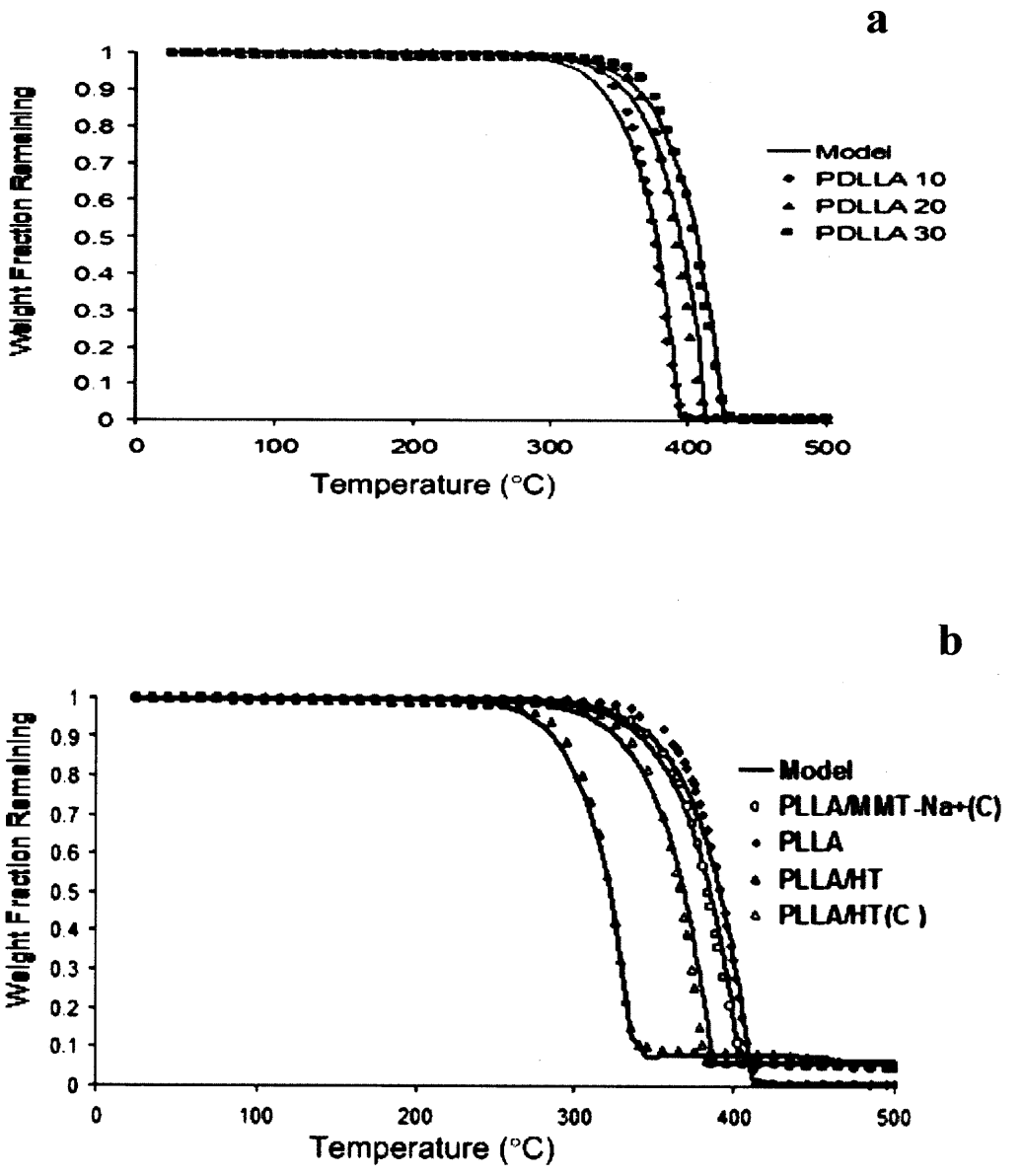

Figure 5.23 TGA model fitting: (a) PDLLA at different heating rate (10, 20 and 30°C/min) under nitrogen; (b) PLLA and its composites at heating rate 20°C/min under nitrogen.

5.4 Hydrolytic Degradation

5.4.1 Effects of Polymer Type

The rate constants k_2^* for the *IV* autocatalyzed model were determined by linear regression from plots of $\ln(IV/IV_0)$ versus time (equation 2.9) at 50 °C in Figures 5.24, 5.25 (MMT and nanocomposites) and Figure 5.28 (MMT and HT calcined or noncalcined clay composites). The *IV*s of the unfilled polymers and the polymers in all composites decrease exponentially with degradation time throughout the experimental time period. The apparent degradation rate constants and the corresponding r^2 correlation coefficients are shown in Tables 5.9 and 5.11. The high correlation coefficients support the validity of the autocatalytic degradation mechanism. Based on information from Figures 5.24 and 5.25 and Tables 5.10 and 5.12, the degradation rate constants decrease in the following order: unfilled PDLLA and its composites > unfilled PLAB blend and its composites > unfilled PLLA and its composites >annealed PLLA and its composites; note that the initial M_{v0} values of the neat amorphous polymer and the polymer in its composites are higher than those of the semicrystalline polymer and its composites (Tables 5.9 and 5.11).

An increase in the number of crystalline domains decreases permeation, increases tortuosity and reduces water absorption. The latter is related to reduction in mobility of polymer chains at higher crystallinity and free volume reduction that would hinder water attack. The formation of additional crystalline regions through isothermal annealing would further inhibit the penetration of water molecules. Plots of water uptake vs. time (Figures 5.26 and 5.27) during the 28-day degradation period support these results. It is shown that the water uptake of the unfilled PDLLA amorphous polymer and its composites is higher than that of the unfilled PLLA semicrystalline polymer and its

composites and much higher than the water uptake of the annealed samples. These results are supported with data from Tables 5.10 and 5.12 indicating that the final/initial *IV* ratios for the semicrystalline PLLA and its composites are higher than those of the equivalent PDLLA and PLAB polymers and their composites, at all degradation temperatures.

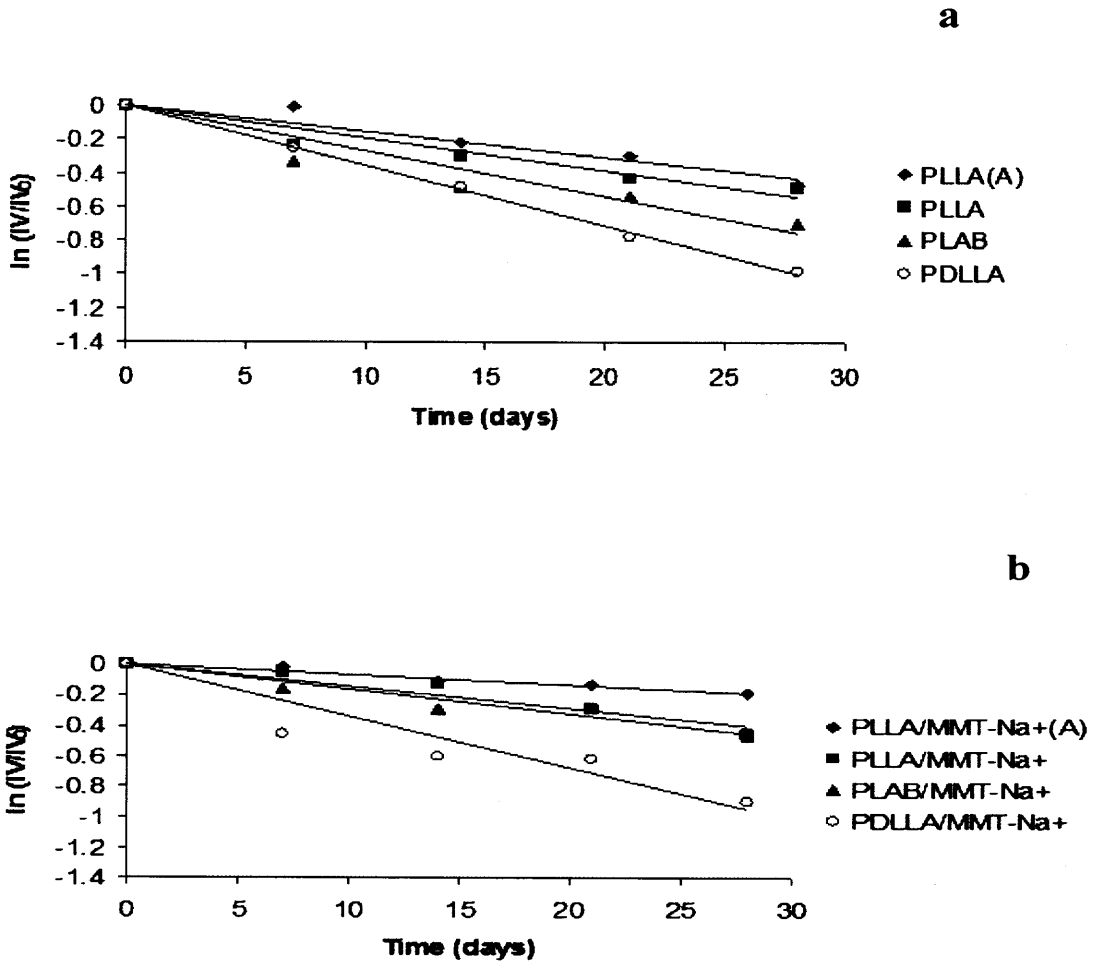

Figure 5.24 Autocatalyzed degradation model at 50°C: (a) unfilled polymers; (b) polymer microcomposites.

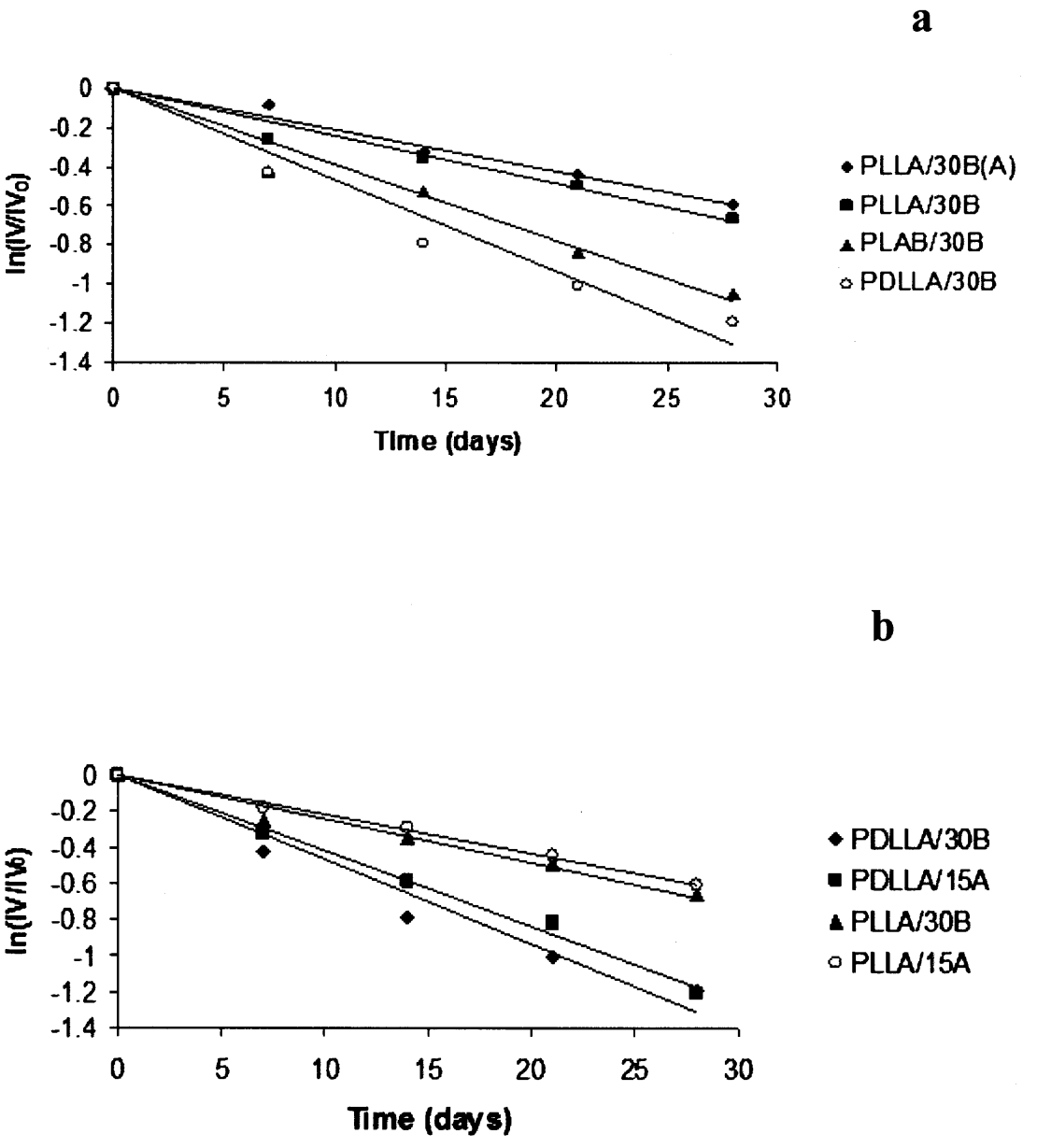

Figure 5.25 Autocatalyzed degradation model at 50°C: (a) polymer nanocomposites (30B); (b) PDLLA/30B, PDLLA/15A, PLLA/30B and PLLA/15A.

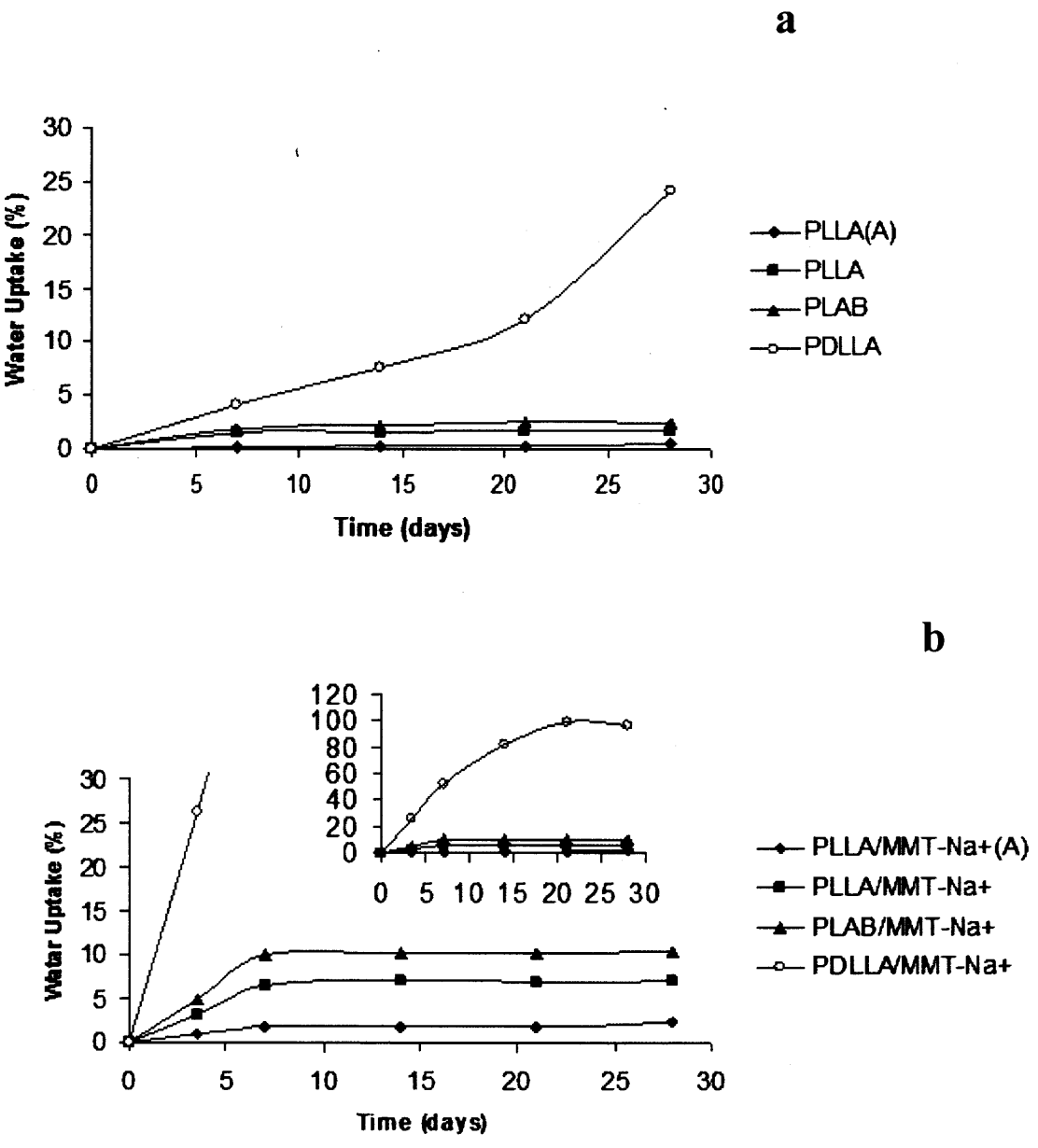

Figure 5.26 Water uptake at 50°C: (a) unfilled polymer; (b) polymer microcomposites ($MMT\text{-}Na^{+}$).

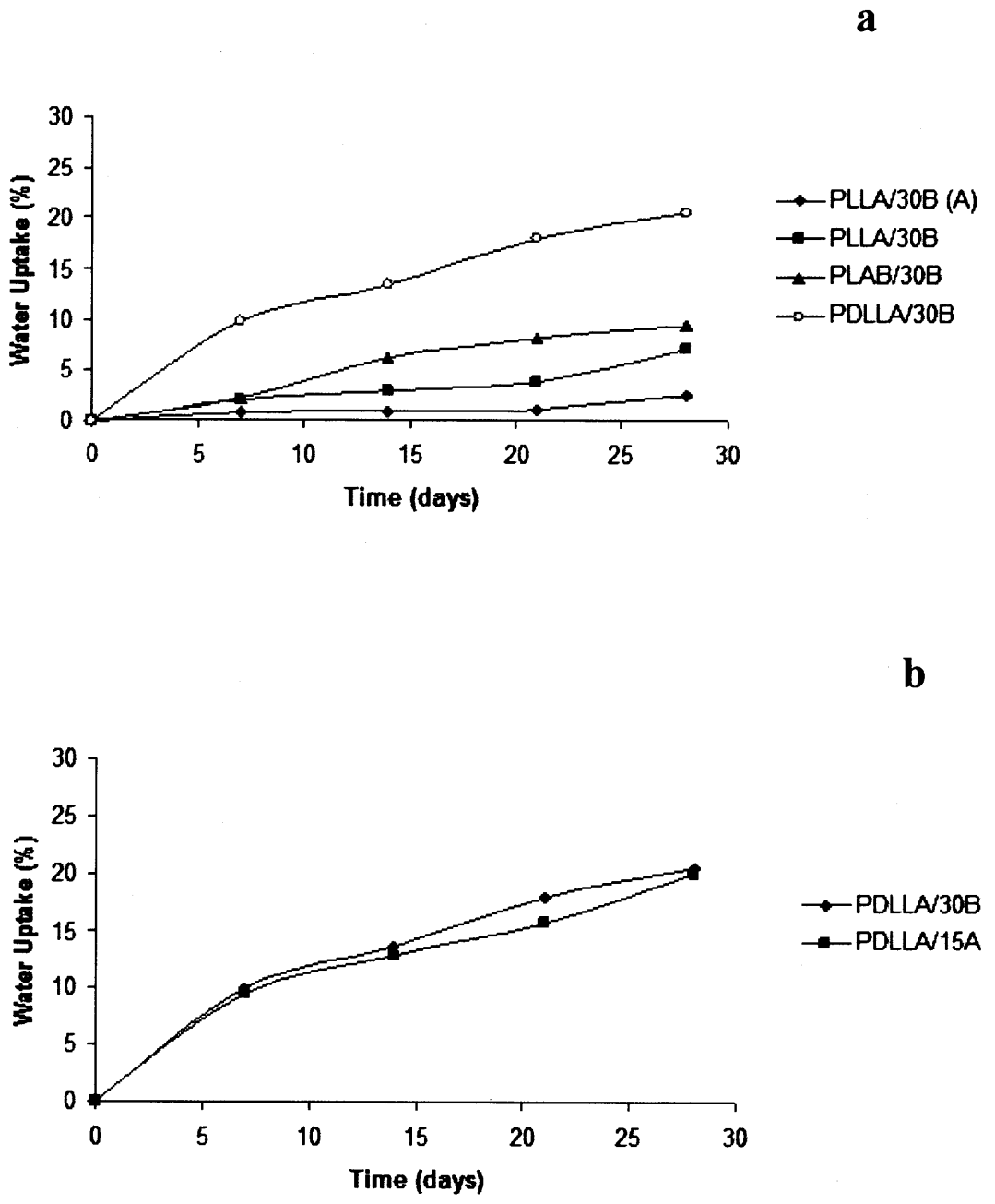

Figure 5.27 Water uptake at 50°C: (a) polymer nanocomposites (30B); (b) PDLLA/30B and PDLLA/15A.

Table 5.9. Autocatalyzed Hydrolytic Degradation Rate Constants for Unfilled Polymers and their MMT Micro and Nanocomposites at Different Test Temperatures

Sample	Degradation Rate Constant, k_2^*, day^{-1} (r^2)		
	50°C	60°C	70°C
PLLA	0.0194 (0.89)	0.0843 (0.98)	0.200 (0.92)
PLLA (A)*	0.0154 (0.92)	N/A	N/A
PLLA/MMT-Na^+	0.0143 (0.94)	0.0639 (0.96)	0.180 (0.99)
PLLA/MMT-Na^+ (A)*	0.00670 (0.95)	N/A	N/A
PLLA/30B	0.0243 (0.97)	0.110 (0.95)	0.249 (0.98)
PLLA/30B(A)*	0.0211 (0.98)	N/A	N/A
PLLA/15A	0.0216 (0.99)	0.0992 (0.97)	0.225 (0.98)
PDLLA	0.0356 (1.00)	0.183 (0.98)	0.309 (0.98)
PDLLA/MMT-Na^+	0.0338 (0.83)	0.169 (0.95)	0.296 (0.89)
PDLLA/30B	0.0466 (0.95)	0.194 (0.96)	0.356 (0.87)
PDLLA/15A	0.0420 (0.99)	0.183 (0.95)	0.350 (0.82)
PLAB	0.0271 (0.88)	N/A	N/A
PLAB/MMT-Na^+	0.0163 (0.92)	N/A	N/A
PLAB/30B	0.0389 (0.96)	N/A	N/A

* Annealed

Table 5.10 Initial IV_0 and M_{v0}, Final/Initial IV Ratios and Final Solution pH* Values after Degradation for Unfilled Polymer and their MMT Micro and Nanocomposites at Selected Temperatures and Times (days)

Sample			50°C		60°C		70°C	
	IV_0	M_{v0}	IV_{28}/IV_0	pH_{28}	IV_{15}/IV_0	pH_{15}	IV_9/IV_0	pH_9
PLLA	1.51	51980	0.62	7.72	0.22	7.49	0.13	4.47
PLLA/MMT-Na^+	1.27	41010	0.64	7.79	0.38	7.82	0.21	6.99
PLLA/30B	1.36	45040	0.51	7.54	0.21	5.83	0.11	4.44
PLLA/15A	1.14	35370	0.58	7.38	0.29	3.9	0.14	3.07
PDLLA	1.2	68430	0.38	7.52	0.08	2.73	0.08	2.55
PDLLA/MMT-Na^+	0.93	49150	0.41	7.27	0.1	2.72	0.1	2.52
PDLLA/30B	1.15	64750	0.3	7.2	0.07	2.66	0.06	2.48
PDLLA/15A	1.07	58970	0.3	6.44	0.08	2.68	0.07	2.38
PLAB	1.45	N/A**	0.5	7.78	N/M***	N/M***	N/M***	N/M***
PLAB/MMT-Na^+	1.11	N/A**	0.63	7.9	N/M***	N/M***	N/M***	N/M***
PLAB/30B	1.25	N/A**	0.35	7.46	N/M***	N/M***	N/M***	N/M***

* Initial pH 10.5

** *B* and *v* values from Eq. (2.8) not available for the blend

*** Not measured

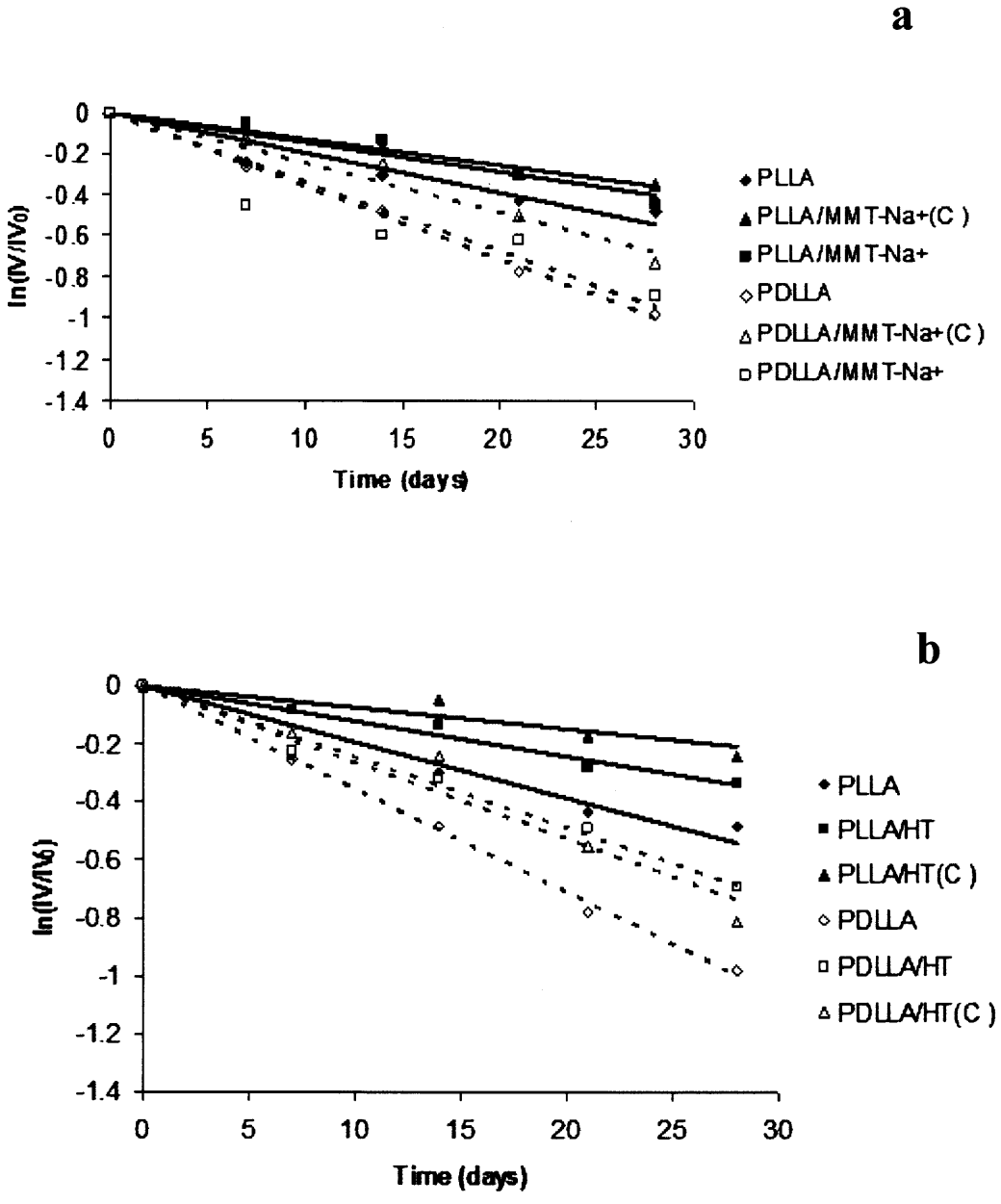

Figure 5.28 Autocatalyzed degradation model at 50°C: (a) unfilled polymers and their MMT-Na^+ and MMT-Na^+(C) composites; (b) unfilled polymers and their HT and HT(C) composites.

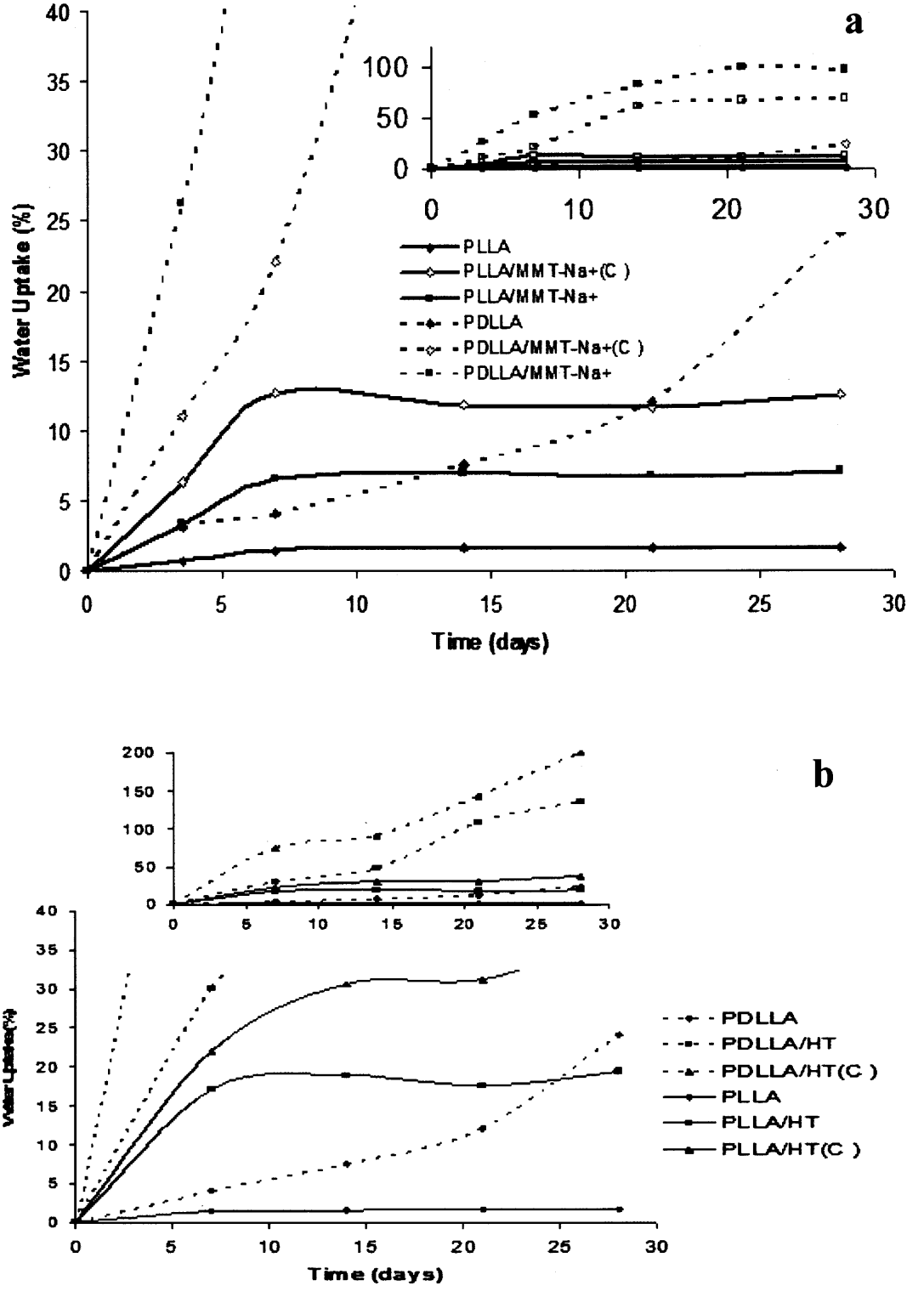

Figure 5.29 Water uptake at 50°C: (a) unfilled polymers and their MMT-Na^+ and MMT-Na^+(C) composites; (b) unfilled polymers and their HT and HT(C) composites.

Table 5.11 Autocatalyzed Hydrolytic Degradation Rate Constants for Unfilled Polymers and their Cationic and Anionic Clay Composites at Different Test Temperatures

Sample Type	Degradation Rate Constant, k_2^*, day^{-1} (r^2)		
	50°C	60°C	70°C
PLLA	0.0194 (0.89)	0.0843 (0.98)	0.200 (0.92)
PLLA/MMT-Na^+	0.0143 (0.94)	0.0639 (0.96)	0.180 (0.99)
PLLA/MMT-Na^+(C)	0.0127 (0.99)	0.0593 (0.98)	0.195 (0.99)
PLLA/HT	0.0121 (0.97)	0.0574 (0.97)	0.162 (0.94)
PLLA/HT(C)	0.0075 (0.83)	0.0418 (0.99)	0.125 (0.91)
PDLLA	0.0356 (1.00)	0.183 (0.98)	0.309 (0.98)
PDLLA/MMT-Na^+	0.0338 (0.83)	0.170 (0.95)	0.296 (0.89)
PDLLA/MMT-Na^+(C)	0.0241 (0.96)	0.174 (0.96)	0.306 (0.96)
PDLLA/HT	0.0244 (0.99)	0.116 (1.00)	0.219 (0.88)
PDLLA/HT(C)	0.0264 (0.95)	0.115 (0.95)	0.230 (0.92)

Table 5.12 Intrinsic Viscosity Change (*IV*) and Final Solution pH* Value after Degradation for Unfilled Polymer and their Cationic and Anionic Clay Composites at Selected Temperatures and Times

Sample	IV_0	M_{v0}	50°C		60°C		70°C	
			IV_{28}/IV_0	pH_{28}	IV_{15}/IV_0	pH_{15}	IV_9/IV_0	pH_9
PLLA	1.51	51980	0.62	7.72	0.22	7.49	0.13	4.47
PLLA/MMT-Na^+	1.27	41010	0.64	7.79	0.38	7.82	0.21	6.99
PLLA/MMT-Na^+(C)	1.3	42340	0.71	8.39	0.40	7.54	0.18	5.35
PLLA/HT	1.05	31600	0.71	8.10	0.44	7.83	0.26	4.28
PLLA/HT(C)	1.39	46410	0.78	9.16	0.53	7.79	0.31	5.77
PDLLA	1.2	70860	0.38	7.52	0.08	2.73	0.08	2.55
PDLLA/MMT-Na^+	0.93	50890	0.41	7.27	0.1	2.72	0.1	2.52
PDLLA/MMT-Na^+(C)	1.04	58840	0.48	7.72	0.09	2.88	0.08	2.70
PDLLA/HT	0.9	48770	0.50	7.04	0.18	4.20	0.18	3.36
PDLLA/HT(C)	1.08	61790	0.44	7.16	0.17	4.33	0.16	3.56

* Initial pH 10.5

5.4.2 Effects of Filler Type

Data in Figures 5.24 and 5.25 and Table 5.9 show that the degradation rate constants of the nanocomposites are significantly higher than those of the unfilled polymers. By contrast, the degradation rate constants of the microcomposites are lower or slightly lower than those of the unfilled polymers. Thus, high filler dispersion (nanoscale) promotes polymer degradation whereas low degree of dispersion (microscale) appears to reduce polymer degradation, in agreement with the ratios of final/initial *IV*s at the three degradation temperatures listed in Table 5.10. Since the water uptake (Figures 5.26 and 5.27) of the nanocomposites is higher or somewhat higher than that of the unfilled polymers, the higher volume of the polymer matrix in contact with the nanoclay edges and surface would result in easier water attack of the polymer chains as compared to the unfilled polymer. Note that although the water uptake of the microcomposites is much higher than that of both nanocomposites and unfilled polymers (Figures 5.26 and 5.27), water may be adsorbed in the gaps between the layers of the MMT-Na^+, as result, they expand as much as several times their original thickness (Karaborni et al., 1996) due to the strong hydrating ability of the Na^+, thus, reducing the amount of water in the polymer matrix.

Data from Table 5.10 also show a significant reduction in the pH of the hydrolysis medium for all samples due to the formation of polylactic acid oligomers/monomer. With respect to PLLA, it is shown that, by contrast to the organophilic 30B and 15A, the presence of the alkaline hydrophilic MMT-Na^+ (pH 9~10) yields a final pH higher than that of the unfilled matrix, possibly through reduction of the autocatalytic effect via neutralization of the formed carboxylic groups (Meer et al., 1996). This trend is also

observed for the PLAB polymer and its composites. However, it does not appear to be the case for the PDLLA/MMT-Na^+ where the resultant pH of the medium is close to that of the unfilled matrix, but still higher than that of the PDLLA nanocomposites at all temperatures. This may be related to the absence of crystallinity in PDLLA vs. PLLA that results in earlier release of oligomers/monomer to the hydrolysis medium. Nanofillers (30B and 15A) that are treated with mostly hydrophobic organic modifiers appear to have little or no neutralization ability. Our experimental results with nanocomposites are in agreement with the conclusions of Ray et al. (2003) and Paul et al (2005). However, the present results of microcomposites differ from those of Paul et al. (2005).

Comparison of the effects of 30B and 15A on the rate constants, based on hydrophilicity and filler dispersion differences, can explain the slightly lower rate constants observed for the PLLA/15A and PDLLA/15A vs. the equivalent composites containing 30B. It is reasonable to consider the slight differences in their water uptake (Figure 5.27b) to explain the small differences in their degradation rate, in agreement with the results of Paul et al. (2005).

Data in Figure 5.28 and Table 5.11 show that the degradation rate constants of the cationic and anionic clay composites are significantly or slightly lower than those of the unfilled polymers. Thus, both cationic and anionic clays (calcined and noncalcined) reduce polymer degradation, in agreement with the ratios of final/initial *IV*s at the three degradation temperatures listed in Table 5.12. The case of cationic clay composites and their water uptake behavior (Figure 5.29) has been mentioned earlier in the beginning of this section. HT composites behave in a different manner by absorbing water at the filler surface due to the presence of surface Mg^{2+} or Al^{3+} ions. Since HT(C) can bind more

cations strongly to the clay surface after heat treatment (Chorom and Rengasamy, 1996), it can absorb much more water on its surface; also, its porous structure would also facilitate water absorption. Thus, the presence of the both cationic and anionic clay would reduce the amount of water in the polymer matrix.

Data from Table 5.12 also show a significant reduction in the pH of the hydrolysis medium for all samples due to the formation of polylactic acid oligomers/monomer. With respect to polymers, it is shown in most cases, that the presence of the MMT and HT alkaline hydrophilic clays yields a final pH higher than that of the unfilled matrix, possibly through reduction of the autocatalytic effect via neutralization of the formed carboxylic groups (Meer and Wolke, 1996).

The lower rate constants observed for the anionic clay composites vs. the equivalent cationic clay composites can be explained based on the higher alkalinities of the HT and HT(C) (Auerbach et al., 2004) These results are also supported with data from Table 5.12 indicating that the final/initial *IV* ratios for the anionic clay composites are, in general, higher than those of the cationic clay composites at all degradation temperatures.

With respect to PLLA, the presence of the calcined clays yields a lower degradation rate compared to the noncalcined clays, except for PLLA/MMT-Na^+(C) at 70°C. It is reasonable to consider that the higher pH value (10~11) of the calcined clays was generated by binding more cations strongly to the clay surface .after heat treatment (Chorom and Pengasamy, 1996). The EDX experimental results (no included) show the Al and Mg elemental contents for both MMT-Na^+ and HT composites increase on the surface by about 50% after calcinations. However, with respect to PDLLA, there are no

differences in the degradation rate constants between calcined and non-calcined composites due to the high water uptake of PDLLA; this would erase the structural differences between calcined and non-calcined clays because of the memory effect (Cavani et al., 1991).

Based on the initial intrinsic viscosity values listed in Tables 5.10 and 5.12 and the calculated rate constants of Tables 5.9 and 5.11, it appears that the degradation rate constants are independent of the initial polymer MW. Thus, it is evident that hydrolysis in the presence of fillers is a complex phenomenon depending on filler dispersion and type, water uptake, thermal history and the hydrating ability of fillers as well as their surface acidity.

5.4.3 Effects of Temperature

Tables 5.9 and 5.11 show results of accelerated degradation in the temperature range from 50°C to 70°C (T_g of polymers is around 60°C) As expected, the rate constants increase with increasing temperature since higher temperatures increase the diffusion rate of water and that of water-soluble oligomers. Note that the degradation rate constant significantly increases at 60°C (around T_g) since water molecules would be able to access the amorphous regions more easily, initiating faster hydrolytic chain scission (Weir et al., 2004). It should be noted that the exact location of the T_g may be below the assumed values of 58-60°C, continuously decreasing as a result of plasticization and/or loss of molecular weight Activation energies calculated from the plot of $\ln k_2^*$ vs 1/T from the Arrhenius-type relationship (Wise et al., 1995):

$$k_2^* = Ae^{-E_a/RT} \tag{5.18}$$

show high linear correlation coefficients (r^2) for both unfilled polymers and polymer composites (Figures 5.30 and 5.31). This suggests that the degradation kinetics do not differ significantly above and below the assumed T_g of 58°C~60°C. The calculated activation energies of unfilled PLLA are in relative good agreement with the data of Weir et al. (2004), although the latter were obtained at different pH.

Usually, high activation energies indicate that degradation started with more difficulty and the degradation rate constants are more sensitive to temperature. As expected, the activation energies for the semicrystalline PLLA and its composites are higher than those for the amorphous PDLLA and its composites (Figures 5.30 and 5.31). The activation energies for the MMT-Na^+ microcomposites are also higher or slightly higher than those of the corresponding unfilled polymers and nanocomposites, (Figure 5.30) in agreement with the previously described differences in degradation rate constants

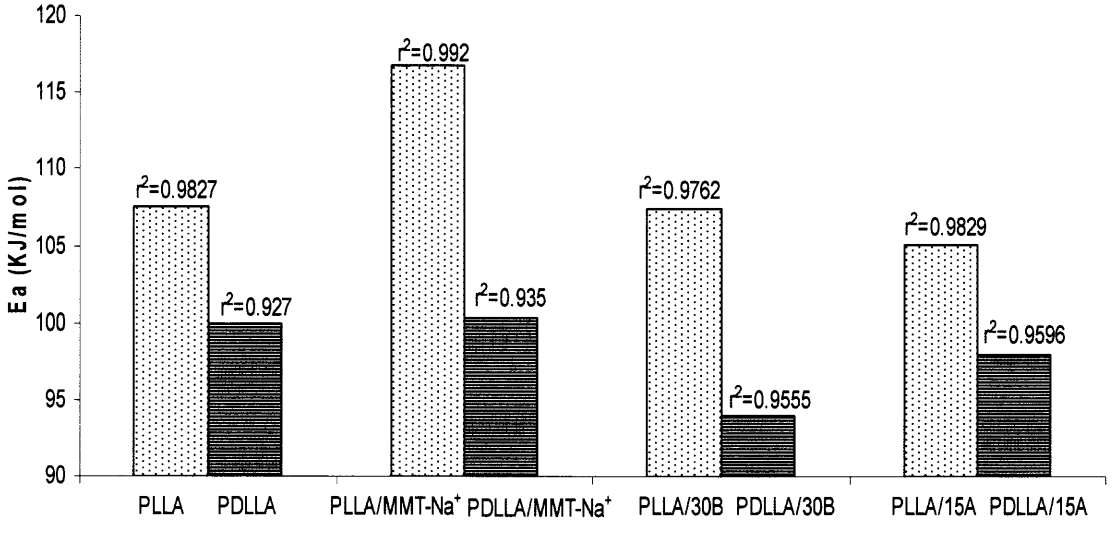

Figure 5.30 Hydrolytic degradation activation energies for PLLA, PDLLA and their micro and nanocomposites.

Compared to unfilled polymers (Figure 5.31), the activation energies of their cationic and anionic clay composites are higher (PLLA) or slightly higher (PDLLA) except for PDLLA/(HT(C)). In the case of PLLA, it is shown that the calcined clays yield higher activation energies than noncalcined clays. The overall results are in agreement with the previously described differences in the degradation rate constants.

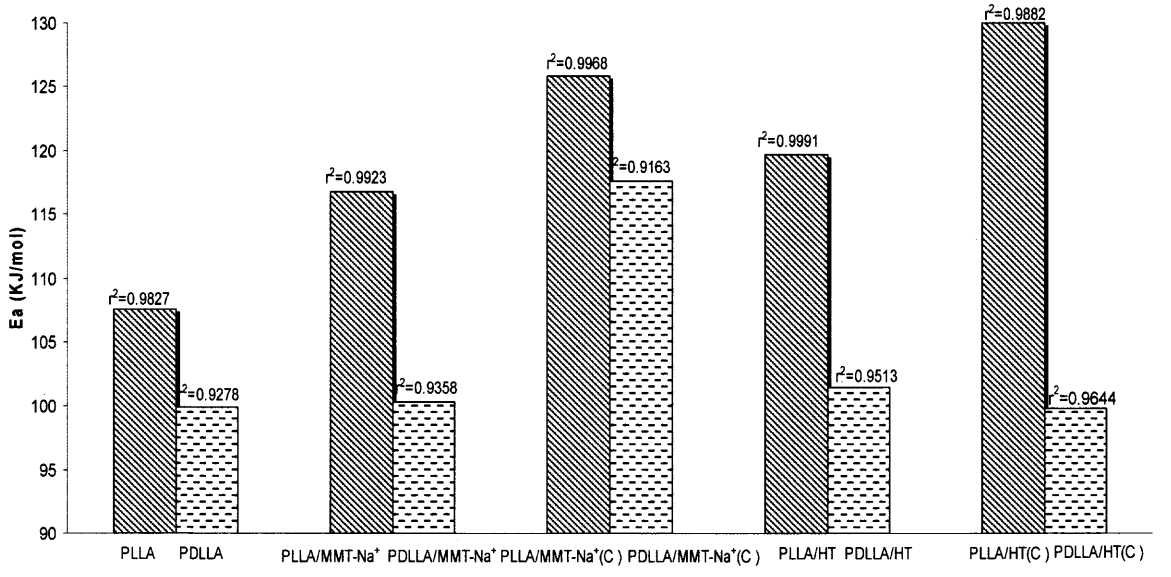

Figure 5.31 Hydrolytic degradation activation energies for PLLA, PDLLA and their cationic and anionic clay composites.

5.4.4 Morphological Changes

Figure 5.32 shows film cross-section surfaces of PLLA and its MMT micro- and nanocomposites after 28 days degradation at 50°C. Both the unfilled polymer and its microcomposite have a much lower concentration of pores over the entire film cross-section surface (Figures 5.32(a) and (b)) than either nanocomposite (Figures 5.32(c) and (d)). Since both unfilled polymer and polymer composites had no apparent pores over their entire surface (SEM micrographs not shown) it is confirmed that hydrolytic

degradation takes place in the bulk of the polymer. Compared to the nanocomposites, the degradation pores of the microcomposites and the unfilled polymer are larger and heterogeneous. Note that the differences in type and extent of filler dispersion responsible for the observed differences in pore size and dispersion suggest that polymer degradation starts at the interface between polymer matrix and fillers.

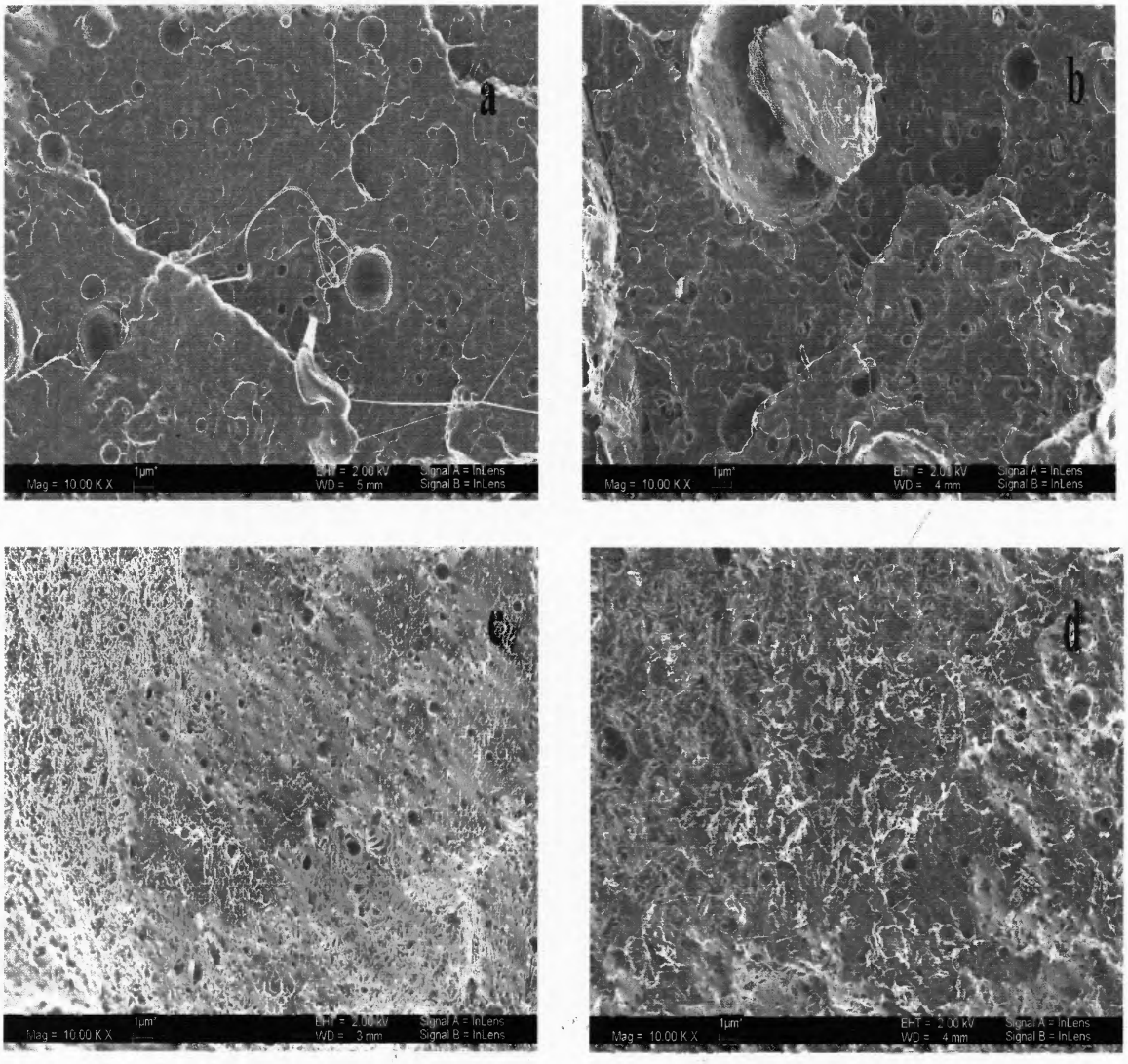

Figure 5.32 Morphology of film cross-section surface after 28 days hydrolytic degradation at 50°C: (a) unfilled PLLA (b) PLLA/MMT-Na^+ (c) PLLA/30B (d) PLLA/15A.

Figure 5.33 shows film cross-section surfaces of PLLA and its cationic and anionic clay composites after 28 days degradation at 50°C. The cationic clay composites have a much lower concentration of larger and heterogeneous pores over the entire film cross-section surface (Figures 5.33 (a) and (b)) than the anionic clay composites (Figures 5.33(c) and (d)). The same comments regarding the type of degradation and the site of its origin as in Figure 5.32 are also valid in the present case of Figure 5.33.

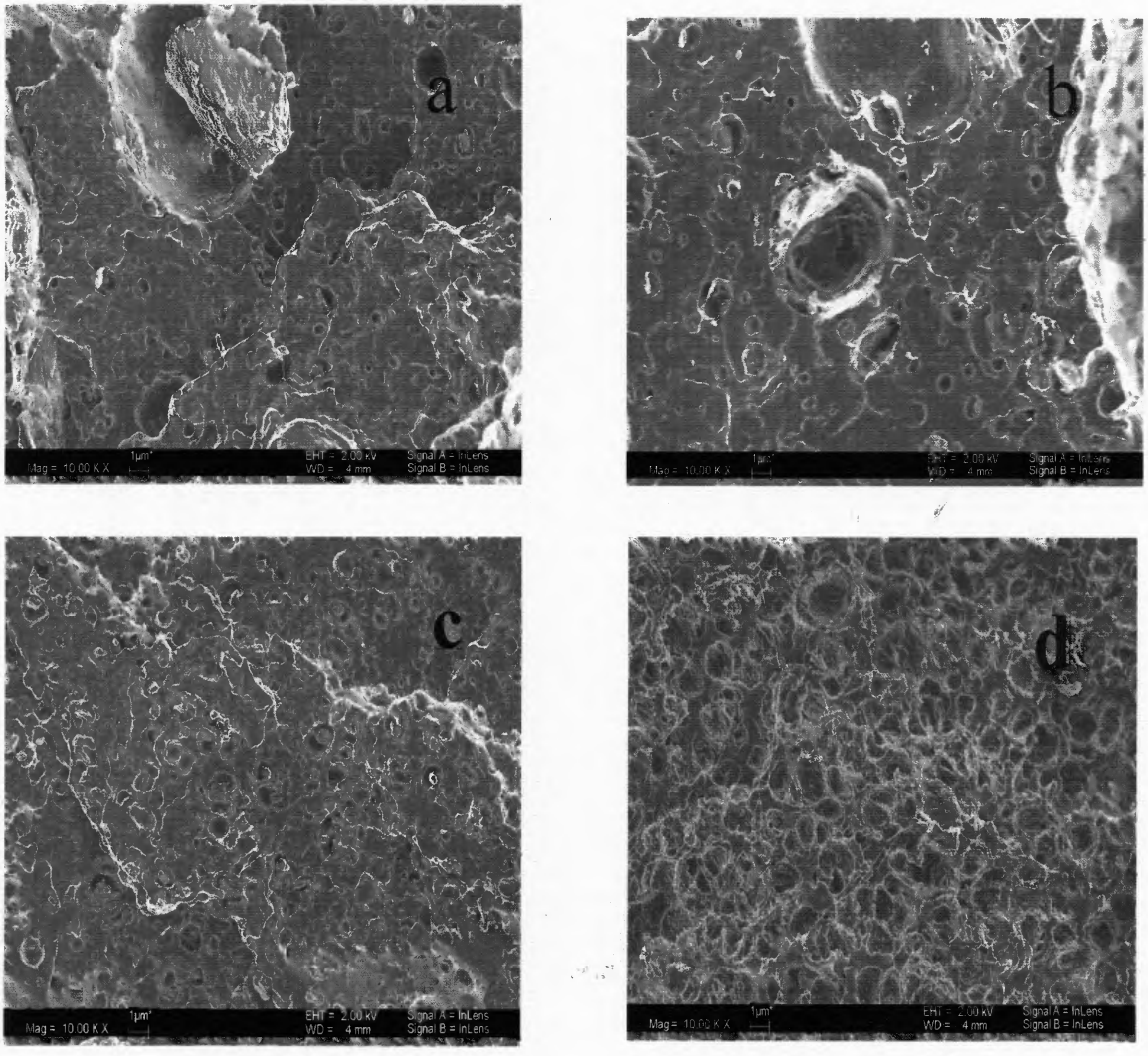

Figure 5.33 Morphology of film cross-section surface after 28 days hydrolytic degradation at 50°C: (a) PLLA/MMT-Na^+ (b) PLLA/MMT-Na^+(C) (c) PLLA/HT (d) PLLA/HT(C).

5.4.5 Effects on Thermal Properties

It has been already shown that 30B as nucleating agent enhanced polymer crystallization during melt blending; thus, it is important to study the effect of 30B on the polymer crystallization behavior during hydrolytic degradation. Firstly, by focusing on the thermal transitions of the PDLLA/30B nanocomposite, it is noted that T_g appears to slightly decrease with immersion time (Figure 5.34(a)) due to MW reduction and the known plasticizing effect of lactic acid oligomers formed during degradation (Paul et al., 2005). 30B appears to promote crystallization of the amorphous polymer since weak T_{cc} and T_m peaks appear after 14 and 21 days hydrolysis. However, it seems that the formed crystalline structure is unstable enough since the peaks disappeared after 28 days.

For the PLLA/30B nanocomposite was T_g was almost relatively constant during immersion (Figure 5.34 (b)), whereas T_{cc} shifted to slightly lower temperatures with increasing hydrolysis time. This T_{cc} change can be related to the lower MW since shorter chains would tend to crystallise at lower temperatures. Enthalpy changes for cold crystallization (ΔH_{cc}) were also significantly reduced after 28 days hydrolysis. T_m is slightly shifted to low temperatures with time, although enthalpy changes for melting (ΔH_m) appear to increase with time. A small endothermic peak observed just before melting commenced is attributed to additional polymer crystallization since near the polymer melting temperature, chain mobility would have increased, allowing some of the amorphous segments to reorder themselves. Although crystallization peaks during cooling of samples immersed up to 21 days are absent, a strong crystallization peak (T_c) appearing after 28 days (Figure 5.35(a)) can be readily related to reduced molecular weight and the 30B's strong nucleating ability.

Comparison of the thermal transitions during heating of PLLA/30B and PLLA (Figures 5.34(b) and 5.35 (b)), suggest that the filler is responsible for the T_g and T_{cc} shifts to lower temperatures as a function of immersion time, but not for the presence of double melting peaks, due to two lamellar populations with different perfection, that are observed in the scans of PLLA (Liu and Petermann, 2001). The presence of one melting peak in the 30B nanocomposites may be due to either the strong H-bonding between the modifier nanofiller and the polymer matrix inhibiting the crystal reorganization process, or to the presence of only one lamellar population.

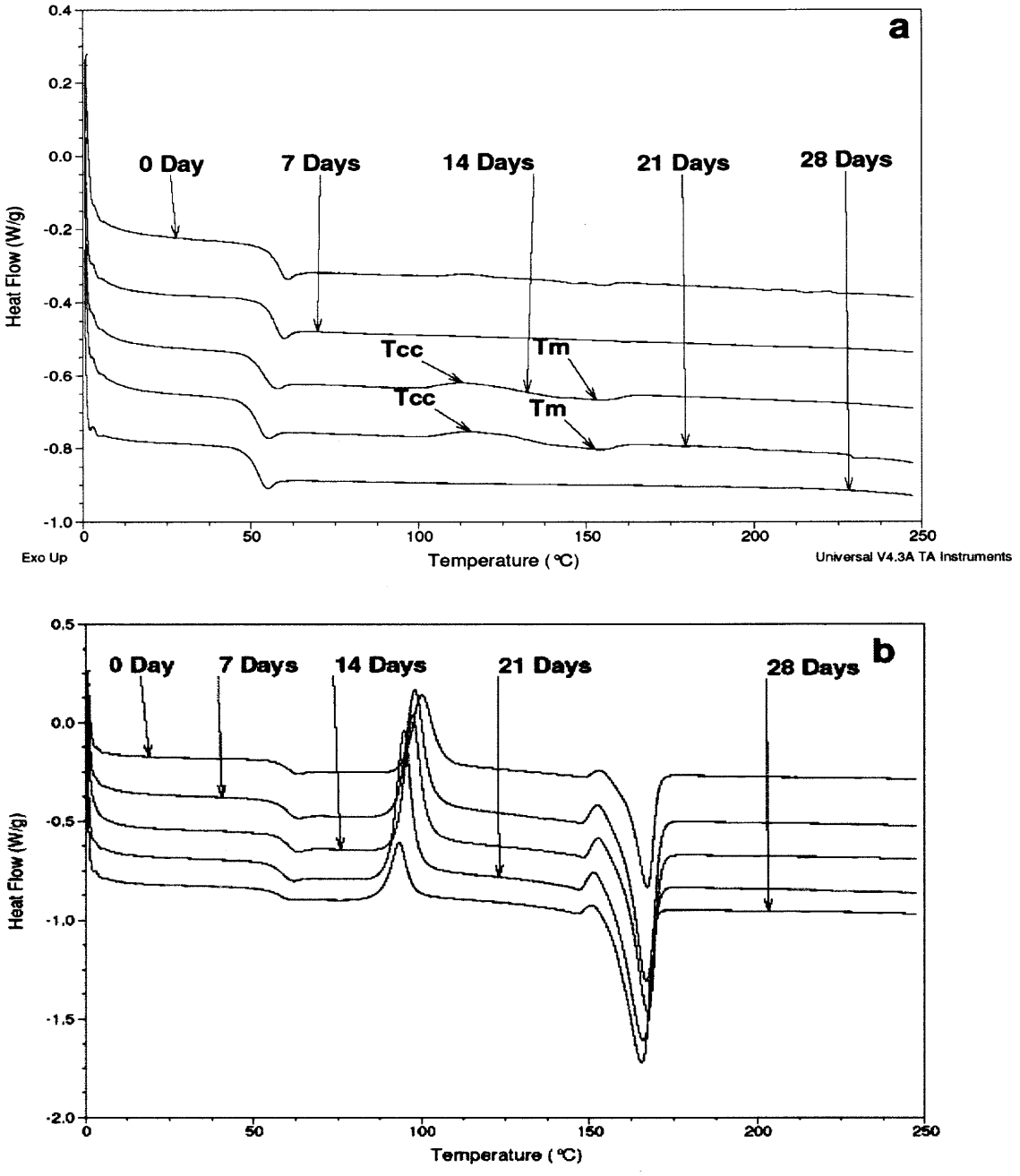

Figure 5.34 DSC curves during hydrolytic degradation at 50°C: (a) PDLLA/30B-2nd heating; (b) PLLA/30B-2nd heating.

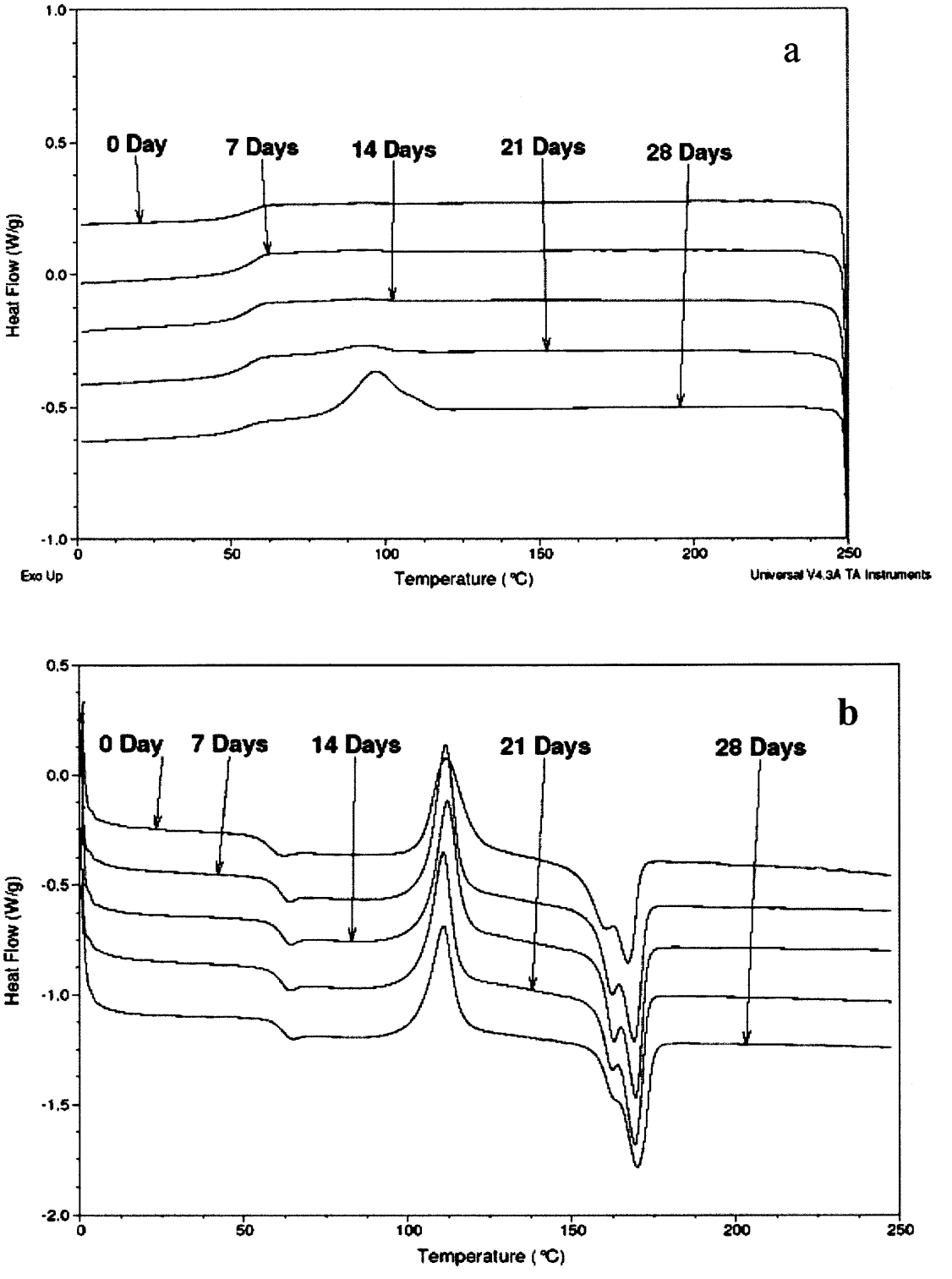

Figure 5.35 DSC curves during hydrolytic degradation at 50°C: (a) PLLA/30B-cooling; (b) PLLA-2nd heating.

PLLA/MMT-Na^+(C) as an example was used to study the thermal transition and crystallization behavior for MMT-Na^+ composites during hydrolytic degradation. Noted that T_g of PLLA/MMT-Na^+(C) was almost relatively constant (Figure 5.36 (a)) whereas T_{cc} slightly shifted to lower temperatures with increasing hydrolysis time. Enthalpy changes for cold crystallization (ΔH_{cc}) were almost constant after 28 days hydrolysis. Peak T_m is slightly shifted to lower temperatures with time, although enthalpy changes for melting (ΔH_m) appear to slightly increase. Like unfilled PLLA (Figure 5.35(b)), a double melting peak is also found in PLLA/MMT-Na^+(C) clay composites due to two lamellar populations with different perfection that are observed in the second heating scans (Liu and Petermann, 2001). The second melting peak increases whereas the first one is reduced with immersion time.

It is well known that the HT dehydration below 200°C is followed by the collapse of the lamellar structure and given rise to mixed oxides between 200°C and 400°C (Bellotto and Rebours, 1996). Thus, it is important to investigate the thermal transitions and crystallization behavior of the PLLA/HT during hydrolytic degradation at different heating temperature range Its T_g appears to somewhat decrease with immersion time (Figure 5.36(b)) during the second heating scan from 0°C to 250°C whereas T_{cc} significantly shifted to higher temperatures with increasing hydrolysis time. Interestingly, T_{cc} was shifted to lower temperature after 28 days degradation. T_m is significantly shifted to low temperatures with time. Also, the single melting peak slowly changed into double peaks during hydrolytic degradation. During the cooling, it is no possible to detect any crystallization peaks. Within the heating temperature range from 20°C to 180°C, T_g is relatively constant with increasing hydrolysis time, whereas T_{cc} slightly shifted to lower

temperatures (Figure 5.37 (a)). Enthalpy changes for cold crystallization (ΔH_{cc}) were also significantly reduced after 28 days hydrolysis. T_m is almost constant with time, although enthalpy changes for melting (ΔH_m) appear to increase with time. Double melt peaks were gradually changed into single peaks with time. Also, a significant crystallization peak (T_c) appeared after 14 days (Figure 5.37 (b)) degradation. A major reason for the observed behavior of HT composites is that HT decomposition above 200°C (Figure 5.15) produces metal oxides which may result in depolymerization of PLLA (Motoyama et al., 2007) and consequent change in the PLLA crystallization behavior.

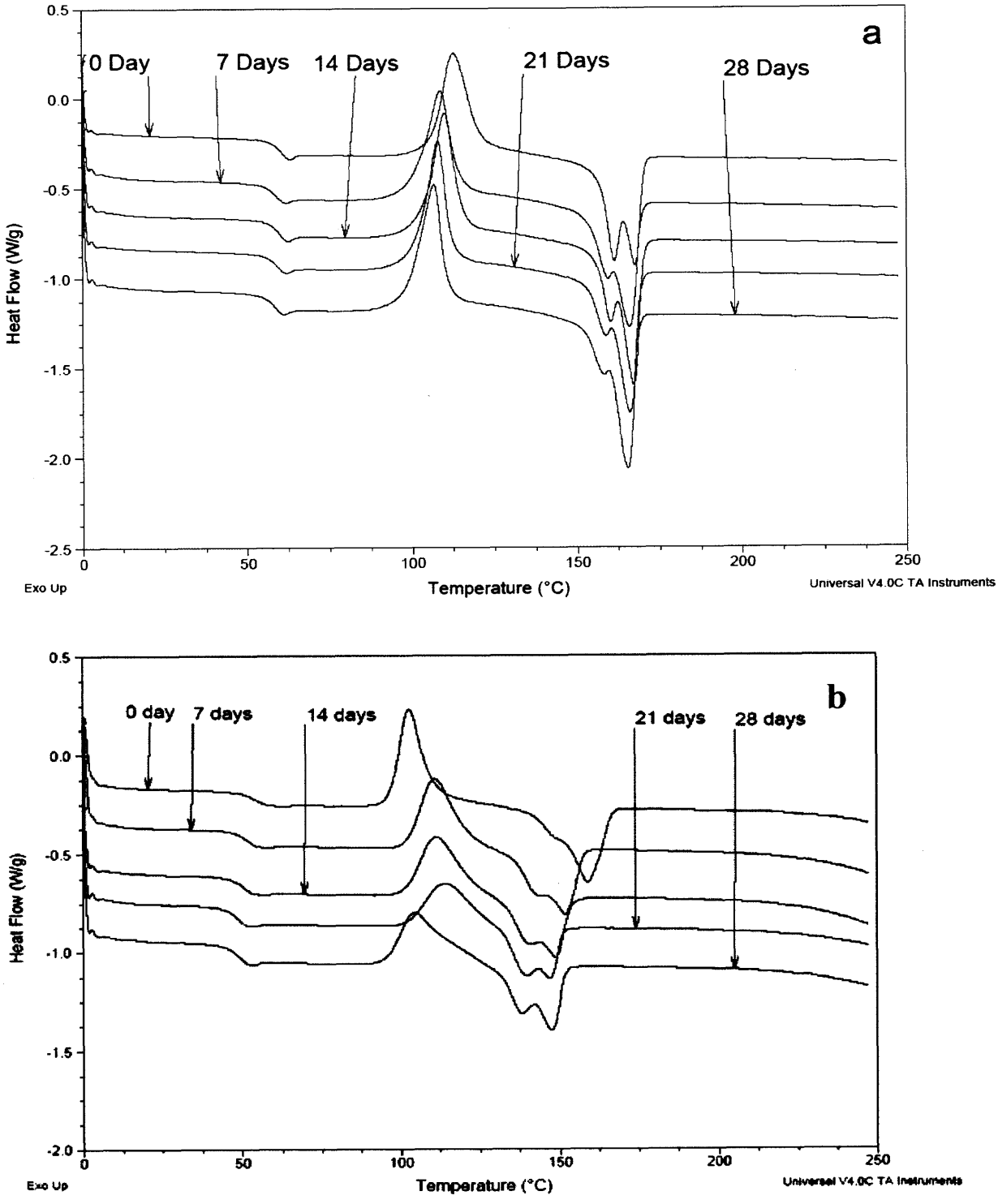

Figure 5.36 DSC curves during hydrolytic degradation at 50°C (a) PLLA/MMT/Na^{+}(C)-2nd heating; (b) PLLA/HT-2nd heating (0°C~250°C).

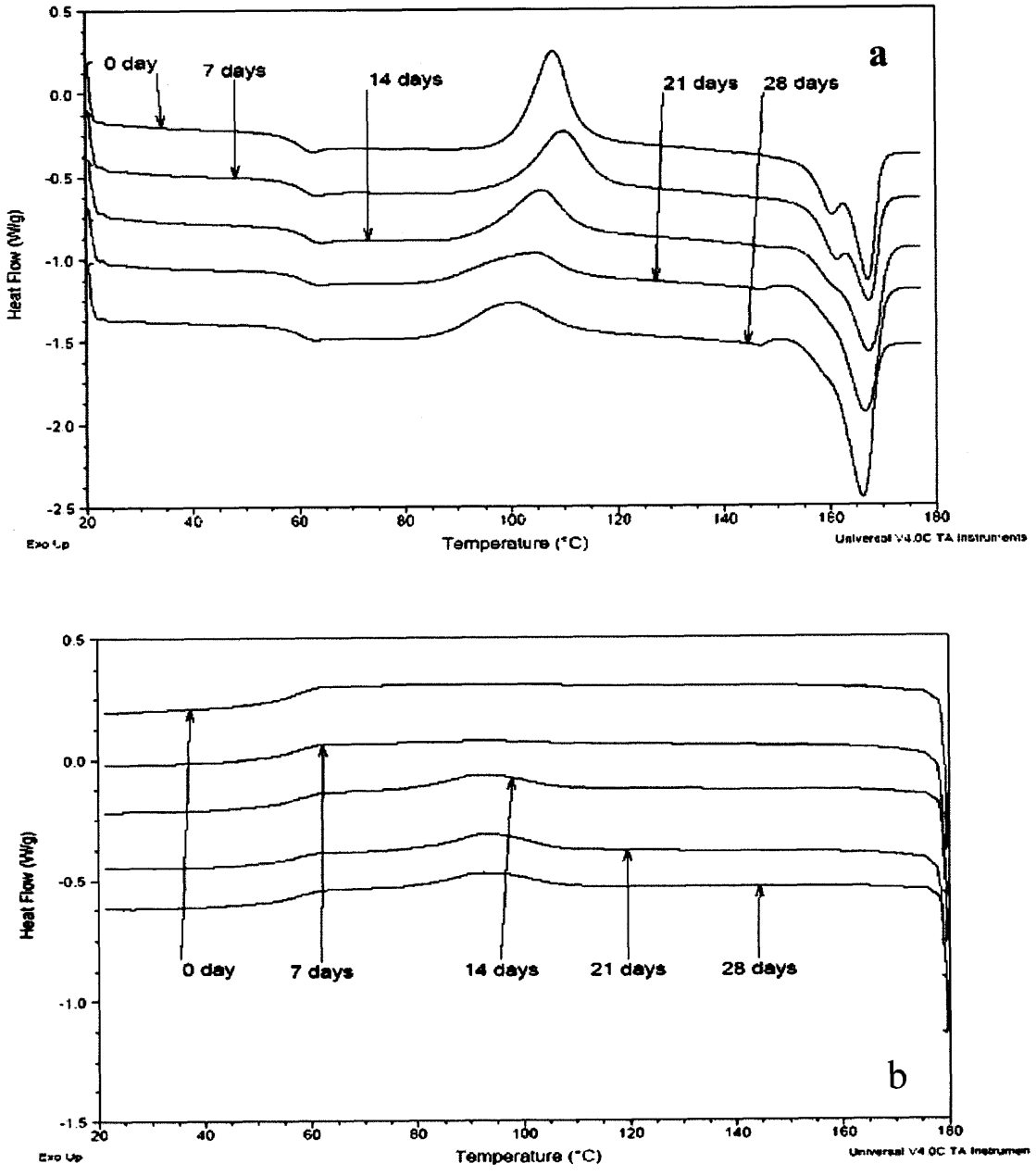

Figure 5.37 DSC curves during hydrolytic degradation at 50°C: (a) PLLA/HT-2nd heating (20°C~180°C); (b) PLLA/HT- cooling (180°C~20°C).

CHAPTER 6

CONCLUSIONS AND RECOMMENDATIONS

6.1 Conclusions

PLA composites based on semicrystalline and amorphous polymers, unmodified, calcined and organomodified cationic MMT clays as well as unmodified and calcined anionic HT clays at 5wt% content were produced by melt mixing and characterized for polymer intrinsic viscosity (*IV*) changes and filler dispersion by WAXD and SEM/EDX prior to thermal and hydrolytic degradation. Melt processing resulted in MW reduction for all unfilled polymer controls and also for the polymer matrices present in the composites. Thermomechanical degradation was more pronounced in the presence of all fillers, which apparently acted catalytically, but to different degrees. Unmodified cationic and anionic clays led to the formation of a microcomposite and nanocomposite respectively, whereas exfoliated/ intercalated nanocomposites were prepared by melt blending PLA with the organomodified cationic clays.

6.1.1 Thermal Degradation

The polymer controls and the composites were subjected to accelerated thermal degradation over a temperature from 180°C to 200°C under air and characterized for changes in polymer *IV* as a function of time. To calculate the degradation rate constants, the experimental *IV* data that increased with degradation time were fitted in a modified statistical random scission model with excellent/good correlation coefficients. The thermal stability of fillers, polymers and polymer composites were recorded by TGA under nitrogen and air at different heating rates. Kinetic analyses were performed by both

the Ozawa–Flynn–Wall and the Horowitz-Metzger methods. All results showed that the extent of degradation of the amorphous PDLLA and its composites is lower than that of the semicrystalline PLA and its composites as a result of the higher initial molecular weight of PDLLA.

In general, the degradation rate of the nanocomposites were significantly lower than those of the unfilled polymers and their cationic microcomposites under air since nanofillers promote char formation during thermo-oxidative treatment that retarded degradation. The exfoliated nanocomposites were more thermally stable than the intercalated nanocomposites. Cationic microfillers had two effects on isothermal degradation: a barrier effect that delayed polymer degradation at 180°C and a catalytic effect that promoted polymer degradation at 200°C. The degradation rate constants of anionic clay composites were lower than those of the cationic clay composites. The presence of the calcined clay in the polymer yielded a higher or slightly higher degradation rate constant than the presence of the non-calcined clays.

Based on TGA data and thermal kinetic analysis, nanofillers reduce polymer thermal stability due to their heat accumulating ability and the degradation of the organomodifiers by the Hoffman elimination effect. Calcined MMT and calcined HT provide better thermal stability than their non-calcined counterparts with HT composites having the lowest thermal stability as a result of the significant structural changes of the clay at elevated temperatures. In general, kinetics analysis results support the findings that the thermal stability of PDLLA and its composites (except for PDLLA/HT(C)) is higher than that of PLLA and its composites (except for PLLA/HT(C)) and also that the

thermal stability of the cationic nanocomposites is higher than that of the microcomposites.

6.1.2 Hydrolytic Degradation

The polymer controls and the composites were subjected to accelerated hydrolytic degradation at pH 10.5 over a temperature range of 50°C ~70°C and characterized for changes in polymer intrinsic viscosity, thermal properties and morphology as a function of immersion time. To calculate the degradation rate constants, the experimental *IV* data that decreased exponentially with degradation time were fitted in a carboxylic group autocatalyzed degradation model with excellent/good correlation coefficients. Degradation rate constants were higher for amorphous PLA and its composites than semicrystalline PLA and its composites as a result of increased permeation through the amorphous domains. Since the MMT-Na^+ lost its neutralization ability after treatment with the organic modifiers the degradation rate constants of the cationic nanocomposites were significantly higher than those of the unfilled polymers; by contrast, those of the cationic microcomposites and anionic nanocomposites were lower or slightly lower than those of the unfilled polymers possibly due to the reduction of the carboxyl group catalytic effect through neutralization with the hydrophilic alkaline filler.

In most situations, lower rate constants were observed for the polymer/anionic clay composites vs. the equivalent composites containing cationic clay. With respect to PLLA, it is shown that the presence of the calcined clays yielded a lower degradation rate than the presence of the non-calcined clay. However, with respect to PDLLA, no such

trend was observed since the high water uptake of PDLLA would erase the structural differences between calcined and non-calcined materials.

Although the degradation rate constants increased with increasing temperature from 50°C to 70°C, based on the calculated activation energies the degradation kinetics did not differ significantly above and below the assumed initial T_g of 58~60°C. Higher activation energies were observed for the semicrystalline polymer and its composites. The hydrolytic degradation of both unfilled polymers and their composites originated from the bulk of the material. After degradation, the differences in pore size and content suggested that polymer degradation originated at the interface between polymer matrix and fillers. Changes of thermal properties as a function of degradation time identified that different clays had different effects on the polymer crystallization behavior during hydrolytic degradation, some acting as nucleators.

6.2 Some Practical Implications

According to the experimental results of this work, the PLA cationic nanocomposites appear to be the best materials for future industrial applications, particularly for food packaging, due to their good thermal stability and high hydrolytic degradation rate constants. During processing and use, high thermal stability and low thermal degradation constant can minimize molecular weight changes which will cause decrease in the material's physical and mechanical properties. However, the high hydrolytic degradation rate constants imply fast disappearance of the material if landfilled. In addition, the filler effect on hydrolytic degradation may be important for drug delivery and tissue engineering applications as long as the organomodified fillers are cleared by regulatory

agencies to be used for such applications. It is understood that the pH value of drugs or additives and their dispersion will affect the drug release rate or tissue regeneration.

It is worth mentioning that the kinetic analysis of both isothermal and hydrolytic degradation is applicable to material degradation at the initial stages. Hydrolytic degradation can be predicted at any temperature since activation energies for all materials are available. At high temperatures, especially for PDLLA and its composites, the entire hydrolytic degradation process could be controlled since the time for a significant material disappearance (very low *IV*) could be available, perhaps through the aid of an estimated time/temperature superposition factor. However, for the isothermal or hydrolytic degradation of PLLA and its composites, some further experiments need to be carried out in order to follow the entire degradation process to much lower *IV* values than the ones measured in this work.

6.3 Recommendations for Future Work

1. A major research project originating from this work is the detailed study of the catalytic effects of (well characterized fillers) on polymer degradation based on their surface chemistry and composition, including the use of acidic bentonite MK10. Further experiments should be conducted with polymers of known structure and D-, L-proportions prepared with known catalysts in order to study their interference with the degradation reactions.

2. A more detailed investigation is required to explore the reasons for HT to reduce polymer degradation during isothermal heating, particularly, in amorphous PLA.

Furthermore the higher thermal stability of HT and HT(C) composites under air rather than nitrogen needs to be explored in detail.

3. Given the importance of foamed PLA in food packaging applications, experiments should be carried out with selected fillers in order to study their combined degradative and nucleating effects.

4. Thermal analysis combined with mass spectroscopy should be used to identify components which are released from polymer composites in the presence of different fillers.

5. The combination of amorphous and semicrystalline PLA matrices should be pursued further since degradation rates and properties could be optimized through the use of two polymers with different characteristics.

APPENDIX

THERMAL DEGRADATION EQUATION DEVELOPMENT

We assume that this degradation occurs by random bond breaking. Based on statistics of random scission mechanism, equation (2.1) can be obtained again as follows (Tanford, 1961):

$$\frac{1}{X_t} - \frac{1}{X_0} = kt \tag{2.1}$$

When both sides of equation (2.1) are multiplied by 1/w, where w is the molecular weight of the repeat unit, we have:

$$\frac{1}{X_t w} = \frac{1}{X_0 w} + \frac{kt}{w} \tag{A-1}$$

Assuming

$$k_n = \frac{k}{w} \tag{A-2}$$

Then

$$\frac{1}{\overline{M}_{nt}} = \frac{1}{\overline{M}_{n0}} + k_n t \tag{A-3}$$

$\overline{M}_{n0}$ and $\overline{M}_{nt}$ are the molecular weights of the polymer at time 0 and t, respectively and k_n is rate constant based on the number average molecular weight.

Since $\overline{M}_v$, the viscosity average molecular weight, is close to the weight average molecular weight, $\overline{M}_w$ which is also proportional to $\overline{M}_n$:

$$\overline{M}_v = c' \overline{M}_n \tag{A-4}$$

Where c' is constant

Equation (A-3) can then be converted into the following equation

$$\frac{1}{\overline{M_{vt}}} = \frac{1}{\overline{M_{v0}}} + \frac{k_n t}{c'} \tag{A-5}$$

Assuming that

$$\frac{k_n}{c'} = k_v \tag{A-6}$$

then

$$\frac{1}{\overline{M_{vt}}} = \frac{1}{\overline{M_{v0}}} + k_v t \tag{A-7}$$

Based on Taylor Series Expansion, if 1/X<< 1, the following relationship is obtained (Spiegel and Liu, 1999)

$$\frac{1}{X} \cong \ln(1+\frac{1}{X}) = \frac{1}{X} - (\frac{1}{X})^2/2 + ... - (\frac{1}{X})^n/n \tag{A-8}$$

So equation (A-7) is changed into the following equation:

$$\ln(\frac{1+\overline{M_{vt}}}{\overline{M_{vt}}}) = \ln(\frac{1+\overline{M_{v0}}}{\overline{M_{v0}}}) + k_v t \tag{A-9}$$

$$\ln(1+\overline{M_{vt}}) - \ln(1+\overline{M_{v0}}) = \ln(\frac{\overline{M_{vt}}}{\overline{M_{v0}}}) + k_v t \tag{A-10}$$

By combining equation (2.8)

$$IV = [\eta] = B(\overline{M_v})^{\nu} \tag{2.8}$$

and equation (A-10), we obtain:

$$\ln(1+\overline{M_{vt}})^{\nu} - \ln(1+\overline{M_{v0}})^{\nu} = \ln(\frac{IV_t}{IV_0}) + k_v \nu t \tag{A-11}$$

If M_v>>1, then based on the Binomial Equation

$$(1+M_v)^v \approx M_v{}^v + 1 \tag{A-12}$$

Substituting equation (A-12) into equation (A-11) we have

$$\ln(\overline{M}_{vt}^{\,v}+1) - \ln(1+\overline{M}_{v0}^{\,v}) = \ln(\frac{IV_t}{IV_0}) + k_v vt \tag{A-13}$$

By combining equations (2.8) and (A-13) we obtain:

$$\ln(\frac{IV_t}{B}+1) - \ln(1+\frac{IV_0}{B}) = \ln(\frac{IV_t}{IV_0}) + k_v vt \tag{A-14}$$

By rearrangement of equation (A-14) we have

$$\ln(\frac{1}{B}+\frac{1}{IV_t}) - \ln(\frac{1}{B}+\frac{1}{IV_0}) = k_v vt \tag{A-15}$$

$$\ln(1+\frac{B}{IV_t}) - \ln(1+\frac{B}{IV_0}) = k_v vt \tag{A-16}$$

Since B/IV<<1, by using equation (A-8) we obtain

$$\frac{B}{IV_t} = \frac{B}{IV_0} + k_v vt \tag{A-17}$$

By rearrangement of equation (A-17) we obtain:

$$\frac{1}{IV_t} = \frac{1}{IV_0} + \frac{k_v vt}{B} \tag{A-18}$$

And by assuming

$$k_{iv} = \frac{k_v v}{B} \tag{5.1}$$

we obtain the following new degradation equation based on *IV* change

$$\frac{1}{IV_t} = \frac{1}{IV_0} + k_{iv} t \tag{5.2}$$

REFERENCES

Agrawal, C. M., Huang, D. Schmitz, J. P. and Athanasiou, K. A. (1997). Elevated temperature degradation of a 50:50 copolymer of PLA-PGA. Tissue Engineering, 3, 345-352.

Albertsson, A. C. and Karlsson, S. (1994). Chemistry and Technology of Biodegradable Polymers. 7-17, Blackie Academic & Professional, an imprint of Chapman & Hall, Glasgow, UK.

Anderson, A. J. and Dawes, E. A. (1990). Occurrence, metabolism, metabolic role, and industrial uses of bacterial polyhydroxyalkanoates. Microbiological Reviews, 54, 450-472.

Arraiza, A. Sarasua, J. R., Verdu, J. and Colin, X. (2007). Rheological behavior and modeling of thermal degradation of Poly(ε-Caprolactone) and Poly(L-Lactide). International Polymer Processing, 5, 389-394.

Auerbach, S., Carrado, K. and Dutta, P. (2004) Handbook of Layered Materials, Marcel Dekker, Inc., New York.

Belbella, A., Vauthier, C., Fessei, H., Devissaguet, J. P. and Puisieux, F. (1996). In vitro degradation of nanospheres from poly(D,L-lactides) of different molecular weights and polydispersities. International Journal of Pharmaceutics, 129, 95-102.

Bellotto, M., Rebours, B., Clause, O., Lynch, J., Bazin, D. and Elkaiim, E. (1996). Hydrotalcite decomposition mechanism: a clue to the structure and reactivity of spinel-like mixed oxides. Journal of Physical Chemistry, 100, 8535-8542.

Berta, M., Lindsay, C., Pans, G. and Camino, G. (2006). Effect of chemical structure on, combustion and thermal behaviour of polyurethane elastomer layered silicate nanocomposites. Polymer Degradation and Stability, 91, 1179-1191.

Bhari, K., Mitomo, H., Enjoji, T., Yoshii, F. and Makuuchi, K. (1998). Radiation crosslined poly(butylene succinate) foam and its biodegradation. Polymer Degradation and Stability, 62, 551-557.

Blumstein, A. (1965). Polymerization of adsorbed monolayers: II. Thermal degradation of the inserted polymers. Journal of Polymer Science: Part A: Polymer Chemistry, 3, 2665-2673.

Bourbigot, S., Gilman, J. and Wilkie, C. (2004). Kinetic analysis of the thermal degradation of polystyrene montmorillonite nanocomposite. Polymer Degradation and Stability, 84, 483-492.

Brownell, W. E., (1976). Structural Clay Products, Springer- Verlag, New York.

Carter, L. W., Hendricks, J. G. and Bolley, D. S. (1950). United States Patent No. 2, 531, 396, (assigned to National Lead Co).

Cavani, F., Trifirb, F. and Vaccari, A. (1991). Hydrotalcite-type anionic clays: preparation, properties and applications. Catalysis Today, 11, 173-301.

Chang, J., Hang, Y. and Sur, G. (2003). Poly(lactic acid) nanocomposites with various organoclays. I. thermomechanical properties, morphology, and gas permeability. Journal of Polymer Science: Part B: Polymer Physics, 41, 94-103.

Chen, G. and Yoon, J. (2005). Morphology and thermal properties of Poly(L-lactide)/Poly(butylene succinate-co-butylene adipate) compounded with twice functionalized clay. Journal of Polymer Science: Part B: Polymer Physics, 43, 478-487.

Chorom, M. and Rengasamy, P. (1996). Effect of heating on swelling and dispersion of different cationic forms of a smectite. Clays and Clay Minerals, 44, 783-790.

Chouzouri, G., Patel, S. H. and Xanthos, M. (2004). Biocomposites based on poly(L-lactic acid) and a functional synthetic filler. Proceedings 62nd Annual Technical Conference of Plastics Engineers, SPE ,50, 3366-3370.

Chouzouri, G. and Xanthos, M. (2003). Modification of biodegradable polyesters with inorganic fillers. Proceedings 61st Annual Technical Conference of Plastics Engineers, SPE, 49, 2561-2565.

Chrissafis, K., Antoniadis, G. Paraskevopoulos, K.M., Vassiliou, A. and Bikiaris, D.N. (2007). Comparative study of the effect of different nanoparticles on the mechanical properties and thermal degradation mechanism of in situ prepared poly(ε-caprolactone) nanocomposites. Composites Science and Technology, 67, 2165-2174.

Chye, S., Loo, J., Ooi, C.P. Hong, S., Wee, E., Chiang, Y. and Boey, F. (2005). Effect of isothermal annealing on the hydrolytic degradation rate of poly(lactide-co-glycolide) (PLGA). Biomaterials, 26, 2827-2833.

Coats, A. W. and Redfern, J. P. (1964) Kinetic parameters from thermogravimetric data Nature, 201, 68-69.

Dabrowski, F., Bourbigot, S., Delobel, R. and Bras, M. (2000). Kinetic modeling of the thermal degradation of polyamide-6 nanocomposite. European Polymer Journal, 36, 273-284.

Degee, P., Dubois, P. and Jerome, R. (1997). Bulk polymerization of lactides initiated by aluminium isopropoxide, 3: Thermal stability and viscoelastic properties. Macromolecular Chemistry Physics, 198, 1985-1995.

Dennis, H. R., Hunter, D. L, Chang, D., Kim, S., White, J.L., Cho, J. W. and Paul, D. R. (2001). Effect of melt processing conditions on the extent of exfoliation in organoclay-based nanocomposites. Polymer, 42, 9513-9522.

Doi, Y., Kasuya, K., Abe, H., Koyama, N., Ishiwatari, S. and Takagi, K. (1996). Evaluation of biodegradabilities of biosynthetic and chemosynthetic polyesters in river water. Polymer Degradation Stability, 5, 281-286.

El-Toufaili, F., Dinse, A., Feix, G. and Reichert, K. (2006). Studies on Hydrotalcite-catalyzed synthesis of Poly(ethylene terephthalate). Macromolecular Materials and Engineering, 291, 1136-1143.

El-Toufaili, F., Feix, G. and Reichert, K. (2006). Kinetics and mechanistic investigation of hydrotalcite-catalyzed melt synthesis of poly(ethylene terephthalate) Macromolecular Materials and Engineering , 291, 1144-1154.

Erickson, K. L., Bostrom, T. E. and Frost, R. L. (2004). A study of structural memory effects in synthetic hydrotalcites using environmental SEM. Materials Letters, 59, 226-229.

Fan, Y. J., Nishida, H., Hoshihara, S., Shirai, Y., Tokiwa, Y. and Endo, T. (2003). Pyrolysis kinetics of poly(L-lactide) with carboxyl and calcium salt end structures. Polymer Degradation and stability, 79, 547-562.

Fan, Y., Nishida, H., Mori, T., Shirai, Y. and Endo, T. (2004). Thermal degradation of poly(L-lactide): effect of alkali earth metal oxides for selective L,L-lactide formation. Polymer, 45, 1197-1205.

Feijoo, J. L. (2005). Development of amorphous PLA-montmorillonite nanocomposites. Journal of Materials Science, 40, 785-788.

Fischer, E. W., Sterzel, H. J. and Wegner, G. (1973). Investigation of the structure of solution grown crystals of lactide copolymers by means of chemical reactions. Kolloid-Zeitschrift & Zeitschrift für Polymere, 251, 980-990.

Fornesa,T. D., Yoona, P.J., Hunterb, D. L., Keskkulaa, H. and Paul, D. R. (2002). Effect of organoclay structure on nylon 6 nanocomposite morphology and properties. Polymer, 43, 5915-5933.

Fornes, T. D., Yoon, P. J. Keskkula, H. and Paul, D. R. (2001). Nylon 6 nanocomposites: The effect of matrix molecular weight. Polymer, 42, 9929-9940.

Freeman, E. S. and Caroll, B. (1958). The application of thermoanalytical techniques to reaction kinetics. The thermogravimetric evaluation of the kinetics of the decomposition of calcium oxalate monohydrate. Journal of Physical Chemistry, 62, 394-397.

Fukui, T. and Doi, Y. (1997). Cloning and analysis of the poly(3- hydroxybutyrate-co-3-hydroxyhexanoate) biosynthesis genes of aeromonas caviae. Journal of Bacteriology, 179, 4821-4830.

Fukui, T., Shiomi, N. and Doi, Y. (1998). Expression and characterization of (R)-specific enoyl coenzyme a hydratase involved in polyhydroxyalkanoate biosynthesis by aeromonas caviae. Journal of Bacteriology,180, 667-673.

Fujimaki, T. (1998). Processability and properties of aliphatic polyester, "bionolle", synthesised by polycondenstaion reaction. Polymer Degradation Stability, 59, 209-214.

Garlotta, D. (2001). A literature review of Poly(Lactic Acid). Journal of Polymers and the Environment, 9, 63-84.

Gilman, J. W. (1999). Flammability and thermal stability studies of polymer layered-silicate (clay) nanocomposites. Applied Clay Science, 15, 31-49.

Gilman, J. W., Jackson, C. L., Morgan, A. B., Harris, R., Manias, E., Giannelis, E. P., et al. (2000). Flammability properties of polymer - layered-silicate nanocomposites. Polypropylene and polystyrene nanocomposites. Chemistry of Materials, 12, 1866-1873.

Göpferich, A. and Tessmar, J. (2002). Polyanhydride degradation and erosion. Advanced Drug Delivery Reviews, 54, 911-931.

Gopakumar, T. G., Patel, N. S. and Xanthos, M. (2006). Effect of nanofillers on the properties of flexible protective polymer coatings. Polymer Composites, 27, 368-380.

Grimshaw, R. W. (1971). The Chemistry and Physics of Clay and Allied Ceramic Materials, Ernest Benn Limited, London.

Gross, R. and Kalra, B. (2002). Biodegradable polymers for the environment. Science, 297, 803-808.

Guan, J. and Hanna, M. A. (2002). Modification of macrostructure of starch acetate extruded with natural fibers. ASAE Paper No. 026148. Chicago, Illinois. ASAE.

Guggenheim, S. and Martin, R. T. (1995). Definition of clay and clay mineral: joint report of the AIPEA nomenclature and CMS nomenclature committees. Clays and Clay Minerals, 43, 255-256.

Hakkarainen M. (2002). Aliphatic polyester: abiotic and biotic degradation and degradation products. Advances in Polymer Science,157, 113-137.

He, H. and Lee, L. (2004). Poly(lactic-co-glycolic acid) and functional hydrogels for drug delivery applications. Proceedings 62nd Annual Technical Conference of Plastics Engineers, SPE, 50, 3356-3360.

Heller, J., Barr, J., Ng, S. Y., Schwach-Abdellauoi, S. and Gurny, R. (2002). Analytical solutions to mathematical models of the surface and bulk erosion of solid polymers. Advanced Drug Delivery Reviews, 54, 1015-1039.

Horowitz, H. H. and Metzger, G. (1963). A new analysis of thermogravimetric traces. Analytical Chemistry, 35, 1464-1468.

Huijberts, G. N., Eggink, G., Waard, P., Huisman, G. W. and Witholt, B. (1992) Pseudomonas putida KT2442 cultivated on glucose accumulates poly(3-hydroxyalkanoates) consisting of saturated and unsaturated monomers. Applied Environmental Microbiology, 58, 536-544.

Hurrell, S. and Cameron, R. E. (2002). The effect of initial polymer morphology on the degradation and drug release from polyglycolide. Biomaterials, 23, 2401-2409.

Hyon, S. H., Jamshidi, K. and Ikada, Y. (1997). Synthesis of polylactides with different molecular weights. Biomaterials, 16, 1503-1508.

Jamshidi, K., Hyon, S. H. and Ikada, Y. (1988). Thermal characterization of polylactides. Polymer, 29, 2229-2234.

Jong, S. J., Ariasa, E. R., Rijkers, DT., Nostrum, C.F., Kettenes, J. J. and Hennink, W.E. (2001). New insights into the hydrolytic degradation of poly(lactic acid): participation of the alcohol terminus. Polymer, 42, 2795-2802.

Karaborni, S., Smit, B., Heidug, W., Urai, J. and Oort, E. (1996). The swelling of clays: molecular simulations of the hydration of montmorillonite. Science, 271, 1102-1104.

Kim, N., Malhotra, S. and Xanthos, M. (2006). Modification of cationic nanoclays with ionic liquids. Microporous and Mesoporous Materials, 96, 29-35.

Kissinger, H. E. (1957). Reaction kinetics in differential thermal analysis. Analytical Chemistry, 29, 1702-1706.

Khan, A. I. and O'Hare, D. (2002). Intercalation chemistry of layered double hydroxides: recent developments and applications. Journal of Materials Chemistry, 12, 3191 - 3198.

Kolybaba, M., Tabil, L.G., Panigrahi, S., Crerar, W. J., Powell, T. and Wang, B. (2003). Biodegradable polymers: past, present, and future Paper Number: RRV03-0007 An ASAE Meeting Presentation.

Kopinke, F. D. and Mackenzie, K. J. (1997). Mechanistic aspects of the thermal degradation of poly(lactic acid) and poly(β-hydroxybutyric acid) Journal of Analytical and Applied Pyrolysis, 43, 40-41.

Kopinke, F. D., Remmler, M., Mackenzie, K., Moder, M. and Wachsen, O. (1996). Thermal decomposition of biodegradable polyesters - II. Poly(lactic acid). Polymer Degradation Stability, 53, 329-342.

Kovanda, F., Kovacsova, E. and Kolousek, D., (1999). Removal of anions from solution by calcined hydrotalcite and regeneration of used sorbent in repeated calcination rehydration anion exchange processes. Collection of Czechoslovak Chemical Communications. 64, 1517-1528.

Lammers, P. and Kromer, K. (2002). Competitive natural fiber used in composite materials for automotive parts. ASAE Paper No. 026167. Chicago, Illinois. ASAE.

Lan, T., Kaviratna, P. and Pinnavaia, T. (1995). Mechanism of clay tactoid exfoliation in epoxy-clay nanocomposites. Chemistry of Materials, 7, 2144-2150.

Lan, T. and Pinnavaia, T, (1996). Nanolayer ordering in an epoxy-exfoliated clay hybrid composite. Materials Research Society Symposium - Proceedings, 435,79-84.

Ledward, D. (1998). Properties and applications of compostable starch-based materials. Trends in Food Science and Technology, 41, 402-405.

Lee, K. M. and Han, C. D. (2003). Rheology of organoclay nanocomposites: effects of polymer matrix/organoclay compatibility and the gallery distance of organoclay Macromolecules, 36, 7165-7178.

Lee, S. R., Park, H. M., Lim, H., Kang, T., Li, X., Cho, W. J. and Ha, C. S. (2002). Microstructure, tensile properties, and biodegradability of aliphatic polyester/clay nanocomposites. Polymer, 43, 2495-500.

Lepoittevin, B., Pantoustier, N., Devalckenaere, M., Alexandre, M., Kubies, D., Calberg, C., Jerome, R. and Dubois, P. (2002). Poly(ε-caprolactone)/clay nanocomposites by in-situ intercalative polymerization catalyzed by dibutyltin dimethoxide. Macromolecules, 35, 8385-8390.

Liu, T., and Petermann, J. (2001). Multiple melting behavior in isothermally cold-crystallized isotactic polystyrene. Polymer, 42, 6453-6461.

Liu, X., Zou, Y., Li, W., Cao, G. and Chen, W. (2006). Kinetics of thermo-oxidative and thermal degradation of poly(D,L-lactide) (PDLLA) at processing temperature. Polymer Degradation and Stability, 91, 3259-3265.

Loyens, W., Jannasch, P. and Maurer, F. (2005). Effect of clay modifier and matrix molar mass on the structure and properties of poly(ethylene oxide)/Cloisite nanocomposites via melt-compounding. Polymer, 46, 903-914.

Maiti, P., Batt, C. and Giannelis, E. (2003). Renewable plastics: synthesis and properties of PHB nanocomposites. Polymer Material Science Engineering, 88, 58-59.

Malinconico, M. and Laurienzo, P. (2007). Nanometric dispersion of a Mg/Al layered double hydroxide into a chemically modified polycaprolactone. Biomacromolecules, 8, 773-779.

Mani, R. and Bhattacharya, M. (2001). Properties of injection moulded blends of starch and modified biodegradable polyesters. European Polymer Journal, 37, 515-526.

Marazzato, C., Peneva, Y., Lefterova, E., Filippi, S. and Minkova, L. (2007). Kinetics of non-isothermal degradation of nanocomposites based on functionalized polyethylenes. Polymer Testing, 26, 526-536.

Marras, S., Zuburtikudis, I. and Panayiotou, C. (2007). Nanostructure vs. microstructure: morphological and thermomechanical characterization of poly(L-lactic acid)/layered silicate hybrids. European Polymer Journal, 43, 2191-2206.

McNeill, I. C. and Leiper, H. A. (1985). Degradation studies of some polyesters and polycarbonates--2. polylactide: Degradation under isothermal conditions, thermal degradation mechanism and photolysis of the polymer. Polymer Degradation and Stability, 11, 309-326.

Meer, S., Wijn, J. and Wolke, J. (1996). The influence of basic filler materials on the degradation of amorphous D- and L-lactide copolymer. Journal of Materials Science: Materials in Medicine, 7, 359-361.

Messersmith, P. B. and Giannelis, E. P. (1995). Synthesis and barrier properties of poly(ε-caprolactone)-layered silicate nanocomposites. Journal of Polymer Science Part A: Polymer Chemistry, 33, 1047-1057.

Miyata, S. Hirose, T. and Iizima, N. (1978). Fire-retarding thermoplastic resin composition. US Patent, 4085 088.

Mohanty, A. K., Drzal, L. T. and Misra, M. (2003). Nano-reinforcement of bio-based polymers—the hope and reality. Polymer Material Science Engineering, 88, 60-61.

Mohanty, A. K., Misra, M. and Drzal, L. (2005). Natural Fibers, Biopolymers, and Biocomposites Taylor & Francis Group, Boca Raton, Florida.

Montaudo, G. and Rizzarelli, P. (2000). Synthesis and enzymatic degradation of aliphatic Copolyesters. Polymer Degradation Stability, 70, 305-314.

Motoyama, T., Tsukegi, T., Shirai, Y., Nishida, H. and Endo, T. (2007). Effects of MgO catalyst on depolymerization of poly-L-lactic acid to L,L-lactide. Polymer Degradation and Stability, 92, 1350-1358.

Mukhopadhyay, P. (2002). Emerging trends in plastic technology. Plastics Engineering, 58, 28-35.

Nair, L. S. and Laurencin, C. T. (2007). Biodegradable polymers as biomaterials. Progress in Polymer Science, 32, 762-798.

Noyan, H., Onal, M. and Sarikaya, Y. (2006). The effect of heating on the surface area, porosity and surface acidity of a bentonite. Clays and Clay Minerals, 54, 375-381.

Okamoto, K., Toshima, K., and Matsumura, S. (2005). Degradation of poly(lactic acid) into repolymerizable oligomer using montmorillonite K10 for chemical recycling. Macromolecular Bioscience, 5, 813-820.

Ortuoste, N., Allen, N., Papanastasiou, M., McMahon, A., Edge, M., Johnson, B. and Keck-Antoine, K. (2006). Hydrolytic stability and hydrolysis reaction mechanism of bis(2,4-di-tert-butyl)pentaerythritol diphosphite (Alkanox P-24). Polymer Degradation and Stability, 91, 195-211.

Ozawa, T. (1965). A new method of analyzing thermogravimetric data. Bulletin of the Chemical Society of Japan, 38, 1881-1886.

Partini, M. (2006). Characterization and degradation mechanisms of aliphatic polyesters Ph D thesis. Department of Chemical and Food Engineering, University Degli Studi Di, Salerno, Italy

Park, J. H., Ye, M. and Park, K. (2005). Biodegradable polymers for microencapsulation of drugs. Molecules, 10, 146-161.

Paul, M. A, Delcourt, C., Alexandre, M., Degee, P., Monteverde, F. and Dubois, P. (2005). Polylactide/montmorillonite nanocomposites: study of the hydrolytic degradation. Polymer Degradation Stability, 87, 535-542.

Paul, M. A., Alexandre, M., Degee, P., Henrist, C., Rulmont, A. and Dubois, P., (2003). New nanocomposite materials based on plasticized poly(L-lactide) and organo-modified montmorillonites: thermal and morphological study. Polymer 44, 443-450.

Philip, S., Keshavarz, T. and Roy, I. (2007). Polyhydroxyalkanoates: biodegradable polymers with a range of applications. Journal of Chemical Technology and Biotechnology, 82, 233-247.

Pitt, C. G., Gratzl, M. M. and Kimmel, G. L. (1981). Aliphatic polyesters II. The degradation of poly (DL-lactide), poly(ε-caprolactone) and their copolymers in vivo. Biomaterials, 2, 215-220.

Pitt, C. and Gu, Z. (1987). Modification of the rates of chain cleavage of polycaprolactone and related polyesters in the solid state. Journal of Controlled Release, 4, 283-292.

Pluta, M., Galeski, A., Alexandre, M., Paul, M. A. and Dubois, P. (2002). Polylactide/montmorillonite nanocomposites and microcomposites prepared by melt blending: Structure and some physical properties. Journal of Applied Polymer Science, 86, 1497-506.

Pluta, M., Jeszka, J. K. and Boiteux, G. (2007). Polylactide/montmorillonite nanocomposites: Structure, dielectric, viscoelastic and thermal properties. European Polymer Journal, 43, 2819-2835.

Porjazoska, A., Kayaman-Apohan, N., Karal-Yilmaz, O., Cvetkovska, M., Baysal, K. and Baysal, B. M. (2002). Synthesis and characterization of glycolide, L-lactide, and PDMS-based terpolymers as a support for cell cultures. Journal of Biomaterials Science, Polymer Edition, 13, 1119-1134.

Qin, H., Zhang, S., Zhao, C. and Yang, M. (2005). Zero-Order kinetics of the thermal degradation of polypropylene/clay nanocomposites. Journal of Polymer Science: Part B: Polymer Physics, 43, 3713-3719.

Ratto, J. A., Steeves, D.M., Welsh, E. A. and Powell, B. E. (1999). A study of polymer/clay nanocomposites for biodegradable applications. Proceedings 57th, Annual Technical Conference of Plastics Engineers, SPE, 45, 1628.

Ray, S. S. and Bousmina, M. (2005). Biodegradable polymers and their layered silicate nanocomposites: In greening the 21st century materials world. Progress in Materials Science, 50, 962-107.

Ray, S. S. Yamadab, K., Okamotoa, M., Fujimotoa, Y., Ogamib, A. and Ueda, K. (2003). New polylactide/layered silicate nanocomposites. 5. Designing of materials with desired properties. Polymer, 44, 6633-6646.

Ray, S. S., Yamada, K., Okamoto, M. and Ueda, K. (2003). Control of biodegradability of polylactide via nanocomposite technology. Macromolecular Materials and Engineering, 288, 203-208.

Reich, L. and Stivala, S. (1971). Elements of Polymer Degradation, McGRAW-Hill Book Company, New York.

Royte, E. (2006). Corn plastic to the rescue. Smithsonian Magazine, August.

Sakiyama-Elbert, S. and Hubbell, J. (2001). Functional biomaterials: Design of novel biomaterials. Annual Review of Materials Research, 31, 183-201.

Saxena, S. K. (2004). Polyvinyl Alcohol (PVA). Chemical and Technical Assessment (CTA). The 61st meeting of the Joint FAO/WHO Expert Committee on Food Additives, JECFA, 3, 1-3.

Schnabel, W. (1981). Polymer degradation principles and practical applications , Hanser International, New York.

Serrano, J., Bertin, V. and Bulbulian, S. (2002). Elution of 235U fission products through a calcined hydrotalcite-packed column. Journal of Radioanalytical and Nuclear Chemistry, Vol. 254, 91-94.

Shih., C. (1995). A graphical method for the determination of the mode of hydrolysis of biodegradable polymers. Pharmaceutical Research, 12, 2036-2040.

Sinha, V. R., Bansal, K., Kaushik, R., Kumria, R. and Trehan, A. (2004). Poly-epsilon-caprolactone microspheres and nanospheres: an overview. International Journal of Pharmaceutics, 278, 1-23.

Sinha, R. S. and Okamoto, M. (2003). Polymer/layered silicate nanocomposites: a review from preparation to processing. Progress in Polymer Science, 28, 1539-1641.

Shirahama, H., Kawaguchi, Y., Aludin, M. and Yasuda, H. (2001). Synthesis and enzymatic degradation of high molecular weight aliphatic polyesters. Journal of Applied Polymer Science, 80, 340-347.

Solomon, O. F. and. Ciuta, I. Z. (1962). Détermination de la viscosité intrinsèque de solutions de polymères par une simple détermination de la viscosité. Journal of Applied Polymer Science, 6, 683-686.

Spiegel, M., and Liu, J. (1999). Mathematical Handbook of Formulas and Tables McGraw-Hill, New York.

Storey, R. F. and Taylor, A. E. (1998). Effect of stannous octoate on the composition, molecular weight, and molecular weight distribution of ethyleneglycol-initiated poly(ε-caprolactone). Journal of Macromolecular Science - Pure and Applied Chemistry, 35, 723-750.

Tammaro, L., Costantino, U., Bolognese, A., Sammartino, G., Marenzi, G., Calignano, A., Tete , S., Mastrangelo, F., Califano, L. and Vittoria, V. (2007). Nanohybrids for controlled antibiotic release in topical applications. International Journal of Antimicrobial Agents, 29, 417-423.

Tanford, C. (1961). Physical Chemistry of Macromolecules , John Wiley & Sons, Inc., New York.

Tian, H. and Tagaya, H. (2007). Preparation, characterization and mechanical properties of the polylactide/perlite and the polylactide/montmorillonite composites. Journal of Materials Science, 42, 3244-3250.

Tichit, D. and Coq, B. (2003). Catalysis by hydrotalcites and related materials. Cattech, 7, 206-217.

Tsuge, T., Fukui, T., Matsusaki, H., Taguchi, S., Kobayashi, G., Ishizaki, A. and Doi, Y. (2000). Molecular cloning of two (R)-specific enoyl-CoA hydratase genes from pseudomonas aeruginosa and their use for polyhydroxyalkanoate synthesis. FEMS Microbiology Letters, 184, 193-198.

Tsuji, H., and Ikada, Y. (2000). Properties and morphology of poly(L-lactide).4. Effects of structural parameters on long-term hydrolysis of poly(L-lactide) in phosphate-buffered solution. Polymer Degradation and Stability, 67, 179-189.

Urayama, H., Kanamori, T., Fukushima, K. and Kimura, Y. (2003). Controlled crystal nucleation in the melt-crystallization of poly (L-lactide) and poly(L-lactide)/poly(D-lactide) stereocomplex. Polymer, 44, 5635-5641.

Usuki, A., Kojima, Y., Kawasumi, M., Okada, A., Fukushima, Y., Kurauchi, T. and Kamigatio, O. (1993). Synthesis of nylon 6-clay hybrid. Journal of Materials Research, 8, 1179-1184.

Uesaka, T., Nakane, K., Maeda, S., Ogihara, T. and Ogata, N. (2000). Structure and physical properties of poly(butylene succinate)/cellulose acetate blends. Polymer 41, 8449-8454.

Usuki, A., Koiwai, A., Kojima, Y., Kawasumi, M., Okada, A., Kurauchi, T. and Kamigaito, O. (1995). Interaction of nylon 6-clay surface and mechanical properties of nylon 6-clay hybrid. Journal of Applied Polymer Science, 55, 119-123.

Vaia, R. A. and Giannelis, E. P. (1997). Lattice of polymer melt intercalation in organically modified layered silicates. Macromolecules, 30, 7990-7999.

Vaia, R. A. and Giannelis, E.P. (1997). Polymer melt intercalation in organically-modified layered silicates: model predictions and experiment. Macromolecules, 30, 8000-8009.

Veld, P. J., Velner, E. M., White, P., Hamhuis, J., Dijkstra, P. J. and Feijen, J. (1997). Melt block copolymerisation of ε-caprolactone and L-Lactide. Journal of Polymer Science: Part A: Polymer Chemistry, 35, 219-226.

Vert, M., Mauduit, J. and Li, S. (1994) Biodegradation of PLA/GA polymers: Increasing Complexity. Biomaterials, 15, 1209-1213.

Vogel, B.M. and Mallapragada, S.K. (2005). The synthesis of polyanhydrides. Handbook of Biodegradable Polymeric Materials and their Applications, 1, 1-19. American Scientific Publishers, Ames, Iowa.

Wachsen, O., Reichert, K. H., Kruger, R. P., Much, H. and Schulz, G. (1997). Thermal decomposition of biodegradable polyesters - III. Studies on the mechanisms of thermal degradation of oligo-L-lactide using SEC, LACCC and MALDI-TOF-MS, Polymer Degradation and Stability, 55, 225-231.

Wang, Y., Steinhoff, B., Brinkmann, C. and Alig, I. (2008). In-line monitoring of the thermal degradation of poly(L-lactic acid) during melt extrusion by UV/vis spectroscopy. Polymer 49, 1257-1265.

Weir, N. A., Buchanan, F. J., Orr, J. F., Farrar, D. F. and Dickson, G. R. (2004). Degradation of poly-L-lactide. Part 2: increased temperature accelerated degradation. Proceedings of the Institute of Mechanical Engineers, Part H: Journal of Engineering in Medicine Proc, 218, 321-330.

Wise, J., Gillen, K. T. and Clough, R. L. (1995). An ultrasensitive technique for testing the Arrhenius extrapolation assumption for thermally aged elastomers. Polymer Degradation and Stability, 49, 403-418.

Wu, T. and Wu, C. (2006). Biodegradable poly(lactic acid)/chitosan-modified montmorillonite nanocomposites: Preparation and characterization. Polymer Degradation and Stability, 91, 2198-2204.

Xie, W., Gao, Z., Pan, W., Hunter, D., Singh, A. and Vaia, R. (2001). Thermal degradation chemistry of alkyl quaternary ammonium montmorillonite. Chemistry of Materials, 13, 2979-2990.

Xing, P., An, Y., Dong, L. and Feng Z. (1998). Miscibility and crystallization of poly(b-hydroxybutyrate)/ poly(vinyl acetate-co-vinyl alcohol) blends. Macromolecules, 31, 6898-6907.

Xu, S. H. and Boyd, S. A. (1995). Cationic surfactant sorption to a vermiculitic subsoil via hydrophobie bonding. Environmental Science and Technology, 29, 312-320.

Yasuda, T. and Takiyama, E. (1995). Biodegradable poly(butylene succinate). US Patent 5391644.

Youan, B. B., Benoit, M. A., Baras, B. and Gillard, J. (1999). Protein-loaded poly(epsilon-caprolactone) microparticles. I. Optimization of the preparation by (water-in-oil)-in water emulsion solvent evaporation. Journal of Microencapsulation, 16, 587-599.

Zanetti, M., Camino, G., Reichert, P. and Mulhaupt, R. (2001). Thermal behaviour of poly(propylene) layered silicate nanocomposites. Macromolecular Rapid Communications, 22, 176-180.

Zhu, L. and Xanthos, M. (2004). Effects of process conditions and mixing protocols on structure of extruded polypropylene nanocomposites. Journal of Applied Polymer Science, 93, 1891-1899.